Nuclear Particle Transport with Emphasis on Monte-Carlo and Shielding Calculations

Kirkegaard, P.

Publication date:
1966

Document Version
Publisher's PDF, also known as Version of record

Risö Report No. 136

Risö Report No. 136

Danish Atomic Energy Commission

Research Establishment Risö

Nuclear Particle Transport with Emphasis on Monte-Carlo and Shielding Calculations

by Peter Kirkegaard

June, 1966

Sales distributors: Jul. Gjellerup, 87, Sölvgade, Copenhagen K, Denmark

Available on exchange from: Library, Danish Atomic Energy Commission, Risö, Roskilde, Denmark

June, 1966 Risø Report No. 136

Nuclear Particle Transport with Emphasis on Monte-Carlo and Shielding Calculations

by

Peter Kirkegaard

The Danish Atomic Energy Commission
Research Establishment Risø
Reactor Physics Department

Abstract

A description is given of a number of methods of calculating the transport of neutrons and γ-rays, mainly in reactor shields. Emphasis has been laid on the Monte-Carlo technique. All the methods described have been programmed for the electronic computer GIER at Risø, and some of them also for the IBM 7090 computer at the Danish Technical University, Lyngby.

A simple bulk shield programme system has been developed which calculates the penetration of neutrons as well as γ-rays throughout a reactor shield. The neutrons are treated according to the removal-diffusion theory with one removal and one diffusion group. The γ-ray calculation relies on the build-up concept.

An improved removal-diffusion neutron shielding programme has been worked out, permitting an arbitrary number of removal and diffusion groups. A cross-section library with the elements most frequently encountered in shielding has been prepared.

A general outline of the Monte-Carlo calculation method for problems in nuclear particle transport is given. Some minor reactor problems concerning self-absorption of γ-rays in fuel rods and distribution of the energy deposition on the various components of a fuel lattice cell are solved by the Monte-Carlo method.

A Monte-Carlo Y-ray shieldirg programme has been written, especially suited for laminated shields, in which case it is superior to build-up methods. The programme calculates the energy deposition rate throughout the shield as well as the dose rate at the external surface.

Finally, a Monte-Carlo method for computing the axial neutron flux distribution in a short, absorbing rod is presented.

Whenever possible, the calculations described in this report have been supported by experimental results.

Contents

		Page
1.	Introduction	5
	1.1. Acknowledgements	6
2.	A Simple Bulk Shield Programme System for Neutrons and γ-Rays	7
	2.1. REMTHERM, A Multi-Layer, Simple Removal Programme for Neutrons	7
	2.2. PRIGAM, a Multi-Layer, Build-up Programme for Core γ-Rays	12
	2.3. SEGAM I and SEGAM II, Programmes for Capture γ-Rays	14
	2.4. Calculation Results	16
3.	A Multi-Group Bulk Shield Programme for Neutrons	16
	3.1. The REMDIFF Method	17
	3.2. The Cross Section Library	23
	3.3. Calculation Results	30
4.	General Outline of the Monte-Carlo Method in Calculating Nuclear Particle Transport	31
	4.1. Principle of the Monte-Carlo Method	32
	4.2. Production of Random Numbers	33
	4.3. Monte-Carlo in Nuclear Particle Transport	35
	4.4. Fundamental Sampling Principle	35
	4.5. Standard Routines in Problems of Nuclear Particle Transport	36
	4.6. Variance-Reducing Devices	40
5.	Some Minor Problems Solved by the Monte-Carlo Method	43
	5.1. Self-Absorption of γ-Rays in Fuel Rods	44
	5.2. Energy Deposition on the Components of a Fuel Lattice Cell, for γ-Rays	46
	5.3. Energy Deposition on the Components of a Fuel Lattice Cell, for Neutrons	49

Page

6. A Monte-Carlo Bulk Shield Programme for Y-Rays 51

6.1. Description of the Problem 52
6.2. Application of the Exponential Transformation 52
6.3. Calculation of Heat Generation and Dose Rate 57
6.4. The Programme 60
6.5. Calculation Results 63

7. Monte-Carlo Calculation of Axial Neutron Flux Distribution in a Short, Absorbing Rod 66

7.1. Description of the Problem 66
7.2. Discussion of the Models 67
7.3. Description of the Monte-Carlo Methods 68
7.4. The Computer Programme System 73
7.5. Presentation of Calculations and Comparison with Experiments 76
7.6. The Risö Measurements 80

References 82

Figures 84

1. INTRODUCTION

When the work described in this report started in the autumn of 1963, it was planned to develop a number of calculation methods for shielding purposes, and to programme them for the electronic computer GIER at Risö. Up to that time, all shielding calculations at Risö had been made with paper, pencil and slide rule, and because of the troublesome and lengthy nature of such calculations the methods applied were restricted to rather crude ones. However, a draft of a computer programme system, worked out by A. Olsen, Risö, already existed. His methods closely followed those applied in his hand calculations for the DOR-type reactor. It was decided, first of all to continue and complete his work. Therefore a reactor bulk shielding programme system calculating neutron flux and γ-dose throughout the shield was made. It was recognized, however, that this programme system would be suitable only for rough estimates, not for detailed and reliable shielding calculations. This is due to several shortcomings and oversimplifications in the models applied; examples are the division of the neutrons into only two energy groups, and the application of the build-up concept in the γ-calculations. Therefore it was planned to replace the simple methods by some other methods giving more accurate and reliable answers. Special attention was given to the possibility of introducing the Monte-Carlo calculation method, which possesses great versatility and is thus superior to most other methods.

It turned out that the shielding calculation methods for γ-rays could advantageously be replaced by Monte-Carlo. Concerning the neutrons, the choice of method is not so clear. Owing to the huge number of cross-section parameters necessary to describe the neutron transport in a Monte-Carlo model, it was decided not to apply Monte-Carlo. Instead, a multi-group method was chosen.

When the investigations of the prospects of Monte-Carlo started, this method was new at Risö, at least in the field of reactor physics. Consequently it was necessary to do some work to gain knowledge of the proper use of the method, and to apply it to rather simple problems so as to gather enough experience to solve problems of some complexity. It is therefore natural that a description of the theory behind the Monte-Carlo technique and of a number of applications to problems in reactor physics should be included in this report.

The first problem in this work solved by the Monte-Carlo technique was a calculation of the fraction of γ-energy escaping from a long rod in

which fission occurs. This simple problem is very instructive as it involves many of the standard devices in the Monte-Carlo technique. The next problem was the calculation of the distribution of the energy deposition on the various components of a fuel lattice cell.

Finally, the report describes Monte-Carlo methods for the solution of two problems considerably more involved than those described above. One is the Y-shielding problem mentioned previously, and the other concerns the longitudinal neutron flux distribution in a short, absorbing rod.

Digital computers have played a very important role for the project in so far as they have been used to carry out almost all the calculations. When the project started, the GIER computer had recently been acquired by Risö. This computer has a small fast memory storage, and it turned out that more complex problems, especially those tackled by the Monte-Carlo technique, required excessive computing time. Fortunately, in the autumn of 1965, an IBM 7090 computer was installed at NEUCC (Northern Europe University Computing Center) at the Technical University of Denmark in Lyngby, and became available also for Risö. A translation of the larger programmes for use in this computer was then carried out with the result that they are now working satisfactorily.

1.1. Acknowledgements

The work presented was carried out in partial fulfilment of the requirements for the lic. techn. degree. It was made possible by a grant from the Technical University of Denmark and by the support of the Danish Atomic Energy Commission, both of which are gratefully acknowledged.

Thanks are also due to the staff of NEUCC, and to all members of the computer group at Risö. In particular, the author wishes to thank Erik Hansen, who was of invaluable help in assisting in the IBM 7090 computations.

For valuable discussions and much help during the work, the author proffers his thanks to P. L. Ølgaard, Head of the Reactor Physics Department, Risö, and to P. B. Suhr, A. Olsen, B. Micheelsen, and H. Neltrup, all of the Reactor Physics Department, Risö.

Finally, the careful measurements by W. Buck, Reactor Physics Department, in support of the Monte-Carlo calculations in section 7 are acknowledged.

2. A SIMPLE BULK SHIELD PROGRAMME SYSTEM FOR NEUTRONS AND Y-RAYS

In almost all reactor shielding design calculations, only neutrons and Y-rays need be taken into account. Other types of radiation, such as α- and β-rays, are easily stopped by a few mm of normal shielding material. In a power reactor the neutrons in the shield originate from fission. Generally, minor effects like those of photoneutrons can be neglected. The Y-rays in the shield originate both from the reactor core and from the shield itself. In the core, Y-rays are produced almost instantaneously by the fission process, further during the decay of the fission products, and by neutron capture in the structural materials of the core, such as Al. The Y-sources in the shield itself are due to capture of thermal (and epithermal) neutrons. In thermal shields of power reactors, iron is a frequently used component, and this metal has a very hard capture-Y line (7.5 MeV). In many reactors these Y-rays give a predominant contribution to the dose rate at the external surface of the biological shield. The following subsections describe simple methods of calculating the attenuation of the neutrons and Y-rays throughout a bulk shield round a reactor and the Y heat generation rate in the shield.

2.1. REMTHERM, A Multi-Layer, Simple Removal Programme for Neutrons

The programme REMTHERM carries out calculations based on simple removal theory of the fast and thermal neutron flux throughout a shield.

The core-shield configuration may be either a sphere, an infinite cylinder or an infinite slab system. The core is assumed to be a homogeneous medium with a spatially constant volume source of fast neutrons. The surrounding shield must consist of a finite number of symmetrical, homogeneous layers. Any reflectors, if present, are considered part of the shield. The result of the calculation is the fast and thermal neutron fluxes in an arbitrary number of shield points.

The simple removal theory adopted here is valid only for mixtures (or laminations) of materials with heavy and light nuclei respectively (e.g. iron and hydrogen). It is then a fair approximation to consider only two groups of neutrons. In the first group are kept those neutrons which have not collided at all, or which have been scattered elastically through a small angle. This flux, called the removal flux, is calculated as the uncollided

flux of source neutrons, the total cross section Σ_t being replaced by Σ_r, the so-called removal cross section, which is smaller than Σ_t. Σ_r is an empirical cross section, experimentally adapted for shielding applications. In the second group are kept all neutrons "removed" from the first group (fast absorption neglected). These neutrons will have a rather small age to thermal energies because of the light nuclei present; therefore they can simply be considered as thermal neutrons and be treated by the aid of diffusion theory.

The definitions of removal flux and removal cross section are somewhat ambiguous and depend on the applications. Although the simple removal theory outlined above is rather crude, this approach is certainly better than two-group diffusion theory. This is due to the fact that the cross section often decreases rapidly in the MeV-region so that at large distances from the sources there are relatively many "penetrating" fast neutrons from the core. On account of the marked anisotropy, this penetrating flux cannot be adequately treated by diffusion theory, but is well described as a virtually uncollided flux.

In the following, analytical expressions for the removal flux ϕ_1 are given in the three geometries.

Spherical geometry:

$$\phi_1 = \frac{S_o}{2\Sigma_{ro}} \int_0^{\text{Arc sin}\frac{a}{r}} \sin\theta \left\{1 - \exp\left[-2\Sigma_{ro}\sqrt{a^2 - r^2\sin^2\theta}\right]\right\} \exp\left\{-\int_a^r \frac{\Sigma_r(\rho)\,\rho\,d\rho}{\sqrt{\rho^2 - r^2\sin^2\theta}}\right\} d\theta \qquad (2.1)$$

Infinite cylinder:

$$\phi_1 = \frac{S_o}{\pi\Sigma_{ro}} \int_0^a \left[Ki_2(f(x,r)) - Ki_2(2\Sigma_{ro}\sqrt{a^2 - x^2} + f(x,r))\right] \frac{dx}{\sqrt{r^2 - x^2}} \qquad (2.2)$$

with $$f(x,r) = \int_a^r \frac{\Sigma_r(\rho)\,\rho\,d\rho}{\sqrt{\rho^2 - x^2}}$$

Infinite slab:

$$\Phi_1 = \frac{S_o}{2\Sigma_{ro}} \left(E_2(S) - E_2(S + 2\Sigma_{ro} a)\right) . \qquad (2.3)$$

In these formulas, Σ_{ro} and Σ_r are the removal cross sections in the core and the shield respectively, 2a is the core thickness, S_o the strength of the volume source of fast neutrons in the core, r the distance from core centre to shield point, and S the optical distance ($\int \Sigma_r dr$) from core surface to shield point. Finally, $E_n(x)$ and $Ki_n(x)$ denote the exponential integral function and the Bickley function respectively:

$$E_n(x) = x^{n-1} \int_x^\infty \frac{e^{-t}}{t^n} dt, \quad Ki_n(x) = \int_0^{\frac{\pi}{2}} e^{-\frac{x}{\cos\varphi}} \cos^{n-1}\varphi \, d\varphi . \qquad (2.4)$$

All the three expressions for Φ_1 are obtained by integrating the simple exponential attenuation kernel over the core volume.

The thermal flux Φ_2 is calculated as the solution of the diffusion equation

$$D \nabla^2 \Phi_2 - \Sigma_a \Phi_2 + Q = 0 ; \qquad (2.5)$$

D is the thermal diffusion coefficient and Σ_a the thermal absorption cross section.

The source term Q is set equal to $\Sigma_r \cdot \Phi_1$. The previously obtained expressions for Φ_1 are too complicated to be used in the solution of (2.5). Instead, Φ_1 is approximated by simple functions, depending on the actual geometry, as described later. The number of equations (2.5) to be solved is equal to N, the number of shield layers. The solution of each equation involves two arbitrary constants; this makes altogether 2 N constants to be determined. The N-1 shield interfaces yield 2N-2 boundary conditions (continuity of flux and current); hence two more conditions are required. One is a prescribed thermal flux value at the core - shield interface. The other is that the thermal flux must vanish at the extrapolated external shield boundary. Now, the 2N constants can be determined by solution of a system of 2N linear equations. Owing to the usually large variation in the order of magnitude of the coefficients, only special methods will succeed in the

numerical solution of these equations. In this programme, a method suggested by Crout and programmed by Lang Rasmussen, Risö, is applied.

In the following, the solution of equation (2.5) is given separately for the three geometrical cases. The solution concerns a definite layer (no. i).

(1) Spherical geometry

The use of $\nabla^2 \Phi_2 = \frac{d^2\Phi_2}{dr^2} + \frac{2}{r}\frac{d\Phi_2}{dr}$ yields

$$\frac{d^2\Phi_2}{dr^2} + \frac{2}{r}\frac{d\Phi_2}{dr} - \varkappa_i^2 \Phi_2 + \frac{Q_i}{D_i} = 0 \qquad (2.6)$$

with $\varkappa_i^2 = \frac{\Sigma_{ai}}{D_i}$.

Further, on the substitution $\Phi_2 = \frac{y}{r}$:

$$\frac{d^2y}{dr^2} - \varkappa_i^2 y + r\frac{Q_i}{D_i} = 0 .$$

It is now convenient to approximate the source term $r \cdot \frac{Q_i}{D_i}$ by an exponential: $r \cdot \frac{Q_i}{D_i} \approx c_i e^{-b_i r}$.

The constants c_i and b_i are uniquely determined by requiring

$$Q_i = \Sigma_{ri} \cdot \Phi_1$$

at the two boundaries of the layer.

The approximated form of the diffusion equation is now

$$\frac{d^2y}{dr^2} - \varkappa_i^2 y + c_i e^{-b_i r} = 0$$

with the general solution

$$y = A_i e^{\varkappa_i r} + B_i e^{-\varkappa_i r} + \frac{c_i}{\varkappa_i^2 - b_i^2} e^{-b_i r}$$

or

$$\phi_2 = \frac{1}{r}\left(A_i e^{\varkappa_i r} + B_i e^{-\varkappa_i r} + \frac{c_i}{\varkappa_i^2 - b_i^2} e^{-b_i r}\right) . \qquad (2.7)$$

(2) Infinite cylinder

The use of $\nabla^2 \phi_2 = \frac{d^2\phi_2}{dr^2} + \frac{1}{r}\frac{d\phi_2}{dr}$ yields

$$\frac{d^2\phi_2}{dr^2} + \frac{1}{r}\frac{d\phi_2}{dr} - \varkappa_i^2 \phi_2 + \frac{Q_i}{D_i} = 0 . \qquad (2.8)$$

Here the source term $\frac{Q_i}{D_i}$ is approximated by a modified, zero-order Bessel function of the second kind:

$$\frac{Q_i}{D_i} \approx c_i K_o (b_i r) .$$

The constants c_i and b_i are uniquely determined by requiring

$$Q_i = \Sigma_{ri} \cdot \phi_1$$

at the two boundaries of the layer. The approximated diffusion equation is now

$$\frac{d^2\phi_2}{dr^2} + \frac{1}{r}\frac{d\phi_2}{dr} - \varkappa_i^2 \phi_2 + c_i K_o(b_i r) = 0$$

with the general solution

$$\phi_2 = A_i I_o(\varkappa_i r) + B_i K_o(\varkappa_i r) + \frac{c_i}{\varkappa_i^2 - b_i^2} K_o(b_i r) \; ; \qquad (2.9)$$

I_o is the modified, zero-order Bessel function of the first kind.

(3) Slab

The use of $\nabla^2 \phi_2 = \frac{d^2\phi_2}{dr^2}$ yields

$$\frac{d^2 \Phi_2}{dr^2} - \varkappa_i^2 \Phi_2 + \frac{Q_i}{D_i} = 0 . \qquad (2.10)$$

Here, $\frac{Q_i}{D_i} \approx c_i e^{-b_i r}$, and the approximated diffusion equation is

$$\frac{d^2 \Phi_2}{dr^2} - \varkappa_i^2 \Phi_2 + c_i e^{-b_i r} = 0 ,$$

where c_i and b_i are determined as before. The general solution of this equation is

$$\Phi_2 = A_i e^{\varkappa_i r} + B_i e^{-\varkappa_i r} + \frac{c_i}{\varkappa_i^2 - b_i^2} e^{-b_i r} . \qquad (2.11)$$

2.2. PRIGAM, a Multi-Layer, Build-up Programme for Core γ-Rays

It is often necessary to know the heat generation rate in the shield of a power reactor in order to design a proper thermal shield and avoid cracks in the biological concrete shield.

In this subsection is described a programme, PRIGAM, which computes the heat production in a shield from core γ-rays. In subsection 2.3 are described analogous programmes computing the heating in the shield from capture γ-sources in the shield itself.

PRIGAM is able to handle a number of shield layers and a number of γ-energy groups. The geometry (fig. 2.1) is the same as for REMTHERM in the slab case. However, for large core dimensions the code will be suitable also for a spherical or cylindrical geometry; the errors will then be small, especially for shield points near the core, where the prediction of heat production is most important (e.g. in the thermal shield and inner parts of the biological shield).

On the addition of an air or tissue layer outside the external surface of the biological shield, PRIGAM may also be used for dose rate calculations.

PRIGAM assumes the sources of γ-rays to be spatially constant over the core. The heat generation from each energy group is calculated separately and the results are added up.

The sympol μ (with or without indices) will in the following denote the total linear γ-absorption coefficient (in cm^{-1}). It includes absorption processes by the photoelectric effect and by pair production, as well as Compton

scattering (without coherent scattering).

The core is assumed opaque to the Y-rays, which permits the back-face correction to be ignored. Under this condition, the volume source S_v (photons/cm^3/sec) in some energy group (g) can be replaced by an equivalent surface source

$$S_{pl} = \frac{S_v}{\mu_{core}} \quad \text{(photons/cm}^2\text{/sec)} \; . \tag{2.12}$$

The calculations are based on the build-up concept, i. e. the desired quantity is calculated from the uncollided Y-flux and then multiplied by a build-up factor B to compensate for the scattered radiation. The build-up factor of choice is in our case the energy build-up factor for the point-isotropic source.

In this work, a quadratic build-up factor

$$B(D) = 1 + \beta D + \gamma D^2 \tag{2.13}$$

was applied. β and γ are energy-dependent coefficients, while D denotes the optical distance (number of Y-relaxation lengths) in the medium between the source point and the shield point. This medium should be infinite and homogeneous, which are the conditions for the point-isotropic build-up factor to be valid. However, neither of these conditions is fulfilled in our problem. First, the shield terminates at the external surface. This causes an overestimation of the flux near this surface. Secondly, the shield may be composed of laminae of different materials. To get round this problem in a simple way, one replaces (2.13) by the expression

$$B(D) = 1 + \sum_{i=1}^{n} \beta_i \mu_i d_i + \sum_{i=1}^{n} \gamma_i (\mu_i d_i)^2 \; , \tag{2.14}$$

where β_i and γ_i are quadratic build-up coefficients for the material in shield layer no. i. The other symbols are explained in fig. 2.1. (2.14) implies that B for a lamination of layers is approximately equal to the product of the B_i's for the individual layers provided none of the B_i's are much greater than one.

This method of constructing build-up factors for laminations is merely a computational trick and has little physical background. Clearly, in this approach, the penetration does not depend on the order of laminations; this is, however, a very crude approximation.

The surface source S_{pl} causes an effective Y-flux at shield point P (fig. 2.1):

$$\phi(t) = \frac{S_{pl}}{2}\left[E_1(X) + \frac{e^{-X}}{X}\sum_i \beta_i X_i + \frac{\sum_i \gamma_i X_i^2}{X^2} e^{-X}(1+X)\right] . \qquad (2.15)$$

(2.15) is obtained by integration of the expression

$$\frac{S_{pl}}{4\pi d^2} e^{-D} \cdot B(D) \qquad (2.16)$$

over the source plane.

The heat generation rate at P from energy group g is

$$W_g(t) = \phi_g(t) \cdot \mu_{Ea} \cdot E , \qquad (2.17)$$

where μ_{Ea} is the Y-energy absorption coefficient at P for energy E.

The total heat generation rate at P is

$$W(t) = \sum_g W_g(t) . \qquad (2.18)$$

The Y cross sections in this work are calculated by the programme itself once the concentrations and atomic numbers of the constituent elements of the layers are given. This was made possible by a study by A. Olsen, Risö, who fitted the Y cross sections of all elements to analytic expressions based on formulas from quantum mechanics. The expressions are in general only valid for $E > 0.5$ MeV because of the absorption edges at lower energies. However, energies below 0.5 MeV are not very important for shielding design calculations.

2.3. SEGAM I and SEGAM II, Programmes for Capture Y-Rays

A prominent radiation source in power reactor shields is the Y-radiation from neutron capture in the shield itself. Such capture processes are mainly caused by thermal neutrons.

The programme SEGAM I calculates the heat production in an infinite slab of shield material from capture Y-rays in the layer itself (fig. 2.2.1). SEGAM II calculates the heat production in a number of adjacent slabs from capture Y sources in an exterior slab (fig. 2.2.2).

The thermal flux, as calculated with REMTHERM (eq. (2.11)), was in each shield layer a sum of exponentials:

$$\Phi_{th}(t) = \sum_k \Phi_{th,k}\, e^{-kt} \quad . \tag{2.19}$$

Then the capture γ sources, $\Sigma_{cap} \cdot \Phi_{th}(t)$, in the source slab will also be a sum of exponentials, both for SEGAM I and SEGAM II:

$$Q(t) = \sum_k Q_{o,k}\, e^{-kt} \quad . \tag{2.20}$$

As in the PRIGAM case, the γ-sources may be distributed over a number of energy groups.

The heat generation is calculated for each exponential term and each energy group and then summed over terms and groups to give the total heat generation rate in a shield point.

The build-up factor applied in the flux calculations is the same as for PRIGAM.

The resulting expression for the effective γ-flux due to one exponential term $Q_{o,k}\, e^{-kt}$ and one group energy E is for the SEGAM I case

$$\Phi(t) = \frac{Q_{o,k}\exp(-\nu X)}{2\mu}\left[F_1(X,\nu) + F_1(X_1-X,\,-\nu) + (\beta+\gamma)\left\{\frac{\exp((\nu-1)X)-1}{\nu-1} + \frac{1-\exp(-(\nu+1)(X_1-X))}{\nu+1}\right\}\right.$$

$$\left. + \gamma\left\{\frac{X\exp((\nu-1)X)}{\nu-1} - \frac{(X_1-X)\exp(-(\nu+1)(X_1-X))}{\nu+1} + \frac{1-\exp((\nu-1)X)}{(\nu-1)^2} + \frac{1-\exp(-(\nu+1)(X_1-X))}{(\nu+1)^2}\right\}\right]. \tag{2.21}$$

The function $F_1(X,\nu)$ is defined as the integral $\int_0^X e^{\nu t} E_1(t)\,dt$.

The other symbols are explained in fig. 2.2.1.

For the SEGAM II case the effective γ-flux at P (fig. 2.2.2) is

$$\Phi(t) = \frac{Q_{o,k}}{2\mu_1}\left[\frac{1}{\nu}\left\{\exp(\nu X)E_1(X) - E_1((1-\nu)X) - \exp(\nu X')E_1(X') + E_1((1-\nu)X')\right\} +\right.$$

$$+(B_2+\gamma X'^2)\left(\frac{\exp(-(1-\nu)X')}{X'}-\frac{\exp(-(1-\nu)X)}{X}\right)+(B_1+\nu B_2-\beta X'+\nu\gamma X'^2-2\gamma X')(E_1((1-\nu)X')$$

$$-E_1((1-\nu)X))+\left[\frac{\beta-2\gamma X'+\gamma}{1-\nu}+\frac{\gamma}{(1-\nu)^2}\right](\exp(-(1-\nu)X')-\exp(-(1-\nu)X))$$

$$+\frac{\gamma(X'\exp(-(1-\nu)X')-X\exp(-(1-\nu)X))}{1-\nu}\Bigg]\cdot\exp(-\nu X)\,. \qquad (2.22)$$

The heat generation rate is calculated from the flux as in (2.17).

SEGAM I and SEGAM II have the same shortcomings due to the build-up factor as PRIGAM. One of the consequences of this is that, e.g. in the SEGAM I slab, the result is independent of the media outside the slab.

2.4. Calculation Results

The programme system described in this section has been used to carry out shielding calculations on the Swedish R2-0 reactor, for which rather comprehensive experimental results are available.

The description of these calculations and comparisons with measurements are presented at the end of sects. 3 and 6, where they are discussed in connection with the results obtained by the more advanced methods described in this report.

3. A MULTI-GROUP BULK SHIELD PROGRAMME FOR NEUTRONS

This section describes an improved calculation method for neutron bulk shield problems. A computer programme, REMDIFF, has been worked out which is superior to REMTHERM in the following respects:

(1) It operates with a number of removal groups and a number of diffusion groups instead of only one of each. In this way a rather detailed picture of the neutron spectrum can be obtained. This is desirable in problems with deep penetration of fast neutrons and in radiation damage problems.

(2) It permits a spatial variation of the fission sources. In many applications, the source density in the outer parts of the core, which give the main contribution to the flux in the shield, is very different from the average density over the whole core region.

(3) An improved method is used to solve the diffusion equations. The improvement consists in the fitting of the diffusion source term to a sum of two expressions rather than to only one. The effect of this change is marked for thick shield layers.

A drawback of the REMDIFF programme is that it handles only slab geometry. For problems with cylindrical or spherical geometry, one possible approach is to calculate the energy spectrum with REMDIFF and then calculate the geometrical corrections with REMTHERM. On the other hand, REMDIFF is provided with an option for the approximate handling of finite slabs.

3.1. The REMDIFF Method

The geometry is shown in fig. 3.1; it is basically the same as the REMTHERM geometry in the slab case.

REMDIFF operates with a number of removal groups, G_m, and a number of diffusion groups, g_m.

In REMTHERM, the removal cross section Σ_r for a definite shield layer was given as an empirical value for the material in question (concrete, water, etc.). REMDIFF calculates Σ_r for each group and each layer from the concentrations of the constituent elements and the microscopic removal cross sections σ_r. The following expression for σ_r is used here:

$$\sigma_r = \sigma_{total} - 2\pi \int_{\mu_o}^{1} \sigma_{el}(\mu)\, d\mu \quad . \tag{3.1}$$

This formula has been proposed by a Swedish group[1], who recommend a fixed value of μ_o equal to 0.6; this value is adopted here. σ_{total} is the total microscopic cross section, $\sigma_{el}(\mu)$ the microscopic differential elastic scattering cross section per unit solid angle, and μ the deflection cosine in the laboratory system of reference. μ_o defines a cone into which the virgin neutrons may be scattered without losing their character of being virtually unscattered. To maintain the physical consistence it is desirable that the energy degradation coupled to the deviation μ_o is not strong enough to reduce the neutrons, originally having the group energy E_G, to the next lower group energy E_{G+1}. This condition is met by the group structure of the cross-section library presented in subsection 3.2, even in the case of scattering on hydrogen. From (3.1) follows that absorption and inelastic scattering processes "remove" the neutrons from the virtually unscattered removal flux.

When $\Sigma_r = \sum_i N_i \sigma_{ri}$ has been calculated for the core and the l_m shield layers in all G_m removal groups, one calculates the G_m removal fluxes throughout the reactor (REMDIFF treats the core just like the shield layers). Actually, the calculation is limited to the set S of points marked in fig. 3.1: the half core is divided by half-points, and each shield layer is divided by third-points. The source of the removal flux calculation is the fission neutrons in the core, divided into G_m energy groups. Spatial variation of the source is allowed: the programme reads in the source (in fact, the thermal flux) in a number of core points, and makes a 6th order polynomial least-square fit. The resulting polynomial, P(x), has no terms with odd powers owing to the requirement of symmetry. With this source, the removal fluxes in all points and groups are calculated as the integral

$$\frac{1}{\Sigma_{r,\,core}} \int_{-a}^{a} P(x)\,dx \cdot \frac{1}{2} E_1(S(X,P)) \quad , \tag{3.2}$$

where S(X, P) is the optical distance ($\int \Sigma_r dr$) from the source element to P. (3.2) is calculated by numerical integration. A small numerical complication arises if P is one of the three core calculation points; as these lie in the source region, zero arguments occur in E_1. This calamity is cured by integrating (3.2) by parts. The result is essentially an integral like (3.2), but with E_1 replaced by the E_2-function, which is regular for zero arguments.

When the removal flux calculation sketched above is finished for all G_m removal groups, one begins the calculation of the g_m diffusion fluxes in core and shield, starting at the fastest group, $g = 1$, and ending with the slowest, $g = g_m$, which is the thermal group.

It is characteristic of the REMDIFF method that each removal group gives a source contribution not only to the fastest diffusion group (the English method), but to all of them. Further, outscattering from diffusion group g gives sources not only to the next slower group, $g + 1$, but to all the groups $g + 1$, $g + 2$, ..., g_m. This treatment of the transfer between groups was proposed by AB Atomenergi, Sweden[1]. The cross-section library, presented in 3.2, utilizes only partially the possibilities of the allowed group transfers.

The diffusion equation in group no. g ($1 \leq g \leq g_m$) and layer no. l ($0 \leq l \leq l_m$) reads

$$D_{gl}\frac{d^2\Phi_{gl}}{dx^2} - (\Sigma_{a,gl} + \Sigma_{outsc,gl})\cdot\Phi_{gl} + Q_{gl}(x) = 0 \quad . \tag{3.3}$$

$\Sigma_{a,gl}$ is the absorption cross section. $\Sigma_{outsc,gl}$ is the cross section for scattering out of group g. D_{gl} is the diffusion coefficient, calculated as

$$D_{gl} = \frac{1}{3\Sigma_{tr}} \text{ with } \Sigma_{tr} = \Sigma_a + \Sigma_{outsc} + \overline{\Sigma_s(1-\mu)} \quad ,$$

where $\overline{\Sigma_s(1-\mu)} = \sum_i N_i \, \sigma_{s,i}(1-\mu_i)$ is the group self-scattering cross section corrected for anisotropy.

The source term $Q_{gl}(x)$ is a sum of removal sources

$$Q_{gl,rem}(x) = \sum_{G=1}^{G_m} \Sigma^{rd}_{G\to g} \, \Phi^{rem}_{Gl}(x) \tag{3.4}$$

and (if $g > 1$) diffusion sources

$$Q_{gl,dif}(x) = \sum_{\gamma=1}^{g-1} \Sigma^{dd}_{\gamma\to g} \, \Phi^{dif}_{\gamma l}(x) \quad . \tag{3.5}$$

The removal→diffusion transference cross sections $\Sigma^{rd}_{G\to g}$ are elements of a $G_m \cdot g_m$ matrix, while the diffusion→diffusion transference cross sections $\Sigma^{dd}_{\gamma\to g}$ are elements of a $g_m \cdot g_m$ matrix with zeros below the diagonal. $\Phi^{rem}_{Gl}(x)$ and $\Phi^{dif}_{\gamma l}(x)$ are removal and diffusion fluxes respectively.

In the following, the technique applied in solving the system of $g_m \cdot (l_m + 1)$ diffusion equations (3.3) is described. The order of solution is chosen so that first the equations with $g = 1$ are solved for all regions ($l = 0, 1, \ldots, l_m$), then all equations with $g = 2$, and so on, ending with the thermal group $g = g_m$.

The equations with $g = 1$ contain only removal sources. By the aid of (3.4) these sources can be calculated at the same set of points, S, as the removal flux, see fig. 3.1. In each region is then constructed an analytic function of exponential or trigonometric type having the correct value at these points. This analytic function is simple enough to allow an analytical solution of the diffusion equation. The diffusion flux for $g = 1$ is then calculated in the points S, whereafter the sources for the equations with $g = 2$

at these points can be calculated from (3.4) and (3.5). The situation is now just the same as for the equations with $g = 1$, and one proceeds in the same way as described until all the equations down to $g = g_m$ are solved.

We now turn to the problem of constructing the analytical expressions for the diffusion sources mentioned above.

Fig. 3.2.1 shows a shield layer with calculated source values k, l, m, n at equidistant points (separation h). It would be desirable to construct a function $A\ e^{\alpha x} + B\ e^{\beta x}$ going through all the four points because such an expression yields very simple solutions of the diffusion equations. However, this is not always possible. Instead it can be shown that a function of one of the following four types:

$$\left.\begin{aligned} &\text{I}: && (A\ e^{\alpha x} + B\ e^{\beta x}) \cos \frac{\pi x}{h} \\ &\text{II}: && A\ e^{\alpha x} + B\ e^{\beta x} \cos \frac{\pi x}{h} \\ &\text{III}: && A\ e^{\alpha x} + B\ e^{\beta x} \\ &\text{IV}: && A\ e^{\alpha x} \cos(b + \beta x) \end{aligned}\right\} \qquad (3.6)$$

will have the desired property. Determination of the type of expression and the constants is carried out by Prony's method. In fact, one searches for an expression of type III above, but accepts one or two complex exponents leading to the other three types. Then, if one puts $e^{\alpha h} = y$, $e^{\beta h} = z$, the following four equations must be satisfied:

$$\left.\begin{aligned} A + B &= k \\ Ay + Bz &= l \\ Ay^2 + Bz^2 &= m \\ Ay^3 + Bz^3 &= n\,. \end{aligned}\right\} \qquad (3.7)$$

Instead of solving for (y, z) one solves for (s_1, s_2), coupled to (y, z) by the requirement that the quadratic equation

$$v^2 + s_1 v + s_2 = 0 \qquad (3.8)$$

must have the roots (y, z). From (3.7) and (3.8) follows that

$$k s_2 + l s_1 + m = A(y^2 + s_1 y + s_2) + B(z^2 + s_1 z + s_2) = 0$$

and

$$l s_2 + m s_1 + n = Ay(y^2 + s_1 y + s_2) + Bz(z^2 + s_1 z + s_2) = 0\,;$$

(s_1, s_2) are then determined as the solution of the equations

$$\begin{aligned} k s_2 + l s_1 + m &= 0 \\ l s_2 + m s_1 + n &= 0 , \end{aligned} \qquad (3.9)$$

whereupon (y, z) are calculated from the symmetrical equations

$$\begin{aligned} y + z &= - s_1 \\ yz &= s_2 \end{aligned} \qquad (3.10)$$

these give complex or real solutions for $y = e^{\alpha h}$ and $z = e^{\beta h}$, which in turn determine α and β. As mentioned, complex values for α or β lead to the types I, II or IV. Finally, A and B are easily determined from eqs. (3.7)

In the corresponding problem for the core region (fig. 3.2.2) the desired function must have the value k at the core centre $x = 0$, 1 at $x = h$, and m at the core edge $x = 2h$. The choice of the function

$$A(\cos \alpha x + \cos \beta x) \qquad (3.11)$$

(α and β may be complex) ensures an expression symmetrical about $x = 0$, which is a natural requirement.

Of course, $A = \frac{k}{2}$. By putting $\cos \alpha h = y$, $\cos \beta h = z$, one obtains the equations

$$\left.\begin{aligned} y + z &= \frac{2l}{k} \\ y^2 + z^2 - 1 &= \frac{m}{k} \end{aligned}\right\} \qquad (3.12)$$

for the determination of (y, z).

An analysis shows that the expression (3.11) may split into seven types of functions, all containing real constants:

$$\left.\begin{aligned} &\text{I} : && A(\cos \alpha x + \cos \beta x) \\ &\text{II} : && A(\cos \alpha x + \cos \beta x) \\ &\text{III} : && A(\cos \alpha x + \cosh \beta x \cos \tfrac{\pi x}{h}) \\ &\text{IV} : && A(\cosh \alpha h + \cosh \beta x) \\ &\text{V} : && A(\cosh \alpha h + \cosh \beta x \cos \tfrac{\pi x}{h}) \end{aligned}\right\} \qquad (3.13)$$

VI : $A(\cosh \alpha x + \cosh \beta x) \cos \frac{\pi x}{h}$

VII: $2A \cos \alpha x \cosh \beta x$.

All the source expressions (3.6) and (3.13) yield fairly handy solutions of the diffusion equations (3.3). By dividing (3.3) by D_{gl} and introducing

$$\varkappa_{gl}^2 = \frac{\Sigma_{a,gl} + \Sigma_{outsc,gl}}{D_{gl}} \tag{3.14}$$

and the constructed source function, one obtains a normalized equation with the common form (indices $g(1, \ldots, g_m)$ and $l(0, \ldots, l_m)$ are suppressed for the sake of clearness)

$$\frac{d^2\Phi}{dx^2} - \varkappa^2 \Phi + \sum_{i=1}^{2} a_i \exp(\alpha_i x) \cos(b_i + \beta_i x) = 0 ; \tag{3.15}$$

(3.15) has the general solution

$$\Phi = A e^{\varkappa x} + B e^{-\varkappa x} + \sum_{i=1}^{2} a_i \exp(\alpha_i x) \frac{(\varkappa^2 - \alpha_i^2 + \beta_i^2)\cos(b_i + \beta_i x) - 2\alpha_i\beta_i \sin(b_i + \beta_i x)}{(\varkappa^2 - \alpha_i^2 + \beta_i^2)^2 + 4\alpha_i^2\beta_i^2} . \tag{3.16}$$

For each diffusion group g we get $l_m + 1$ flux expressions, so that $2 l_m + 2$ arbitrary constants have to be determined. The requirement of symmetry at once yields A = B for the flux in the core; hence $2 l_m + 1$ boundary conditions are necessary:

Φ and $D\frac{d\Phi}{dx}$ have to be continuous at the l_m region interfaces. Φ must vanish at the extrapolated external boundary.

The extrapolation length is taken to be

$$d = \frac{0.71}{\Sigma_{tr}} = 2.13\, D ; \tag{3.17}$$

D refers to group g and layer l_m.

The solution of the $2 l_m + 1$ linear equations for determining the A's and B's proceeds just as in REMTHERM.

It was mentioned at the beginning of this section that REMDIFF could handle a finite slab geometry approximately. On the assumption of a rect-

angular shape of the slabs (a x b) it does so by adding $(\frac{\pi}{a})^2 + (\frac{\pi}{b})^2$ to the expression for $\varkappa_{gl}^2$ (3.14).

The REMDIFF programme accounts for the resonance absorption in the core by U^{238} in a way which will be discussed in 3.2.

3.2. The Cross Section Library

A cross section library containing some frequently encountered nucleides in shielding design has been worked out. These nucleides are given in table 3.1.

Table 3.1

Nucleide No.	Symbol
1	H
2	D
3	C
4	O
5	Mg
6	Al
7	Si
8	Ca
9	Fe
10	Zr
11	Pb
12	U-235
13	U-238

The group structure chosen is seen in fig. 3.3. Although one has the liberty of choosing the energy group limits arbitrarily, it is practical to avoid "overlaps" between the removal and the diffusion groups. The present group structure has two removal groups and nine diffusion groups, the two highest of which have the same limits as the removal groups. The upper energy limit is 10 MeV. Apart from the two lowest diffusion groups, all the groups have a lethargy width of 2.25. This value fits well into the structure of the GAM I library[2], which has provided much of the raw cross section information used in preparing the present library. The reason for choosing the lower limit of group 8 to be 0.414 eV was that this value is generally accepted as the upper limit of thermal energies. All the micro-

scopic cross sections collected in tables 3.2 - 3.6 are given in units of barn.

Removal cross sections

The removal cross sections are calculated from formula (3.1). A weighted average, according to the fission spectrum of U^{235}, is calculated for each removal group. Raw cross-section information is taken mainly from ref. 2, and to some extent from ref. 3. Calculation of $\int_{\mu_o}^{1} \sigma_{el}(\mu)\, d\mu$ requires knowledge of the angular distribution (differential cross section). This knowledge is provided by ref. 4.

In table 3.2 the calculated removal cross sections are collected.

Fission sources

By integration of the fission spectrum over the two removal groups it is found that 72.0% of the neutrons are born in group 1, the remaining 28.0% in group 2.

Removal→diffusion cross section

Next, the transference cross sections $\sigma^{rd}_{i\to j}$ for scattering from removal group i to diffusion group j are calculated. On account of the open group structure it is a good approximation to assume that all cross sections other than $\sigma^{rd}_{i\to i}$ and $\sigma^{rd}_{i\to i+1}$ are zero. As before, the group averaging is made by weighting with the fission spectrum. The results are collected in table 3.3.

The remaining cross sections concern the diffusion groups only. It was decided not to prepare microscopic data for the thermal group (no. 9) in the library, but instead to read into the programme the macroscopic thermal data Σ_a and D for all the regions. The reason for this is that Σ_a and D for thermal neutrons are not always uniquely determined from concentrations and microscopic data.

Proper averaging of the cross sections over the diffusion groups requires knowledge of the energy spectrum. For group 1 this is assumed to be a somewhat degraded fission spectrum, while for the groups 2-8 it is assumed to be an 1/E-spectrum.

Absorption cross section

These appear from table 3.4.

The quoted absorption cross sections for U^{238} do not include the resonance absorption. Instead, the resonance escape probability p is taken as an input quantity in the REMDIFF programme. In the present library it is assumed that p can be written as

$$p = p_5\, p_6\, p_7 \ , \tag{3.17}$$

where p_5, p_6, p_7 are group escape probabilities for the groups 5, 6, 7, and further that

$$p_5 = p_6 = p_7 = \sqrt[3]{p} \ . \tag{3.18}$$

This is a rather crude approximation, but is justified by the minor importance of the correct calculation of diffusion fluxes in the core for a shielding design programme such as the present. The equivalent increment of Σ_a for group g (g = 5, 6, 7) is calculated as

$$\Delta \Sigma_{a,g} = \Sigma_{outsc,\ g} (1 - \sqrt[3]{p}) \ . \tag{3.19}$$

Diffusion transference cross sections

The transference cross sections $\sigma^{dd}_{i\to j}$ for scattering from diffusion group i to diffusion group j are calculated under the same assumption as that made for $\sigma^{rd}_{i\to j}$, namely that $\sigma^{dd}_{i\to j} = 0$ for $j > i+1$. Nucleide no. 7, Si, forms an exception. Here, inelastic scattering in group 1 degrades the energy so much that after the scattering it corresponds to group 4 or 5. The cross sections are

$$\text{Si: } \sigma^{dd}_{1\to 4} = 0.1774 \quad \text{and} \quad \sigma^{dd}_{1\to 5} = 0.1276 \ .$$

The cross sections $\sigma^{dd}_{i\to i}$ and $\sigma^{dd}_{i\to i+1}$ for all 13 nucleides are found in table 3.5.

Finally, table 3.6 shows the cross sections $\sigma^{dd}_{i\to i}(1-\mu)$. They are used to calculate the diffusion coefficients.

Table 3.2

Nucleide No.	1	2	3	4	5	6	7	8	9	10	11	12	13
Group 1	0.9623	1.7088	1.3282	1.5457	1.7340	1.8021	1.3828	1.5619	1.8285	2.6931	3.3781	2.9220	3.9867
Group 2	1.9588	2.5120	2.8174	2.9667	3.5220	2.4082	2.5010	1.4036	1.8170	4.7661	3.5020	3.7386	4.2229

Table 3.3

Nucleide No.	1	2	3	4	5	6	7	8	9	10	11	12	13
Gr. 1 → 1	0.0871	0.5418	1.0411	1.2195	1.5195	1.4738	1.0074	1.2357	1.1741	2.0758	2.9276	1.5753	1.5784
1 → 2	0.8752	1.1670	0.2871	0.3084	0.1918	0.3231	0.0704	0.3262	0.6544	0.6173	0.4505	1.3467	2.2690
2 → 2	0.9688	1.9770	2.8174	2.9667	3.4786	2.4082	2.5010	1.4036	1.8123	4.7551	3.5020	3.4354	3.8706
2 → 3	0.9900	0.5350	0.0000	0.0000	0.0000	0.0000	0.0000	0.0000	0.0000	0.0000	0.0000	0.2916	0.2100

Table 3.4

Nucleide No.	1	2	3	4	5	6	7	8	9	10	11	12	13
Gr. No. 1	0	0	0	0.0177	0.0223	0.0052	0	0	0.0018	0	0	0	0.1393
2	0	0	0	0	0.0722	0.0022	0	0	0.0052	0.0178	0	0.0484	0.1644
3	0	0	0	0	0.3289	0.0189	0	0	0.0076	0.0789	0	0.4657	0.0311
4	0	0	0	0	0	0.0111	0	0	0.0080	0.3700	0	1.8411	0.0047
5	0	0	0	0	0	0	0	0	0.0222	0.6711	0	8.0955	0.0128
6	0.0033	0	0	0	0	0.0067	0	0	0.0679	0.0022	0.0033	29.5000	0.0536
7	0.0278	0	0	0	0.0033	0.0178	0	0	0.2089	0.0144	0.0144	27.2211	0.2022
8	0.0620	0	0	0	0.0100	0.0600	0	0	0.6130	0.0340	0.0400	11.8520	0.4970

Table 3.5

Nucleide No.	1	2	3	4	5	6	7	8	9	10	11	12	13
Gr. 1→1	1.1010	0.3968	1.6663	1.8992	2.2173	2.6163	2.2932	2.9243	2.4112	4.2054	5.8467	4.4054	5.0050
1→2	1.5720	1.9376	0.2321	0.3221	0.1918	0.3231	0.0704	0.3262	0.6544	0.6173	0.4505	1.3467	2.2690
2→2	4.6076	2.1740	3.3906	4.1302	5.5703	4.1777	2.2050	1.9740	3.0803	8.2792	6.9839	6.7795	8.1239
2→3	3.0412	1.0378	0.2560	0.2326	0.1497	0.1472	0.0181	0.0260	0.0576	0.0748	0.0393	0.4560	10.0339
3→3	9.6049	2.2961	4.2698	3.4611	6.1104	3.8931	1.4892	1.4670	5.2991	8.1631	10.5328	10.2634	11.5182
3→4	6.3395	1.0961	0.3224	0.1949	0.1085	0.0386	0.0541	0.0330	0.0722	0.0654	0.0450	0.0399	0.0496
4→4	11.8673	2.3014	4.3605	3.4611	3.3755	1.4017	2.3753	1.9530	6.6208	9.0383	10.6877	10.4604	14.4700
4→5	7.8347	1.0986	0.3292	0.1949	0.1245	0.0472	0.0803	0.0470	0.1225	0.0584	0.0479	0.0396	0.0633
5→5	12.0480	2.3403	4.3784	3.4611	3.3755	1.3744	2.3859	1.9420	10.1892	5.4467	11.1521	10.4604	23.6322
5→6	7.9520	1.1171	0.3306	0.1949	0.1245	0.0456	0.0695	0.0580	0.1730	0.0600	0.0479	0.0396	0.0335
6→6	12.0480	2.3210	4.3795	3.4611	3.3755	1.3680	2.1805	2.6370	10.8270	6.1400	11.1521	12.1477	53.7272
6→7	7.9520	1.1079	0.3306	0.1949	0.1245	0.0453	0.0695	0.0630	0.1730	0.0600	0.0479	0.0401	0.0283
7→7	12.0480	2.3014	4.3793	3.4611	3.3755	1.3696	2.1805	2.6370	10.8270	6.1400	11.1521	11.8861	11.8357
7→8	7.9520	1.0986	0.3306	0.1949	0.1245	0.0460	0.0695	0.0630	0.1730	0.0600	0.0479	0.0483	0.0309
8→8	8.5860	1.4280	4.1059	3.3448	3.2759	1.4311	2.1249	2.6120	10.7578	6.1160	11.1138	13.7429	8.2443
8→9	11.4140	1.9720	0.5941	0.3552	0.2241	0.0889	0.1251	0.0880	0.2422	0.0840	0.0862	0.0971	0.0557

Table 3.6

Nucleide No.	1	2	3	4	5	6	7	8	9	10	11	12	13
Gr. 1	0.3670	0.3320	1.5737	1.4402	1.0479	1.2435	0.7508	1.1212	0.6947	1.2309	2.0276	1.3390	1.4875
2	1.5359	1.8190	3.2021	2.7189	3.7566	2.6123	1.4937	1.2503	1.9655	4.9071	4.1680	3.7097	4.4454
3	3.2016	1.5307	4.0324	3.3168	5.9430	3.7969	1.4555	1.4426	5.2360	8.1035	10.4991	10.2347	11.4859
4	3.9558	1.5354	4.1181	3.3168	3.2830	1.3671	2.3216	1.9206	6.5420	8.9723	10.6535	10.4311	14.4295
5	4.0160	1.5602	4.1350	3.3168	3.2830	1.3405	2.3320	1.9098	10.0679	5.4069	11.1164	10.4311	23.5670
6	4.0160	1.5473	4.1360	3.3168	3.2830	1.3342	2.1312	2.5932	10.6982	6.0952	11.1164	12.1137	53.5768
7	4.0160	1.5343	4.1358	3.3168	3.2830	1.3358	2.1312	2.5932	10.6982	6.0952	11.1164	11.8528	11.8026
8	2.8620	0.9520	3.8776	3.2053	3.1861	1.3958	2.0769	2.5686	10.6298	6.0714	11.0782	13.7044	8.2212

3.3. Calculation Results

Calculations performed by means of REMDIFF have been compared with measurements carried out on the Swedish reactor R2-0 at Studsvik[15]. This reactor is a 100 kW swimming-pool reactor, intended primarily for shielding experiments and critical studies. The core is of box shape, with the dimensions 61.7 x 60.0 x 32.4 cm.

Two of the mock-ups described in ref. 15 were selected for the purpose of comparison between measurements and REMDIFF calculations. These two configurations include two of the most common shielding materials, water and concrete. The arrangements are shown schematically in figs. 3.4 and 3.5. The geometry is essentially one-dimensional slab geometry. In configuration 1 (fig. 3.4) water is the only shielding material. In configuration 2 (fig. 3.5), the bulk shield of magnetite concrete ($\rho = 3.74$) is preceded by 20 cm water and 1 cm aluminium. The REMDIFF calculations were not carried out for more than about 1 metre of water or concrete, although the actual thickness of the mock-ups was considerable greater. This restriction on the calculation stems from troubles caused by the rather limited numerical range of the IBM 7090 computer. These troubles have now been overcome, but it was not found worth while to repeat the calculations with the increased shield thicknesses. In fact, good estimates could be obtained by a simple extrapolation of the flux curves presented here.

The Swedish measurements comprise the thermal flux Φ_{th}, the epithermal flux per lethargy unit Φ_{epi}, and the fast flux in the range 0.3 - 2 MeV, Φ_{fast}. Owing to the coarse structure in the fast-energy range of the present cross-section library of REMDIFF, comparative calculations could not be made for Φ_{fast}, but were restricted to Φ_{th} and Φ_{epi}. The thermal flux Φ_{th} in some types of shield (iron, heavy concrete, etc.) has a direct effect on the production of hard capture-γ rays, which in turn often yield the dominant contribution to the total dose at the external surface of the biological shield. Also the epithermal flux Φ_{epi} may be important in shielding work as it is responsible for part of the damage to shield materials like concrete. The measured epithermal flux is determined as that part of the flux which has a 1/E-spectrum[15]. The calculated value of Φ_{epi} is obtained from the flux results in diffusion group no. 5 (130-1230 eV); the flux results for the neighbouring groups 3, 4, 6, and 7 were almost the same as that for no. 5, indicating a 1/E-spectrum in these groups.

The flux curves as obtained with REMDIFF were corrected for the finite lateral extension of the core (61.7 x 60.0 cm). The correction factor

described in ref. 16 for the transformation from infinite plane source to disk source was applied; its value varied from 1 near the core to about 1/3 far from the core.

The results of the comparison between calculations and experiments are seen in figs. 3.4 and 3.5. The agreement is always inside a factor of three, and in most cases much better. In shielding work such a result must be considered very good, in fact better than one would expect for a calculation scheme like the present. The thermal flux points in the core, used as input in REMDIFF, are marked with crosses in figs. 3.4 and 3.5. One sees that these points are very close to the calculated thermal flux curves in the core region, indicating an internal consistency and soundness of the calculation method.

Also calculation results for the thermal flux obtained with the simple removal-diffusion code REMTHERM mentioned in 2.1 are shown in the figures. The results are corrected for the finite core just as in the case of REMDIFF. The agreement with experiments is not good for the water shield, but better for the concrete shield.

A proposal for improvements of the REMDIFF cross-section library would probably include a more detailed group structure for the energy range above 0.1 MeV, where most of the cross sections decrease rapidly with increasing energy. The number of removal groups should probably be increased from two to about five.

The REMDIFF programme is very fast. The two problems discussed here were solved on the IBM 7090 computer in less than 20 seconds each.

4. GENERAL OUTLINE OF THE MONTE-CARLO METHOD IN CALCULATING NUCLEAR PARTICLE TRANSPORT

The remaining part of the present report is devoted to the Monte-Carlo method and applications of it.

Monte-Carlo is often referred to as the method of random sampling, in fact a very appropriate designation.

A most important field of application is problems in nuclear particle transport, and only such problems will be considered in this report.

However, also other sorts of problems, both in physics and in applied mathematics, have been solved successfully by means of Monte-Carlo. Examples are problems in statistical mechanics, calculation of polymer molecule structures, solution of very large equation systems, and calculation of multidimensional integrals.

Monte-Carlo problems must always be solved on digital computers, preferably of high speed and large size.

4.1. Principle of the Monte-Carlo Method

Quite generally, the principle of Monte-Carlo may be explained as follows: One wishes to calculate some quantity - say a multidimensional integral or a neutron transmission - which is so complicated that an analytic solution is impossible or not feasible. One abandons the calculation of the exact (true) value Q of the quantity and instead tries to obtain a so-called statistical estimate Q_{est}. This estimate is calculated as an average:

$$Q_{est} = \overline{Q}_i = \frac{1}{N} \sum_{i=1}^{N} Q_i (R_i) \; ; \qquad (4.1)$$

R_i is a so-called "sample", which determines the representative value Q_i of the quantity. In the first example, where the quantity was a multidimensional integral, R_i will be a multidimensional point. In the other example, with neutron transmission R_i is the "history" of a neutron, i. e. a set of consecutive values of neutron energies, positions, and directions, simulating in some way the neutron events from birth to death. In both cases, each sample R_i will be constructed by the aid of a series of "random numbers" $r_{i1}, r_{i2}, \ldots$, all lying between zero and one; their properties and the production of them on digital computers will be discussed in 4. 2.

In most cases the estimate is "unbiased", i. e. the mean value of Q_{est} is Q:

$$\mu(Q_{est}) = Q \; . \qquad (4.2)$$

(4. 2) holds in all our applications.

(Note the difference between the terms mean and average: the mean value μ refers to the theoretical probability distribution, while the average (marked with a bar) is determined from the actual samples.)

Restricting oneself to considering only applications in nuclear particle transport, one finds it tempting to define Monte-Carlo merely as a simulation of real particle histories: as each nuclear scattering event is of a probabilistic nature, it can be simulated by the aid of one or more random numbers. However, this definition of Monte-Carlo as a statistical process by which one follows the particle from birth to death, is too narrow. This "random walk" or "direct simulation" method is only the simplest of several possible approaches in the field of Monte-Carlo, and - as will be

discussed later - direct simulation is in fact unsuitable for problems of some complexity, where it must be modified by the inclusion of variance-reducing devices, to be discussed later.

The variance of Q_{est} is defined as the mean square deviation:

$$\text{var}\,(Q_{est}) = \mu (Q_{est} - Q)^2 \quad , \tag{4.3}$$

where Q is the true value of the quantity.

In an actual Monte-Carlo calculation one usually obtains a set of M estimates Q^j_{est} $(1 \leqslant j \leqslant M)$ of the type (4.1). Then the following formulas will be approximately valid:

$$\text{var}(Q_{est}) \approx \frac{1}{M-1} \sum_{j=1}^{M} (Q^j_{est} - \overline{Q_{est}})^2 \quad , \tag{4.4}$$

and

$$\text{var}(\overline{Q_{est}}) \approx \frac{\text{var}(Q_{est})}{M} \quad . \tag{4.5}$$

In these formulas, $\overline{Q_{est}}$ is the set average,

$$\overline{Q_{est}} = \frac{1}{M} \sum_{j=1}^{M} Q^j_{est} \, . \tag{4.6}$$

For practical Monte-Carlo calculations concerning neutron or photon transport, the number of histories, N, used to provide a single estimate Q_{est} will normally be of the order of a few thousand, while the number, M, of independent estimates is, say, ten. The advantage of having several independent estimates (M > 1) is obviously that it is possible to judge the variance of the result (eqs.(4.4) and (4.5)).

A good Monte-Carlo calculation is one in which the variance of the result as well as the computing time are small. This will be further discussed in 4.6.

4.2. Production of Random Numbers

As mentioned in 4.1, a Monte-Carlo calculation involves the use of "random numbers". Customarily, these numbers are restricted to the open interval between 0 and 1.

Random numbers have a probability density function of rectangular shape.

The production of random numbers is carried out on the digital computer itself. A great variety of random number generators exists, but most of them are tailored for some specific computer type. A multiplicative generator, suited for ALGOL and FORTRAN, has been proposed by L. Hansson, Risö, and has been adopted in all the Monte-Carlo calculations described in this report.

The generator utilizes the following simple algorithm:

$$\left.\begin{aligned} Y &= [A\,X/M] \\ Z &= AX - MY \\ r &= Z/M \\ X &= Z \end{aligned}\right\} \qquad (4.7)$$

The square bracket stands for the largest integer $\leqslant$ the argument. The integers A and M have the values 125 and 2,796,203 respectively. r is the resulting random number, always satisfying the inequality $0 < r < 1$. The generator is started by assigning to X an arbitrary positive integer $< M$. By a new "call" of the generator, the foregoing X-value is used for calculating the new r-value. In this manner one can obtain an infinite number of such r-values between 0 and 1, and the sequence will be periodic with a period of M-1[5] calls. All the r-values within a period are different from each other.

Such a series of r-values cannot be truly random because each r-value is uniquely determined by the foregoing. However, the simulation of random numbers is very well established by the algorithm (4.7), provided the total number of calls of the algorithm in the actual problem is below M. If this is not the case, there is a risk of introducing a periodicity in the whole Monte-Carlo calculation. Troubles from this periodicity did not seem to occur in practical calculations till after at least several hours' computing time on the same problem, run on the fast IBM 7090 computer.

An algorithm like (4.7) may be characterized as a generator of "pseudo-random" numbers.

The "randomness" of the numbers generated by (4.7) has been tested in several ways. One of these tests[5] is a χ^2-test both of the rectangular distribution of the r-values and of their independence of each other. The result of this test was satisfactory.

4.3. Monte-Carlo in Nuclear Particle Transport

The further discussion of the Monte-Carlo method is restricted to applications to the transport of nuclear particles, of which furthermore only neutrons and photons are considered. These particles travel independently of each other. The Monte-Carlo procedure then consists in the generation of a set of independent particle histories. The particles are followed from their birth at the source to their death, caused by absorption, escape or any other "category of loss". Random numbers are used to sample path lengths, energy degradation and angular deflection on collision with nuclei, and so on. How this is done in detail, is discussed in the following subsections. As mentioned previously, one seldom simulates slavishly all the events of the particle history because the variance of the results is then too large. A number of "tricks" are frequently applied, some of which are mentioned in 4.6.

The following question naturally arises: What kind of neutron- and γ-problems can profitably be solved by Monte-Carlo? It is very difficult to give a general answer, but one may mention the problems described in sections 6 and 7 as typical examples of problems for which Monte-Carlo is suitable. They are of moderate complexity, too involved to permit analytic solutions, but simple enough to be solved by efficient Monte-Carlo methods. On the other hand, in simple problems permitting solution by an analytic method, the latter will generally be superior to Monte-Carlo.

4.4. Fundamental Sampling Principle

A standard problem in Monte-Carlo is the following:

Given the probability density function (pdf) for some variable; one wishes to set up a procedure for obtaining a statistically correct sampling of this variable by the aid of a random number $r(0 < r < 1)$.

Such a procedure must of course reproduce the original pdf; for a very large number of samples, the values obtained of the variable in question must be distributed in close accordance with the pdf.

As an example, consider the selection of deflection angle θ, or rather the cosine μ of such an angle, for a certain scattering event when the angular distribution is given (fig. 4.1) in terms of a pdf in μ, denoted $f(\mu)$. The first step is to normalize $f(\mu)$ so that

$$\int_{-1}^{1} f(\mu)\, d\mu = 1. \qquad (4.8)$$

Next, one constructs the distribution function

$$F(\mu) = \int_{-1}^{\mu} f(\mu')\, d\mu' \qquad (4.9)$$

with the properties $F(-1) = 0$, $F(1) = 1$.

Finally, one inverts the function $r = F(\mu)$. The inverted function is denoted

$$\mu = \psi(r), \quad 0 < r < 1. \qquad (4.10)$$

It is now shown that (4.10) is the statistically correct sampling rule for μ when r is identified as a random number:

If a large number, N, of μ-values are sampled by means of N random numbers, the number of r-values between r and $r + dr$ is $dN \approx N\, dr$, while the μ-values obtained lie between μ and $\mu + d\mu$ with $\mu = \psi(r)$. The density of μ-samples at μ is

$$\frac{dN}{d\mu} = \frac{N\, dr}{d\mu} = N \cdot F'(\mu) = N \cdot f(\mu) \qquad (4.11)$$

so that $\frac{dN}{N} = f(\mu)\, d\mu$ q. e. d.

The formula (4.10) constitutes the fundamental sampling principle in Monte-Carlo. The above treatment refers to a continuous pdf; however, the discrete case is handled in quite a similar manner.

4.5. Standard Routines in Problems of Nuclear Particle Transport

A Monte-Carlo programme is constructed by linking together a number of subroutines, each corresponding to a certain stage of the calculation. The programme is advantageously described in terms of a flow diagram. The subroutines in such a diagram appear as single "boxes" or as blocks of boxes. A number of the subroutines are common for a great variety of problems.

The subroutines depend on the choice of the set of parameters used to determine the history of the particle followed. These parameters include the particle energy E together with geometrical co-ordinates.

The geometrical co-ordinates are the momentary co-ordinates of the position and the direction vector of the particle. As a rule, rectangular co-ordinates are preferable, even in cases with cylindrical symmetry. Only

for spherically symmetrical problems should other co-ordinates be used. In cartesian space, the momentary state of the particle is characterized by the seven-dimensional vector (E, x, y, z, u, v, w). The direction cosines u, v, w satisfy the relation $u^2 + v^2 + w^2 = 1$.

We now proceed to a description of the most common subroutines. They are described more thoroughly in ref. 6.

Isotropic source

The problem is to select the direction cosines u, v, w for a starting source particle with isotropic distribution. It is tantamount to choosing a point (u, v, w) uniformly distributed on the unit sphere $u^2 + v^2 + w^2 = 1$. This is done by selecting first the cosine w uniformly in $-1 < w < 1$. The corresponding formula is

$$w = 2r - 1 \; ; \tag{4.12}$$

here and in the following, r denotes a random number ($0 < r < 1$). Then a new random number is used to select an angle φ from a uniform distribution in $-\pi < \varphi < \pi$:

$$\varphi = \pi \cdot (2r - 1) . \tag{4.13}$$

Finally, u and v are calculated as

$$\left.\begin{aligned} u &= \sqrt{1 - w^2} \cos \varphi \\ v &= \sqrt{1 - w^2} \sin \varphi \end{aligned}\right\} \tag{4.14}$$

Sampling of particle flight distances

Consider an infinite homogeneous medium with a total macroscopic cross section Σ for the particle in question, say a photon of energy E. The problem is to select the free flight distance of the photon.

According to the fundamental sampling principle, we construct the probability density function (pdf) for flight distances l; it is

$$p(l) = \Sigma \cdot \exp(-\Sigma l) . \tag{4.15}$$

The distribution function is

$$r = F(l) = \int_0^l p(l')dl' = 1 - \exp(-\Sigma l) . \tag{4.16}$$

By solving with respect to l one obtains

$$l = - \frac{1}{\Sigma} \ln(1 - r) . \tag{4.17}$$

The random number r may be replaced by 1 - r. The final sampling formula is simply

$$l = - \ln r / \Sigma. \tag{4.18}$$

Decision of escape from a zone

An actual Monte-Carlo problem normally involves several zones separated by boundaries, and hence one needs a routine which decides whether such a boundary is crossed or not during the particle flight. The routine is easily established once the distance L along the flight to the boundary is calculated; one simply compares L with the sampled track length l.

The calculation of L is normally carried out by solving the flight equations $(x', y', z') = (x, y, z) + t(u, v, w)$ together with the equation for the boundary, $\varphi (x', y', z') = 0$. Since (u, v, w) is a unit vector, the resulting t-value is simply L. This shows one of the advantages of the cartesian co-ordinate set (x, y, z, u, v, w) even in cases where the boundary is, e.g., cylindrical.

If escape from one zone to another occurs, one "forgets" the previous piece of flight and samples a new flight distance from (4.18), starting from the boundary, but of course with unchanged (u, v, w). That this procedure is statistically correct, follows both from the pdf, eq. (4.15), and from physical considerations.

Selecting of nucleus type for collision

This problem arises when a mixture of different nuclei is present. One then writes the total macroscopic cross section for the mixture as a sum of components corresponding to each type of nucleus:

$$\Sigma = \Sigma_1 + \ldots + \Sigma_i + \ldots + \Sigma_n . \tag{4.19}$$

Sampling of the type i, from these cross sections and the random number r, is an example of the discrete analogy of the general sampling problem for continuous variables (see 4.4).

One first normalizes all the cross sections by division by Σ:

$$1 = \Sigma_1^{\mathcal{H}} + \ldots + \Sigma_i^{\mathcal{H}} + \ldots + \Sigma_n^{\mathcal{H}} . \qquad (4.20)$$

Then a table $s_o, s_1 \ldots, s_n$ is constructed so that

$$s_o = 0, \quad s_1 = \Sigma_1^{\mathcal{H}}, \; s_2 = s_1 + \Sigma_2^{\mathcal{H}}, \ldots, \quad s_n = 1 . \qquad (4.21)$$

Finally, the type i is determined as that i-value which satisfies the inequality

$$s_{i-1} < r < s_i . \qquad (4.22)$$

Selecting of type of collision

Having determined the type i of nucleus in the collision (if several nuclei are present), one may wish to select the type of collision event (absorption, elastic scattering, inelastic scattering, fission, etc.). This procedure is exactly similar to the one discussed above.

Deflection angle in scattering

The sampling technique here depends on the physical problem; it will be discussed in the following sections.

Direction parameters after the collision

Given the incident cosines of direction, u, v, w, and the scattering angle ψ (in the laboratory system) with cosine a. One wishes to set up a routine to determine the direction cosines of the deflected line of flight, u', v', w'. We omit the derivation (given in ref. 6) and present the result:

$$\left.\begin{aligned} u' &= (bcwu - bdw)/\sqrt{1 - w^2} + au \\ v' &= (bcwu + bdu)/\sqrt{1 - w^2} + av \\ w' &= -bc\sqrt{1 - w^2} + aw . \end{aligned}\right\} \qquad (4.23)$$

Here, $b = \sqrt{1 - a^2}$, $c = \cos\delta$, $\delta = (2r - 1)\pi$, $d = (\operatorname{sgn}\delta)\sqrt{1-c^2}$. It is clear that ψ alone does not suffice to determine u', v', w'; therefore, also the azimuthal scattering angle δ must be fixed.

Other subroutines

In the final flow diagram of the Monte-Carlo calculation some registration subroutines will appear.

A starting routine which counts the number of particles fed into the

system must be present. This routine stops the calculation when the number of particle histories has reached the prescribed figure.

In order to "kill" a particle which in some sense has become sufficiently unimportant, one must have one or more cut-off routines.

Further, some scoring routines must be present to account for changes in the desired physical quantity (transmission, energy deposition, etc.) during the Monte-Carlo calculation.

4.6. Variance-Reducing Devices

As mentioned in 4.1, the result of a Monte-Carlo calculation has a certain sampling variance

$$V = \sigma^2 , \tag{4.24}$$

where σ is the standard deviation.

V is inversely proportional to the total number of samples, i.e. roughly to the computing time t:

$$\left.\begin{aligned} V &= k^2 \cdot \frac{1}{t} \\ \sigma &= k \cdot \frac{1}{\sqrt{t}} \quad . \end{aligned}\right\} \tag{4.25}$$

Sometimes the variance V in an actual calculation is larger than can be tolerated. An obvious way of decreasing the variance is to increase the computing time. However, eq. (4.25) indicates a rather low rate of convergence, and a sufficient reduction of V frequently requires unacceptably long computing times.

This calamity may often be cured by altering some of the subroutines in the calculations. The modifications are carried out by introducing so-called variance-reducing devices. A great variety of such devices have been developed, and some of them are discussed in the following.

For the sake of simplicity, most of the discussion until now of the various subroutines has referred to the "direct simulation" method, where each elementary event is treated by a statistical game (call of a random number) in close accordance with the real physical situation. As already pointed out in subsection 4.1, direct simulation is not sufficiently effective for complicated problems. If instead one replaces part of the entirely statistical calculation by analytical calculations, the resulting answer will show reduced variance, but an unchanged mean value. In principle, there is no limitation of this procedure: if one replaces all the statistical calcula-

tions by analytical calculations, one obtains a "conventional" calculation, and the variance is zero. However, Monte-Carlo is applied in just the problems in which analytical solutions are impossible or not feasible. Hence, in each Monte-Carlo problem an optimum exists for the relative amounts of "random walk" and analytical calculations.

We now proceed to describe various devices for reduction of the variance. Most of them have been applied in the work described in this report.

The weight concept

Utilization of most of the variance-reducing devices presupposes the weight concept.

As a simple and illustrative example, consider a collision between a neutron and a nucleus; the total cross section is the sum of an absorption and a scattering cross section: $\Sigma_t = \Sigma_a + \Sigma_s$. As described earlier, the process type can be decided by a random number. Alternatively, one could introduce a weight parameter W, ascribed to the neutron. Assuming W = 1 before the collision, one now makes the assumption that the fraction Σ_a/Σ_t of the neutron is absorbed, and the fraction Σ_s/Σ_t is scattered; this scattered part is then treated as a neutron with the reduced weight $W = \Sigma_s/\Sigma_t$. Fluctuations due to sampling of collision type are thus eliminated.

The use of the weight concept normally requires a cut -off value W_o for the weight W. As the particle is killed if W drops below W_o, the computer time spent on an unimportant particle (i. e. one of low weight) will be saved.

Weight parameters may be assigned to a particle already at its birth at the source. This facilitates the reproduction of a fission spectrum.

Importance sampling

This device consists in sampling from another pdf, $f_1(x)$, than the correct one, f(x). Having sampled the quantity x, one has to multiply the weight of the particle by $f(x)/f_1(x)$, correcting the distortion of the pdf. As one has the liberty of choosing $f_1(x)$ arbitrarily, it is possible to "emphasize" a certain range of x-values, which explains the term "importance sampling".

An example in which this device is advantageous is the calculation of a detector response to a source far away. The angular distribution of the source particles is here transformed in order to emphasize directions towards the detector.

Another example is found in 7.3.2, where track lengths are sampled from the scattering cross section instead of from the total cross section.

Splitting

This technique consists in splitting a single particle with the weight W into n identical particles, each with the weight W/n. These n particles are then treated as individual particles. For instance, one can choose n = 2 and let the two split particles have opposite directions. Such a procedure has been applied successfully to criticality calculations[5].

A technique related to splitting has been applied in the solution of the problem in subsection 5.2 of this report.

Russian Roulette

"Russian Roulette" is a statistical game played in order to kill unimportant particles. This game gives the particle a certain surviving probability p, but compensates by multiplying the weight of a surviving particle by $\frac{1}{p}$. This technique is applied in 6.4.

Stratified sampling

Stratified sampling is a device which is normally restricted to source routines. As an example, consider the emission of neutrons from a surface. Instead of the source points being sampled at random, the surface is divided into a number of "strata", nos. 1, 2, ..., n. One starts by selecting a source neutron in a point of region no. 1; after the history of this neutron has terminated, the next neutron is selected in region no. 2, and so on, until region no. n, whereafter the cycle is repeated. Weights may be assigned to each of the regions.

This device has a limited variance-reducing power, but is easy to establish, and the use of it is therefore rather extended.

Stratified sampling is also possible for selecting of energies of source particles.

The exponential transformation

When trying to solve deep-penetration problems by straightforward Monte-Carlo, one often has to emit a prohibitively large number of source particles to get a reasonable response far from the source. This trouble may be overcome by transforming the Bolzmann transport equation by the so-called exponential transformation. The random walk procedure is then adjusted to the transformed equation. This method is applied for the solu-

tion of the Y-shielding problem described in section 6.

The semi-analytic method

Sometimes it is possible to treat one or more particle parameters by completely analytic means so that sampling variations are restricted to the remaining parameters. Such a procedure is described in ref. 5 for the solution of a Y-shielding problem in slab geometry. It is here the collision abscissae z that have been "separated" from the other variables and treated analytically, so that the random sampling is restricted to energies and deflection angles. The efficiency gain by this method is claimed to be very large (2500).

Statistical estimates

This device concerns the scoring routines.

When the direct simulation method is used, the situation frequently arises that the scoring events for some physical quantity to be calculated occur too seldom.

A good example of this is the calculation of the neutron current distribution on a black rod, which problem is treated in section 7. Here, all collisions outside the rod will be "dummies" in the direct simulation. Only when a neutron hits the rod does scoring take place. The scoring routine was therefore modified to permit a statistical estimate of the current in every collision; this is done by letting the neutron lose part of its weight, the loss being equivalent to the probability of hitting the rod after collision. This "spray technique" is described in 7.3.

Another example is the flux scoring routine for grey rods, described in 7.3. This example is the same as that mentioned in connection with importance sampling. The point is here that for each track in a zone of the rod one makes a statistical estimate of the flux increment in that zone instead of waiting until a collision takes place in the zone.

5. SOME MINOR PROBLEMS SOLVED BY THE MONTE-CARLO METHOD

This section describes the solution of some minor problems by Monte-Carlo. The problems are so simple that crude Monte-Carlo (direct simulation) works satisfactorily.

5.1. Self-Absorption of Y-Rays in Fuel Rods

A GIER programme (MC3) has been written which finds the fraction of Y-energy escaping from an infinite, cylindrical rod containing Y-sources.

The rod is assumed homogeneous and surrounded by vacuum, i.e. backscattering is neglected. This is often a good approximation. The Y-source is assumed to be a function of the radial co-ordinate r. The dependence of r must be given as an arbitrary step function. The source spectrum is assumed to be the Y-spectrum from fission, but other spectra, e.g. single lines, may be handled by a slight modification of the library tape of the programme. This library tape contains the Y cross sections of the five elements H, C, O, Al, U.

The photon collisions are assumed to result in only two types of process: Compton scattering and absorption. That is, the annihilation radiation from pair production is assumed to be entirely absorbed by the rod. The error hereby introduced is normally of minor importance.

Fig. 5.1 shows the flow diagram, which should make the calculation procedure sufficiently clear.

An energy group structure identical with the GAM-I structure[2] was used. All groups have the same lethargy width, 0.25. The upper limit is 10 MeV. Group g covers the interval

$$10\,\exp\left(-\frac{g}{4}\right) < E < 10\,\exp\left(\frac{1-g}{4}\right), \qquad E \text{ in MeV.} \tag{5.1}$$

A cut-off energy of nearly 0.01 MeV was chosen.

In the calculation, all energy values are transformed from MeV to "normalized units" (1 n.u. = 0.51083 MeV). This simplifies the treatment of Compton scattering considerably.

Some of the elements of the flow diagram are discussed in the following.

The microscopic total Y cross sections were prepared from data in ref. 7 by double logarithmic interpolation. Compton cross sections were evaluated by means of the expression (ref. 8, p. 147).

$$\sigma(E) = 0.499\left[\frac{1+E}{(1+2E)^2} + \frac{2}{E^2} + \frac{E^2-2E-2}{2E^3}\ln(1+2E)\right] \text{ barn/electron} \quad (E \text{ in n.u.}) \tag{5.2}$$

The shape of the source spectrum was chosen as

$$N(E) = \text{const} \cdot e^{-1.1E} \tag{5.3}$$

(E in MeV).

This expression fits rather well the sum spectrum of γ-rays from fission and from decay of fission products[8]. The value of the constant is not relevant for our purpose.

Source energies were selected by stratified sampling (see 4.6).

Sampling of the start position was not mentioned in the last section and will therefore be briefly described here. One applies the fundamental sampling principle to the given source distribution to set up a procedure giving the radius ρ of the starting photon, see fig. 5.2 (the thermal fluxes $\Phi_1, \Phi_2, \ldots, \Phi_m$ are proportional to the zone sources). As a result, the following procedure is set up for determining ρ : A set of numbers, $r_0, r_1, \ldots, r_m$, are constructed so that

$$\begin{aligned} r_o &= \rho_o = 0 \\ r_i &= r_{i-1} + a\,\Phi_i(\rho_i^2 - \rho_{i-1}^2), \qquad 1 \leqslant i \leqslant m \\ \text{where } \frac{1}{a} &= \sum_{i=1}^{m} \Phi_i(\rho_i^2 - \rho_{i-1}^2), \quad \text{yielding } r_m = 1 \end{aligned} \tag{5.4}$$

After calling for a random number r, one selects the zone i by finding the i-value which satisfies the inequality

$$r_{i-1} < r < r_i \,. \tag{5.5}$$

The exact position ρ inside zone i is determined by

$$\rho = \rho(r) = \sqrt{\frac{r - r_{i-1} + a\,\Phi_i\,\rho_{i-1}^2}{a\,\Phi_i}} \tag{5.6}$$

The remaining elements of the diagram fig. 5.1 have been discussed in the last section except the sampling of the deflection angle θ ($a = \cos\theta$) and the energy degradation E - E' by a Compton scattering. It follows from Compton's formula

$$a = 1 + \frac{1}{E} - \frac{1}{E'} \tag{5.7}$$

where E and E' are in n.u., that one need sample only one of the quantities a and E'. The procedure applied here is due to Bengt Carlson[6]. On the basis of the Klein-Nishina formula for the differential scattering cross section

$$\sigma(E,a) = 0.0397 \frac{1+a^2}{(1+E(1-a))^2} \left[1 + \frac{E^2(1-a)^2}{(1+a^2)(1+E(1-a))}\right] \text{ barn/elec./ster.} \tag{5.8}$$

Carlson has constructed an approximate sampling scheme for E'. His formula reads

$$E' = \frac{E}{1 + s \cdot r + (2E - s) \cdot r^3} , \tag{5.9}$$

where $s = \frac{E}{1 + 0.5625\,E}$ and r is a random number.

(5.9) is used only up to E = 4 n.u. For E > 4, E' is increased by the quantity

$$\Delta E' = \frac{1}{2}(E - 4)(r - r^2)^2 . \tag{5.10}$$

Carlson's approximate device is surprisingly simple in view of the complexity of formula (5.8). It has been analysed for photons up to 10 MeV (E = 20) and has been found to reproduce the distribution (5.8) very well[9].

The running time for MC3 is about 3 min. on GIER. The programme is well suited for calculation of Y-energy escape from fuel rods of either uranium, uranium oxide or uranium carbide.

5.2. Energy Deposition on the Components of a Fuel Lattice Cell, for Y-Rays

The problem to be solved in this subsection concerns the distribution of the Y-energy deposited on the different atoms in a lattice cell which is assumed to be infinitely long and part of an infinite square lattice in a critical reactor. Only the primary energy exchange at the atoms due to the photon collisions will be calculated.

The solution of this problem is useful as the starting point for calculation of the energy deposition on the various components of a reactor.

The corresponding GIER-ALGOL programme has the name MC1. In order to have a fairly simple calculation model one devides the square cell into two homogenized zones: a cylindrical fuel zone (1) and a surrounding moderator zone (2) (fig. 5.3).

The calculation results are given for each of the zones as the deposited Y-energy in MeV per type of atom per thermal fission.

Permissible isotopes are for zone 1 H, D, C, O, Al, Fe, Zr, U-235,

U-238, and for zone 2 H, D, O.

In this problem the sources of Y-radiation will be restricted to the fuel zone. The radiation is naturally divided into four contributions according to origin:

(a) Prompt Y-radiation due to fission

(b) Y-radiation due to decay of fission products

(c) Y-radiation due to neutron capture (resonance and thermal)

(d) Y-radiation due to inelastic scattering.

The total liberated prompt Y-radiation energy per fission is 7.2 ± 0.8 MeV[8] with the spectrum given in eq. (5.3). The corresponding value for the Y-radiation from fission products is 5.5 MeV/fission[8], and the spectrum should be nearly the same. Hence the contributions (a) and (b) may be treated as originating from a single source with the spectrum (5.3) and the total energy 12.7 MeV liberated per fission.

In calculating the contribution from resonance capture, only U-238 is taken into account as an absorber. Neglecting the neutron leakage and fast fission effect, approximately $\nu = 2.5$ neutrons will enter the resonance region per thermal fission. Of these, $\nu(1-p)$ will be captured by resonance absorption in U-238, while νp become thermal (p = resonance escape probability). One thermal neutron causes fission in U-235; the remaining $\nu p - 1$ are absorbed by H, Al, Fe, Zr, U-235, U-238, in accordance with the respective thermal capture cross sections (flux depression neglected). On the basis of these cross sections and the corresponding Y-spectra[10, 11, 12], both the magnitude and the spectral shape of the Y-radiation may be obtained. In most cases, the contributions (c) will amount to about 6 MeV/fission.

The Y-ray contributions from inelastic scattering (type (d)) were left out of consideration. This was decided after a test calculation with a special version of MC2 (the neutron analogy to MC1, which will be described in the next subsection).

The spatial distribution of the sources in zone 1 is given as annular regions with constant source strengths, just as for MC3 (see 5.1). The distribution follows that of the thermal neutrons.

In the Monte-Carlo calculation, the cell periodicity is taken into account simply by mirroring the paths of those photons which would otherwise have escaped from the cell, in the plane cell boundaries (by reversing one direction cosine).

The same assumptions for photon collisions are made here as in 5.1 for the MC3-problem.

The Monte-Carlo calculation is mapped in the flow diagram fig. 5.4. The energy group structure is the same as that in MC3. The library tape of the programme contains Y cross sections in all groups, cross sections and spectra for radiative neutron capture, and data of the Y-spectrum from fission.

The Monte-Carlo technique applied in this problem is mainly direct simulation, and the standard routines have been discussed previously. However, at one point a deviation from direct simulation occurs: the collisions of photons with atoms are treated as described in 4.6 in the description of the weight concept, so that one avoids the decision of absorption or scattering and instead always gets a scattered photon with the weight reduced by the factor $\Sigma_s/(\Sigma_s + \Sigma_a)$. Furthermore, since the Compton scattering depends essentially on the electrons only, not on the nuclei, the colliding photon may be split into m photons (m = number of different atom types in the zone), each carrying a weight W_i proportional to the concentration of electrons belonging to the atom type i. The partial photon i is assumed to collide with an atom of type i and to exchange energy with it. The variance-reducing power of this device as compared with that of sampling of the target atom appeared to be vary great, especially for the less abundant elements.

As an example of the use of MC1, a calculation for a DOR-type cell was carried out. Here the moderator is D_2O; the fuel zone is limited by a zirconium tube encircling a bunch of UO_2-rods surrounded by the organic coolant $C_{18}H_{14}$. In addition, some structural graphite is present in the fuel zone. One wants to know the energy deposited in the coolant and that deposited in the moderator. The calculation procedure is now to homogenize zone 1, calculate the atomic concentrations, and use the programme. The output in the DOR example was (MeV/thermal fission)

	H	D	C	O	Al	Zr	U
fuel zone	0.52		0.42	0.76	0.12	0.69	11.5
moderator zone		0.89		3.7			

For the moderator one simply adds the two contributions to obtain the result 4.6 MeV/thermal fission.

As regards the coolant in zone 1, the situation is a little more involved. One has to correct the C-value (0.42 MeV) for the structural graphite. The ratio of coolant-graphite to the total amount of graphite is

in our example 0.90. Then the γ-energy deposited in the coolant is 0.52 + 0.42 · 0.90 = 0.90 MeV/thermal fission.

For a problem like the present the effect of homogenizing the fuel zone is not believed to introduce any great error because the coolant is well distributed over the fuel zone. Incidentally, the energy deposition calculated for Zr is too high because the Zr-tube is situated in a field of lower gamma flux than the average flux in zone 1.

In the example, the total γ-energy per fission is calculated to be 18.6 MeV, i.e. 13.5 MeV is absorbed by the fuel rods and various structural materials.

The running time on GIER is about 20 minutes.

5.3. Energy Deposition on the Components of a Fuel Lattice Cell, for Neutrons

The physical problem to be solved in this subsection is the same as that described in 5.2, except that neutron energy deposition instead of γ-energy deposition is calculated. As the problem structure is the same as for the γ-problem, no flow diagram is given. The GIER-ALGOL programme MC2 has been worked out for routine calculations.

The source of fast neutrons originates from fission. The value 1.98 MeV is used for the mean energy carried by a fission neutron[10]. If one assumes $\nu = 2.5$, this means a total neutron energy release of 5.0 MeV per (thermal) fission. The fission spectrum used in these calculations is that proposed by Cranberg[10]:

$$N(E) = \text{const.} \cdot \exp\left(-\frac{E}{0.965}\right) \cdot \sinh\sqrt{2.29E} \quad (E \text{ in MeV}). \qquad (5.11)$$

MC2 deals with the same spatial source distribution as MC1; the cell periodicity is taken into account by the same mirroring process as in MC1.

For the fast neutrons in our problem, the following four reaction types have sufficient importance to be taken into account:

(1) elastic scattering
(2) inelastic scattering
(3) fast fission
(4) absorption.

The last two reactions, however, play a rather limited role.

Different collision routines had to be prepared for the different target nucleus types. This is in contrast to the corresponding gamma

problem, and it complicates the Monte-Carlo calculation very much. A number of simplifying assumptions were made for the collisions in order to limit the complexity of the programme structure.

Elastic scattering is assumed to proceed isotropically in the CM-system. This is quite a good approximation when the neutron energy is below 0.1 MeV. Above this energy an increasing anisotropy occurs. In deep-penetration problems (e.g. shielding problems) serious errors may result from the isotropic assumption. However, our problem involves rather short optical distances and no preferred directions, so the error is expected to be of minor importance.

Inelastic scattering is normally accepted to proceed isotropically in the CM-system. Here it is assumed isotropic even in the L-system. The error thus introduced is tolerable because inelastic scattering is a rather infrequent process. The accompanying γ-rays are neglected (cf. 5.2), which makes the two programmes MC1 and MC2 independent of each other.

Fast fission in U-235 and U-238 leads to ejection of about three fast neutrons[2]. In the present calculation it is assumed that the neutrons causing fast fission continue with triple weight and unchanged energy. This approximation gives a rather good picture of the situation.

The energy group structure in MC2 is the same 27-group structure as in MC1 and MC3 (the GAM-I structure). All neutron cross sections used in the library tape of MC2 have been taken from ref. 2.

In the Monte-Carlo calculation only the collision routines are different in MC1 and MC2. In the following, the Monte-Carlo treatment of the two main reaction types, elastic and inelastic scattering, will be given.

Elastic scattering is treated according to the previously mentioned isotropic assumption. For hydrogen, especially simple formulas are valid. If E is the energy before, E' the energy after the H-collision, and r a random number, one has

$$E' = E \cdot r \,. \tag{5.12}$$

The deflection cosine a in the L-system is

$$a = \sqrt{r} \tag{5.13}$$

with the same r as before.

For the other nuclei, the relevant set of formulas is

$$\mu = 2 \cdot r - 1 \tag{5.14}$$

$$E' = \frac{E}{(A+1)^2}(A^2 + 1 + 2A\mu) \tag{5.15}$$

$$a = \frac{1 + A\mu}{\sqrt{1 + A^2 + 2A\mu}} ; \tag{5.16}$$

u is the deflection cosine in the CM-system, A the mass number of the target nucleus. Other symbols are as before.

As mentioned above, inelastic scattering is assumed isotropic in the L-system. The only problem is then the sampling of the energy after scattering. This is done by the aid of the so-called inelastic scattering matrix, giving cross sections $\sigma_{g\to h}$ for scattering from group g to group h. Such matrices are listed in ref. 2. The sampling itself proceeds in analogy with the "type sampling", eqs. (4.19) to (4.22).

As a calculation example for MC2 is taken the same DOR cell as in 5.2 for MC1. The results in MeV/thermal fission were

	H	D	C	O	Al	Zr	U-235	U-238
Fuel zone	2.630		0.072	0.091	0.016	0.040	0.000	0.010
Moderator zone		1.850		0.227				

In the same manner as in 5.3 one obtains:

Neutron energy deposited in coolant = 2.630+ 0.072 · 0.90 =

2.69 MeV/thermal fission

Neutron energy deposited in moderator = 2.08 MeV/thermal fission .

The running time for MC2 is in most cases 1-2 hours.

6. A MONTE-CARLO BULK SHIELD PROGRAMME FOR Y-RAYS

As pointed out in section 2, the application of build-up methods (such as PRIGAM, SEGAM I, SEGAM II) in shielding calculations is rather doubtful when the shield or part of it consists of laminae of widely different materials. This is the case with thermal shields with alternating layers of water and iron or water and lead. Analytic methods for Y-transport calculation, such as Laplace transform, the method of successive scattering and the method of moments, are not feasible for heterogeneous geometry

either[8]. It seems that Monte-Carlo, owing to its great versatility, is the best alternative method.

6.1. Description of the Problem

A computer programme, MC4, has been worked out which carries out a Monte-Carlo calculation of the heat generation rate throughout a laminated shield and the external dose rate due to a distributed Y-source. MC4 exists in GIER-ALGOL as well as in FORTRAN IV for the IBM 7090.

The shield configuration consists of a number of infinite slabs (fig. 6.1). The slab system is at both sides adjacent to vacuum. The chosen orientation of the z-axis depends on the natural penetration direction in the problem, which also determines the surface where the dose rate will be calculated (the "external surface").

Each layer is homogeneous and may be composed of a number of elements. The programme is not able to handle all the elements; the permissible elements are listed in table 6.1.

The Y-source has the form

$$S(E, z) = S_0 \exp(-k(z-z_1)) \cdot \delta\,(E-E_0)\text{phot.}/(\text{cm}^3 \cdot \text{sec} \cdot \text{MeV}), \qquad (6.1)$$

$$z_1 \leqslant z \leqslant z_2$$

i.e. a single-line source with exponential spatial variation (fig. 6.1).

The core and reflector regions may be included in the calculations as part of the shield.

By repeated application of MC4 it is possible to solve any problem which can be solved by PRIGAM, SEGAM I and SEGAM II.

As was the case in the problems treated in section 5, the photon collisions are assumed to result in either Compton scattering or absorption, that is, the annihilation radiation from pair production is assumed to be entirely absorbed at the photon collision point. The error hereby introduced is normally of minor importance.

6.2. Application of the Exponential Transformation

As mentioned in 4.6, an efficient device for deep-penetration problems is to modify the Bolzmann transport equation by an exponential transformation and adjust the random walk procedure to the transformed equation. As this method is described in detail in refs. 13 and 14, only a rather short outline will be given here.

The one-dimensional transport equation in plane geometry is

$$\omega \frac{\delta \Phi(E,\omega,z)}{\delta z} + \Sigma(E,z)\Phi(E,\omega,z) = \int \Sigma(E',z)\,\Phi(E',\omega',z) \cdot$$

$$\cdot\, C(E',\omega';\, E,\omega,z)\,dE'd\omega' + S(E,\omega,z) \qquad (6.2)$$

in conventional notation. We introduce the substitutions

$$\Phi(E,\omega,z) = \Phi^{*}(E,\omega,z)\exp(-cz) \qquad (6.3)$$

$$\Sigma^{*}(E,\omega,z) = \Sigma(E,z) - \omega c \qquad (6.4)$$

$$C^{*}(E',\omega';\, E,\omega,z) = \frac{\Sigma(E',z)}{\Sigma^{*}(E',\omega',z)}\, C(E',\omega';\, E,\omega,z) \qquad (6.5)$$

$$S^{*}(E,\omega,z) = \exp(cz)\cdot S(E,\omega,z) \qquad (6.6)$$

and obtain a new transport equation, formally identical with eq. (6.2)

$$\omega \frac{\delta \Phi^{*}(E,\omega,z)}{\delta z} + \Sigma^{*}(E,\omega,z)\,\Phi^{*}(E,\omega,z) = \int \Sigma^{*}(E',\omega',z)\Phi^{*}(E',\omega',z)\cdot$$

$$\cdot\, C^{*}(E',\omega';\, E,\omega,z)\,d\omega'dE' + S^{*}(E,\omega,z)\,. \qquad (6.7)$$

Note that Σ^{*} has an angular dependence through eq. (6.4). The constant c compensates for the normally steep source and flux variation. For fixed (E,ω) the Σ^{*} in (6.7) takes on constant values Σ_i^{*} in each region (i refers to region i).

The random walk method can now be used to solve the transformed problem, i.e. to find the γ-flux Φ^{*} in a medium with the cross section Σ^{*} and the collision kernel C^{*}. This procedure will be described in the following.

The first step is sampling of the starting position z of a new (source) photon. This is done according to the z-variation of S^{*} (eqs. (6.1) and (6.6)):

$$S^{*}(z) = \text{const}\cdot\exp(-(k-c)z),\quad z_1 \leqslant z \leqslant z_2\,. \qquad (6.8)$$

The source directions are isotropically distributed, and the source photons start with the weight W = 1.

Sampling of flight length is the same for a new photon as for a photon after collision. We therefore discuss the probability density function (pdf) for intercollision distances x. This is the major problem in applying the

exponential transformation. The sampling method described in the following is due to M. Leimdörfer[14].

Referring to fig. 6.1, the photon starts at P_s (collision or source point) in the direction ω in the region s. According to (6.2) the track length in this region should have been sampled from the pdf

$$f_s(x) = \Sigma_s \exp(-\Sigma_s x) \ , \tag{6.9}$$

where the subscript s refers to the region number.

As Σ is replaced by Σ^* when the exponential transformation is applied, (6.9) will be replaced by

$$f_s^*(x) = \Sigma_s^* \exp(-\Sigma_s^* x) \tag{6.10}$$

with $\Sigma_s^* = \Sigma_s - \omega c$.

One could then sample an x from (6.10) and decide whether the region boundary is crossed. If so, a track length in the next region (i in fig. 6.1) with the intersection point P_i as a new starting point could be sampled from the pdf

$$f_i^*(x) = \Sigma_i^* \exp(-\Sigma_i^* x) \tag{6.11}$$

valid for region i. Repeating this procedure, one reaches a terminal point B, or the photon escapes at E.

The transformed equation (6.7) has another collision kernel than the original equation (6.2). This difference must be compensated for at the new collision point B by multiplying the photon weight by

$$\gamma = C^*/C = \Sigma_n/\Sigma_n^* \ . \tag{6.12}$$

The above sampling method for flight distances is simple, but it suffers from a couple of drawbacks:

(a) $\Sigma^* = \Sigma - \omega c$ may happen to be < 0. In this case (6.10), (6.11) and (6.12) become meaningless.

(b) The photons may travel through the whole configuration and escape uncollided. This means waste of computing time.

In order to cure both the calamities (a) and (b), Leimdörfer[14] followed a somewhat changed procedure, which is applied also in the present work:

The pdf in the starting region, eq. (6.10), is replaced by

$$f_s^{**}(x) = \frac{\Sigma_s^*}{1-\exp(-\Sigma_s^* X_s)} \exp(-\Sigma_s^* x), \qquad 0 \leq x \leq X_s \ , \tag{6.13}$$

where X_s is $> x_s$, but otherwise, so far, arbitrary.

By means of eq. (6.13) a flight distance in region s is sampled. In the case shown in fig. 6.1 the region boundary is reached. The probability of this, according to eq. (6.13), is

$$p_s^{**} = 1 - \int_0^{x_s} f_s^{**}(x)dx = \exp(-\Sigma_s^* x_s) \frac{1-\exp(-\Sigma_s^*(X_s-x_s))}{1-\exp(-\Sigma_s^* X_s)} \ . \tag{6.14}$$

According to (6.10) the correct probability of reaching the boundary of region s was (in the transformed problem)

$$p_s^* = 1 - \int_0^{x_s} f_s^*(x)dx = \exp(-\Sigma_s^* x_s) \ . \tag{6.15}$$

Therefore, at the intersection point P_i the weight must be multiplied by

$$\beta_s = \frac{p_s^*}{p_s^{**}} = \frac{1-\exp(-\Sigma_s^* X_s)}{1-\exp(-\Sigma_s^*(X_s-x_s))} \ . \tag{6.16}$$

One then considers P_i as the starting point for further track length sampling. The sampling in an arbitrary intermediate region (no. i, fig. 6.1) proceeds just as above, and equations quite analogous to (6.13) - (6.16) are obtained by replacing index s by i:

$$\text{pdf: } f_i^{**}(x) = \frac{\Sigma_i^*}{1-\exp(-\Sigma_i^* X_i)} \exp(-\Sigma_i^* x), \qquad 0 \leq x \leq X_i \ . \tag{6.17}$$
$$(X_i > x_i)$$

Transmission probability from (6.17):

$$p_i^{**} = 1 - \int_0^{x_i} f_i^{**}(x)dx = \exp(-\Sigma_i^* x_i) \frac{1-\exp(-\Sigma_i^*(X_i-x_i))}{1-\exp(-\Sigma_i^* X_i)} \ . \tag{6.18}$$

Correct transmission probability from (6.11):

$$p_i^{\ast} = 1 - \int_0^{x_i} f_i^{\ast}(x)dx = \exp(-\Sigma_i^{\ast} x_i) \quad . \tag{6.19}$$

Weight multiplier:

$$\beta_i = \frac{p_i^{\ast}}{p_i^{\ast\ast}} = \frac{1-\exp(-\Sigma_i^{\ast} X_i)}{1-\exp(-\Sigma_i^{\ast}(X_i-x_i))} \quad . \tag{6.20}$$

In the terminal region (n) one obtains:

$$\text{pdf: } f_n^{\ast\ast}(x) = \frac{\Sigma_n^{\ast}}{1-\exp(-\Sigma_n^{\ast} X_n)} \exp(-\Sigma_n^{\ast} x), \quad 0 \leqslant x \leqslant X_n \quad . \tag{6.21}$$
$$(X_n > x_n)$$

Probability of collision at B per unit length, from (6.21):

$$q_n^{\ast\ast} = f_n^{\ast\ast}(x_n) = \frac{\Sigma_n^{\ast}}{1-\exp(-\Sigma_n^{\ast} X_n)} \exp(-\Sigma_n^{\ast} x_n) \quad . \tag{6.22}$$

Correct probability of collision at B per unit length, from (6.11):

$$q_n^{\ast} = f_n^{\ast}(x_n) = \Sigma_n^{\ast} \exp(-\Sigma_n^{\ast} x_n) \, . \tag{6.23}$$

Weight multiplier:

$$\beta_n = \frac{q_n^{\ast}}{q_n^{\ast\ast}} = 1-\exp(-\Sigma_n^{\ast} X_n) \quad . \tag{6.24}$$

Finally, we have the weighting factor Y (eq. (6.12)) from the straightforward exponential transformation. The total weighting factor for the flight is then

$$F = \left\{ \prod_{j=s}^{n-1} \frac{1-\exp(-\Sigma_j^{\ast} X_j)}{1-\exp(-\Sigma_j^{\ast}(X_j-x_j))} \right\} \cdot (1-\exp(-\Sigma_n^{\ast} X_n)) \cdot \frac{\Sigma_n}{\Sigma_n^{\ast}} \quad . \tag{6.25}$$

Regardless of the sign of the $\Sigma_j^{\ast}$, F is certainly positive. The same is true of the expressions for the pdf, eqs. (6.13), (6.17), (6.21). In this

manner the drawback (a) is removed.

Until now, the only restriction on the X_j's has been $X_j > x_j$. We now assign to X_j the value (see fig. 6.1)

$$X_j = P_j E, \quad s \leqslant j \leqslant n \ , \tag{6.26}$$

where E is the escape point of the elongated photon path.

Since

$$\int_0^{X_j} p_j^{**}(x)dx = 1 \ , \tag{6.27}$$

it is easily seen that the photons can never escape through the problem boundary. Hence, drawback (b) is also removed.

Sampling of scattering angle and energy decrease is not affected by the exponential transformation.

6.3. Calculation of Heat Generation and Dose Rate

On the basis of the results of the Monte-Carlo calculations for the "transformed problem", the problem is now to estimate some real, physical quantities. These quantities are the energy deposition rate in each of the j_{max} zones[*)] into which the configuration has been divided (fig. 6.1) and the dose rate at the external surface.

From eq. (6.8), which gives the spatial distribution of the emission of source photons in the transformed problem, it follows that the number of Monte-Carlo photons emitted between z and z + dz is

$$dN^* = a \exp(-k^* z)\, dz \tag{6.28}$$

with $k^* = k - c$ (6.29)

and $$a = \frac{N^*}{\int_{z_1}^{z_2} \exp(-k^* z)dz} = \frac{N^* k^*}{1-\exp(-k^* d)} \exp(k^* z_1) \ ; \tag{6.30}$$

d stands for $z_2 - z_1$. N^* is a large number, equal to the total number of Monte-Carlo photons emitted in a calculation.

*) Note the term "zones" for the result domains, not to be confused with the term "region" for a physical layer.

The number of photons in the real problem which corresponds to dN^* in the transformed problem is

$$dN = dN^* \exp(-cz) = a \exp(-kz)\,dz \quad . \tag{6.31}$$

However, it is known from eq. (6.1) that the number of photons emitted in the real problem between z and z + dz per sec and per cm^2 of a plane perpendicular to the z-axis is

$$dN_1 = S_o \exp(-k(z-z_1))dz \quad . \tag{6.32}$$

Hence, to convert from some energy quantity obtained by the Monte-Carlo calculation to the corresponding energy quantity per cm^2 per sec in the physical problem, it is necessary to multiply by the ratio

$$f = \frac{dN_1}{dN} = \frac{S_o(1-\exp(-k^*d))}{N^* k^*} \exp(\, cz_1) \tag{6.33}$$

In the Monte-Carlo calculation the accumulated score of transformed deposited energy E_j^* in each zone and the accumulated transformed energy escape E_{esc}^* have been recorded at the termination of the N^* photon histories. E_{esc}^* is determined as

$$E_{esc}^* = \sum_{\nu} e_{esc,\nu}^* \quad , \tag{6.34}$$

where the summation extends over all collisions in the N^* histories with a final direction $\omega > 0$, each collision giving the statistical estimate $e_{esc,\nu}^*$.

To convert E_j^* to the real energy deposition per cm^3 per sec in zone j, the first step is to calculate the quantity E_j which in the real problem corresponds to E_j^* in the transformed:

$$E_j = E_j^* \exp(-cz_j) \; ; \tag{6.35}$$

z_j is the co-ordinate of a "characteristic point" in zone j, to be discussed later. By multiplication of E_j by f (eq. (6.33)), the energy deposition per cm^2 per sec in zone j is obtained:

$$W_j = E_j \cdot f = \frac{S_o}{N^*} \frac{1-\exp(-k^*d)}{k^*} E_j^* \exp(c(z_1-z_j)) \quad . \tag{6.36}$$

The energy deposition w_j per cm^3 per sec is found by dividing W_j by Δ_j, the width of zone j. It is convenient to express w_j in the unit watt/

cm^3/sec, but to measure the Monte-Carlo energy E_j^K in "normalized units" (n.u.). By the aid of the conversion relations

$$\left.\begin{aligned} &1 \text{ n.u.} = 0.51083 \text{ MeV} \\ &1 \text{ MeV/sec} = 1.602 \cdot 10^{-13} \text{ watt} \end{aligned}\right\} \tag{6.37}$$

(6.36) is recast in the form

$$w_j = 0.818 \cdot 10^{-13} \cdot \frac{S_o}{N^K} \frac{1-\exp(-k^K d)}{k^K \Delta_j} E_j^K \exp(c(z_1 - z_j)) \tag{6.38}$$

(w_j in watt/cm^3, E_j^K in n.u.).

The other problem is to convert E_{esc}^K to dose rate D at the external surface in mr/h. Relating D simply to the escape energy means that the current definition of dose rate (thin and flat detector) is used instead of the flux definition (small spherical detector). The current method is the more efficient of the two in the Monte-Carlo sense[13].

In the range 60 keV - 7 MeV the following relation is valid with max. 25% error[8]:

$$1 \text{ MeV/cm}^2\text{/sec} \quad \text{equivalent to } 1.54 \cdot 10^{-3} \text{ mr/h.} \tag{6.39}$$

The conversion from E_{esc}^K to D is very similar to that from E_j^K to w_j: First the equivalent escape energy in the real problem is calculated as

$$E_{esc} = E_{esc}^K \exp(-cZ) , \tag{6.40}$$

where Z is the co-ordinate of the external surface. The real energy escape per cm^2 per sec is then

$$I_{esc} = E_{esc} \cdot f . \tag{6.41}$$

Inserting the expressions for E_{esc} and f and using the conversion relation (6.39), one obtains the dose rate formula

$$D = 0.000787 \cdot \frac{S_o}{N^K} \frac{1-\exp(-k^K d)}{k^K} E_{esc}^K \exp(c(z_1 - Z)) \tag{6.42}$$

(D in mr/h, E_{esc}^K in n.u.).

6.4. The Programme

A flow diagram of the computer programme MC4 is shown in fig. 6.2. Some of the principal elements of this diagram will now be discussed.

The programme library contains the total group cross sections of the elements in table 6.1, calculated from data in ref. 7 by double logarithmic interpolation. Compton cross sections were evaluated by means of expression (5.2). The energy group structure is the same as in (5.1).

After input of cross-section library and problem data, the programme calculates for each group g and each region i the macroscopic total and scattering cross sections $\Sigma^{tot}_{g,i}$ and $\Sigma^{sc}_{g,i}$ ($1 \leqslant g \leqslant 27$, $1 \leqslant i \leqslant i_{max}$).

Next, the exponential transformation constant c is calculated from the formula

$$c = 1.25 \cdot \Sigma^{tot}_{gs,\,av} , \qquad (6.43)$$

where $\Sigma^{tot}_{gs,\,av}$ is the total cross section at the source energy, averaged over the entire configuration. This seems to be the optimum choice in most practical cases in the sense that it gives the least variance of the results for a given computer-time consumed.

The heart of the MC4 programme is mapped between the two dashed lines in fig. 6.2. The starting position z of the source photons is sampled on the basis of the pdf, eq. (6.8). This z determines a region, i. An isotropic starting direction was assumed, leading to the expression $\omega = 2r-1$ for the cosine of the angle between direction and z-axis (eq. (4.12)).

We have now come to the label "flightstart" in the diagram. A cross section $\Sigma = \Sigma^{tot}_{g,i}$ is ascribed to the photon, which is now characterized by the quantities E, ω , i, z, Σ, W, g. Next, the transformed cross section $\Sigma^{*} = \Sigma - \omega c$ is calculated. Now, depending on the sign of ω , there are two possibilities in the flow diagram. The purpose of this distinction is to suppress the backward direction ($\omega < 0$) and favour the forward one. In the case $\omega < 0$, a game of "Russian Roulette" (see 4.6) is played with a surviving probability $p = \Sigma/\Sigma^{*}$. This is done by sampling a random number r ($0 < r < 1$) and examining whether $r > p$. If this is the case, the photon is killed, otherwise it survives with its weight increased by the factor $\frac{1}{p} = \Sigma^{*}/\Sigma$. In the case $\omega > 0$, one passes through a dose score routine, described below. Both branches, $\omega > 0$ and $\omega < 0$, lead to the label "Distance selecting".

The dose score routine records the escape energy E^{*}_{esc}, given by (6.34). $e^{*}_{esc,\nu}$ is calculated as

$$e^{\kappa}_{esc,v} = EW\exp(-\sum_i \Sigma^{\kappa}_i x_i) \quad . \tag{6.44}$$

The exp-factor in (6.44) contains the optical distance to the escape point in the transformed problem and is formally equal to the probability of uncollided escape, also in the transformed problem.

The next step is sampling of a flight distance. This is done by the aid of equations (6.13) - (6.27). The previous description of these equations should make it easy to follow the different links in the distance sampling routine in the flow diagram. Therefore, at this place it should suffice to discuss the sampling formulas applied in connection with (6.13), (6.17), (6.21). A common form of these equations is

$$f^{\kappa x}(x) = \frac{\Sigma^{\kappa}}{1-\exp(-\Sigma^{\kappa}X)} \exp(-\Sigma^{\kappa}x), \qquad 0 \leq x \leq X \quad . \tag{6.45}$$

Such a truncated exponential leads to the sampling formula

$$x = -\frac{1}{\Sigma^{\kappa}} \ln\left[1-r(1-\exp(-\Sigma^{\kappa}X))\right] \quad . \tag{6.46}$$

(6.46) implies both an ln- and an exp-calculation. In ref. 14 is given an alternative sampling formula:

$$x = \begin{cases} \frac{1}{\Sigma^{\kappa}} \mathrm{UDR}\left\{\frac{-\ln(r)}{\Sigma^{\kappa}X}\right\} & \text{for } \Sigma^{\kappa} > 0 \\ X + \frac{1}{\Sigma^{\kappa}} \mathrm{UDR}\left\{\frac{-\ln(r)}{-\Sigma^{\kappa}X}\right\} & \text{for } \Sigma^{\kappa} < 0 \quad . \end{cases} \tag{6.47}$$

UDR stands for the undivided remainder, e.g. UDR $(\frac{13.83}{6}) = 1.83$. (6.47) involves no exp-calculation and is much faster than (6.46). It is applied in our case.

The collisions may be treated in two different ways:

(a) A game is played to decide whether an absorption or a scattering occurs.

(b) The collision is always treated as a scattering, but the weight is reduced to

$$W \cdot \frac{\Sigma^{sc}}{\Sigma^{tot}} \quad .$$

Normally, (b) is the more favourable method, but for photons of little importance (small E and W) it is desirable to kill the photon, and then (a) is best.

In this work a combination of (a) and (b) is used. Above the energy E_{cr} = 1 n.u. (0.51 MeV), (b) is used, otherwise (a).

In both cases one easily accounts for the contribution to energy deposition of the collision. In the case of scattering, the energy E' after collision must be sampled. This is done by Carlson's method, see 5.1. The cosine a of the deflection angle is calculated by means of Compton's formula

$$a = 1 + \frac{1}{E} - \frac{1}{E'} \quad . \tag{6.48}$$

From a and the direction cosine ω before scattering, the direction ω' after scattering is sampled by means of the formula

$$\omega' = a\omega - \sqrt{(1-\omega^2)(1-a^2)} \cdot \cos(r\pi) \quad . \tag{6.49}$$

(6.49) is a one-dimensional version of eqs. (4.23).

Finally, the new group number, g, determined by E', is assigned and one returns to "flightstart", where a new flight starts, and so on.

When the prescribed number of photon histories is reached, one jumps out from the heart of the programme, and the results as obtained by the formulas (6.38) and (6.42) will be printed out. However, formula (6.38) is somewhat ambiguous owing to the z_j, the co-ordinate of a "characteristic point" P_j in zone j. The choice of P_j as the central point of the zone is not adequate and will introduce a significant error, unless the thickness Δ_j of the result zone is much smaller than $\frac{1}{c}$ (in most cases Δ_j and $\frac{1}{c}$ are of the same order of magnitude). A better estimate of z_j is obtained by assuming constant density of energy deposition in the transformed problem. This leads to the equation

$$\int_{a_j}^{a_j + \Delta_j} \exp(-cz)dz = \Delta_j \exp(-cz_j) \quad , \tag{6.50}$$

where a_j is the co-ordinate of the left boundary of result zone j. When (6.50) is introduced into (6.38), the latter equation is modified to

$$w_j = 0.818 \cdot 10^{-13} \frac{S_o}{N^x} \frac{1-\exp(-k^x d)}{k^x} \cdot \frac{1-\exp(-c\Delta_j)}{c\Delta_j^2} E_j^x \exp(c(z_1-a_j)) \qquad (6.51).$$

(w_j in watt /cm^3, E_j^x in n.u.) ,

in which form we use it.

6.5. Calculation Results

Calculations performed by means of MC4 have been compared with measurements. The arrangement is the Swedish R2-0 reactor with a bulk shield of magnetite concrete preceded by 20 cm water and 1 cm aluminium. It is identical with the second of the two configurations studied in 3.3.

The problem is to calculate the Y-radiation absorbed throughout the concrete shield, in watt/cm^3 or in mrad/h. In the MC4 calculations the thickness of the concrete was limited to about 1 metre just as in the REMDIFF problem discussed in 3.3. Also here the restriction is due to trouble, now overcome, with the limited range of the IBM 7090.

The Y-radiation field in the concrete is almost exclusively due to two sources. The first is the Y-source in the core; it originates from fissions, from decay of fission products, and from neutron captures. The second is the capture-Y source in the concrete shield itself.

The spectrum of the Y-source in the core region is given in a rather detailed form in ref. 15. It appears reasonable to approximate the spectrum with a single Y-line of 2 MeV energy. This source is assumed constant over the source region ($k = 0$ in eq. (6.1)). In the same manner, the capture-Y source in the concrete, mainly due to neutron absorption in the iron component, is well approximated by a single Y-line of 7 MeV energy. The spatial variation of this source follows the thermal flux curve. Three points of the latter are available as experimental results, see fig. 3.5. They lie approximately on a straight line in this figure, so that the capture-Y source can be approximated by a single exponential with $k = 0.119$ (eq. (6.1)). The strengths of the Y-sources in core and concrete are calculated by means of data from ref. 15.

It was not found worth while to correct for the finite lateral extension of the core as was done in 3.3 for REMDIFF. Of course, only the core-Y radiation (primary radiation) should have been corrected, but at those distances from the core where the correction factor becomes significant, the primary radiation is weak as compared with the secondary (capture-Y)

radiation.

The results of the calculations together with the R2-0 measurements are presented in fig. 6.3. The figure shows the MC4 results for the primary radiation (upper diagram), the secondary radiation (middle diagram) and the sum radiation (lower diagram). In the last curve, the absorbed radiation energy (watt/cm^3) was converted to dose rate (mrad/h) by multiplication by $\frac{3.6 \cdot 10^{11}}{\rho} = 0.963 \cdot 10^{11}$. This curve can then be compared directly with the three experimental points taken from ref. 15. The agreement is quite satisfactory. No estimated statistical errors are given in fig. 6.3 because they are small, in fact only slightly greater than the errors in drawing.

The same problem has been solved by the aid of the simple build-up programmes PRIGAM and SEGAM I (sect. 1). The result of these calculations is shown as the three dashed curves in fig. 6.3. The agreement between the total dose curve and the experimental points is hardly inferior to that in the MC4 calculation. This good agreement is not surprising in view of the comments given in sect. 1 on the validity of the build-up codes: they are valid for infinite, homogeneous shield layers, which condition is met to a fair degree of approximation in the present bulk concrete shield.

Note that the energy deposition calculated with PRIGAM diverges at the core-water interface. The reason for this is that PRIGAM operates with an "equivalent surface source", giving infinite flux at the surface itself. PRIGAM results are only applicable some relaxation lengths from the surface.

While, as we have seen, the PRIGAM and SEGAM codes are quite suitable for bulk shields, they cannot handle pronouncedly laminated shields correctly. As an illustrative example, consider a shield composed of 2 cm lead and 30 cm water. On one side of this system is situated a uniform isotropic surface source of photons with the energy 0.5 MeV, and one wishes to find the dose rate at the opposite (external) surface. The answer to this problem depends on the order of the laminae [8, 10]. It is clear, however, that a calculation with the build-up code (in this case SEGAM II) gives a result independent of the order of the layers, unless special "tailor-made" build-up coefficients depending on the said order are applied; but such a device does not fit well into the simple build-up programme system described in sect. 1. On the other hand, MC4 is sensitive to the lamina order, as seen from the results obtained with this code for the problem mentioned above:

Lead followed by water: Dose rate = 1.32 ± 0.06 mr/h

Water followed by lead: Dose rate = 0.63 ± 0.03 mr/h.

The surface source strength was 10^7 photons/cm^2/sec.

This result has not been tested experimentally, but it is in harmony with results from similar calculations[8,10].

The running time for an MC4-problem is of the order of 10 min. on the IBM 7090.

Table 6.1

Permissible Elements for MC4

Atomic no.	Symbol
1	H
3	Li
4	Be
5	B
6	C
7	N
8	O
11	Na
12	Mg
13	Al
14	Si
15	P
16	S
19	K
20	Ca
22	Ti
24	Cr
25	Mn
26	Fe
27	Co
28	Ni
29	Cu
40	Zr
42	Mo
56	Ba
74	W
82	Pb
92	U

7. MONTE-CARLO CALCULATION OF THE AXIAL NEUTRON FLUX DISTRIBUTION IN A SHORT, ABSORBING ROD

In this section is presented a Monte-Carlo method for calculating the relative axial neutron flux distribution in a finite cylindrical rod consisting of a homogeneous, absorbing material.

The rod may be surrounded by either a homogeneous, purely scattering medium or concentric layers of absorbing and scattering materials.

Also the relative surface distribution of the neutron current on black cylindrical rods of finite length is calculated.

The computer programme exists in a GIER-ALGOL version as well as in a FORTRAN IV version for the IBM 7090.

Comparison between calculations and measurements has been carried out for a number of cases.

7.1. Description of the Problem

If a cylindrical rod of absorbing material is placed in a scattering medium, it is a well-known fact that the axial neutron flux in the rod will increase from its unperturbed value far from the ends to a somewhat larger value near the ends. This effect is sometimes referred to as Wilkin's effect. It plays an important role, e.g. for the heat production along a fissile specimen in a reactor, and an estimate of its magnitude is therefore of importance.

The problem has previously been solved theoretically by using one-group diffusion theory[17]. However, diffusion theory is a rather doubtful method when applied to thin and strongly absorbing rods. This section presents a Monte-Carlo method of solution.

In the following, relative one-group flux distributions are described. The programme system (Monte-Carlo 5) is able to handle three types of problems:

(a) Calculation of the neutron current along the surface of a black rod surrounded by a homogeneous and isotropically scattering medium without absorption. The source may be either a volume source outside the rod or a surface source on a cylinder concentric with the rod.

(b) Calculation of the axial flux distribution in a grey rod under the same conditions as for (a).

(c) Calculation of the axial flux distribution in a periodic system of grey rods separated by spacers and surrounded by a number of concentric regions of different materials. No source is allowed in the column formed by the rods and the spacers between them. Isotropic scattering is assumed, and each region is characterized by a scattering cross section (corrected for anisotropy) and an absorption cross section. This "heterogeneous" model can also be used to solve single rod problems.

7.2. Discussion of the Models

It is the grey rod calculations (types (b) and (c)) which are most important for the applications. However, as will be clear from the following, an efficient method of solving these problems is to divide the calculation into two steps, the first of which is a black rod calculation.

In the case of the grey rod in a homogeneous medium (type (b)) one considers the whole number, N, of neutrons which in a certain time interval pass into the rod region. These N neutrons can be divided into two categories: those which have never been in the rod before (N_0) and those which have been there before (N_1), so that $N = N_0 + N_1$.

The N_0 neutrons can be interpreted as the source in the Monte-Carlo calculation. This source is an inward-directed surface source, distributed over the whole surface of the rod. The spatial and angular distribution of the source is exactly the same as the distribution of neutrons on the surface of a black rod, with the same dimensions as the grey rod and immersed in the same medium. Thus, this method of treating the grey rod requires an auxiliary calculation of the current distribution on the black rod. This distribution is not uniform because of the shadowing effect, which decreases towards the ends of the rod. Of course the grey rod problem could be solved without any recourse at all to the black rod calculation, by direct simulation of the source neutrons. From a computational viewpoint, however, the method of introducing the black rod is much more favourable because in the grey rod calculation one can save the computer time necessary to follow the neutrons from their real source points to their entrance into the rod. Furthermore, the black rod problem is simple enough to permit a Monte-Carlo solution, although several refinements of the straightforward Monte-Carlo technique were necessary to avoid excessive computing time. The black rod problems contains very few parameters: If the rod is not so short that a coupling between the ends occurs, the result depends only on the quantity

$$\alpha = 2a\Sigma \,, \qquad (7.1)$$

i. e. the rod diameter measured in mean free paths of the surrounding medium. If coupling occurs, the rod length will enter as another parameter. Owing to this small number of parameters, it is possible to run a number of black rod calculations and to express the results in condensed form (polynomial fits). These fits can be used for grey rod calculations. Thus, a grey rod routine calculation involves only a calculation with a source on the rod itself, which means favourable conditions for a Monte-Carlo run.

In the heterogeneous case (type (c)) a similar argumentation as above leads to a model where the neutrons in the Monte-Carlo calculation start uniformly distributed from the entire curved surface of the infinite cylinder, of which the rod in question is a part - independently of the radial distribution of the sources outside this cylinder. The sources are of course assumed to be axially uniformly distributed. The application of this model is clearly restricted to cases where no sources are present inside the infinite cylinder mentioned above.

7.3. Description of the Monte-Carlo Methods

7.3.1. The black rod calculation

Fig. 7.1 shows the geometry in the black rod problem. The extension of the medium around the rod should be infinite, but application of the Monte-Carlo technique requires a spatial cut-off. This cut-off is chosen as the surface of a large cylinder. In practice, the cut-off cylinder is "large" when no part of it is nearer the rod than 2.5 - 3 mean free paths of the medium outside the rod.

The black rod surface is divided into 2Z current scoring zones, arranged symmetrically about the middle plane $z = 0$. Two types of zones appear: plane end (radial) and curved (axial) zones. For an arbitrary collision point (x, y, z) one has a set of probabilities $p_i(x, y, z)$ of hitting zone i in the next flight, and a total probability $p(x, y, z) = \sum_1^{2Z} p_i(x, y, z)$ of hitting the rod. Straightforward Monte-Carlo would then kill the neutron if a sampled random number $r(0 < r < 1)$ was less than p, and would otherwise continue with the neutron without giving any contribution at all to the score from this collision point. This method gives poor statistics, especially for small rods. Another method was applied which in every collision gives a contribution to the current in all the visible zones (the "spray method"). The neutron with the weight W, colliding at (x, y, z), will lose the fraction

$W \cdot p(x, y, z)$ by absorption on the rod surface, and this amount of absorption is distributed on all the zones visible from (x, y, z) according to the $p_i(x, y, z)$-values. After that, a new flight direction $\vec{\Omega}$ is sampled (isotropic scattering), and also a new track length l. This flight may result in a hit of the rod. This event must, however, be considered as forbidden because the amount of absorption has already been taken into account. It is therefore necessary to try a new sampling $(\vec{\Omega}, l)$ from the previous collision point. Sooner or later an "allowed" sample is obtained, and the neutron then continues its history, now carrying the reduced weight $W \cdot (1-p(x, y, z))$. Escape through the cut-off cylinder cannot occur because this surface is regarded as reflecting in the optical sense. The only possibility of a termination of a neutron history is then loss of weight to such an extent that W drops below a certain cut-off value, W_{cut}. The previously mentioned probabilities $p_i(x, y, z)$ and $p(x,y,z) = \Sigma p_i$ are continuous functions of (x, y, z). One possible approach is to calculate these quantities whenever a new collision point (x, y, z) has been sampled. This method is rather time-consuming. Instead, we have chosen a discrete representation of the p_i's and p's, corresponding to the network shown in fig. 7.1. Because of the cylindrical symmetry, the network is essentially plane (we set $y = 0$ at each new collision). It appeared to be favourable to have two different mesh systems, a fine network near the rod and a coarse one farther from the rod. The mesh probabilities p_{ijk} (rod zone i, mesh indices j, k) and p_{jk} (total hit probability from mesh jk) are taken as the $p_i(x, y, z)$ and $p(x, y, z)$, calculated in the middle point of the mesh. $p_{jk} = \sum_{i=1}^{2L} p_{ijk}$ will be denoted $p_{2L+1, jk}$. All the p_{ijk} form a three-dimensional set of numbers, which is calculated before the real Monte-Carlo run and stored in the programme.

Calculation of these probabilities leads to double integrals. To be specific, consider first the probability s_p that a neutron, after being scattered isotropically at $P(x, 0, z)$ outside the rod (fig. 7.1), reaches a plane, annular zone with the radii ρ_1 and ρ_2 on the end face $z = k$. Of course, $s_p = 0$ for $z < k$. Assuming $z > k$, one has

$$s_p = \int_{\Omega} e^{-\Sigma r} \frac{d\Omega}{4\pi} \quad \text{with } d\Omega = \frac{\rho d\rho d\varphi \cos\theta}{r^2} \text{ and } \cos\theta = \frac{z-k}{r},$$

φ is the angular position of the area element $dA = \rho d\rho d\varphi$, and r is the distance from P to dA.

$$s_p = \int_{\rho_1}^{\rho_2} \frac{\rho d\rho}{2\pi} (z-k) \int_0^{\pi} \frac{e^{-\Sigma r}}{r^3} d\varphi ,$$

and insertion of $r^2 = x^2 + (z-k)^2 + \rho^2 - 2\rho\, x\cos\varphi$ yields

$$s_p = \frac{z-k}{2\pi}\int_{\rho_1}^{\rho_2} \rho\, d\rho \int_o^{\pi} \frac{\exp(-\Sigma(x^2+(z-k)^2+\rho^2-2\rho x\cos\varphi)^{1/2})}{(x^2+(z-k)^2+\rho^2-2\rho x\cos\varphi)^{3/2}} d\varphi \quad . \quad (7.2)$$

The corresponding probability of hitting a cylindrical surface zone on the rod limited by the planes $z = z_1$ and $z = z_2$ is denoted s_c. We have $s_c = 0$ if $x \leqslant a$, where a is the radius of the rod, and for $x > a$:

$$s_c = \int_\Omega e^{-\Sigma r} \frac{d\,\Omega}{4\pi} \quad \text{with} \quad d\,\Omega = \frac{a\,d\varphi\; d\zeta \cos\theta}{r^2}$$

and $\cos\theta = \frac{(x-a\cos\varphi\,,\; -a\sin\varphi\,,\; z-\zeta)}{r} \cdot (\cos\varphi\,,\; \sin\varphi\,,\; 0) = \frac{x\cos\varphi - a}{r}$.

ζ is the z-co-ordinate of the area element $a\, d\varphi\, d\zeta$.

One now has

$$s_c = \int_{z_1}^{z_2} \frac{a\,d\zeta}{2\pi} \int_o^{\varphi_o} e^{-\Sigma r} \frac{x\cos\varphi - a}{r^3} d\varphi \quad \text{with} \quad \varphi_o = \text{Arc cos}\, \frac{a}{x},$$

and substitution of $r^2 = x^2 + (z-\zeta)^2 + a^2 - 2ax\cos\varphi$ yields

$$s_c = \frac{a}{2\pi} \int_{z_1}^{z_2} d\zeta \int_o^{\varphi_o} \frac{(x\cos\varphi - a)\exp(-\Sigma(x^2+(z-\zeta)^2+a^2-2ax\cos\varphi)^{1/2})}{(x^2+(z-\zeta)^2+a^2-2ax\cos\varphi)^{3/2}} d\varphi$$

(7.3)

The Monte-Carlo procedure itself is mapped in the flow diagrams fig. 7.4 (coarse diagram fig. 7.4.1, detailed diagram fig. 7.4.2).

The neutrons start either from the volume between the rod and the cut-off cylinder or from the surface of the cut-off cylinder, according to the type of source. The neutron has a weight parameter W, which is 1 at the starting point. The y-co-ordinate of the source is always zero; further, x and z are both positive. This is bound up with the cylindrical symmetry of the problem. Referring to fig. 7.4.2, a neutron flight starts at the label "flight", either as a source neutron or as a scattered neutron. The co-ordinates are in both cases normalized to the form (x, 0, z) with $x > 0$, $z > 0$. If $x < a$, one goes directly to the label "inner". The flight routine has a main label "escol" (escape or collision), to which one jumps if the black rod is not

hit. During the tracing of the flight, several possibilities of jumping to "escol" occur.

If $x > a$, the following consecutive tests are made:

(1) Sign of x-direction cosine u. $u > 0$ leads to "escol".

(2) Intersection of the flight line with the surface $x^2 + y^2 = a^2$. The case of no intersection point leads to "escol".

(3) Comparison of the distance t along the flight path to the intersection point P_s with the sampled disposal length l. $t > l$ leads to "escol".

(4) z-co-ordinate z_s of intersection point P_s. $|z_s| > h$ leads to "escol", while $|z_s| < k$ means hitting of the rod.

The third possibility in test (4), $k \leqslant |z_s| \leqslant h$, leads to entrance into the "inner" region, given by $x^2 + y^2 \leqslant a^2$, $k \leqslant |z| \leqslant h$. However, before further tracing of such a neutron, one renormalizes $P_s(x_s, y_s, z_s)$ to the form $(a, 0, z_s)$ by simultaneously transforming the components (u, v) of the direction vector to (u', v') by rotating an angle $-\varphi$ ($\operatorname{tg} \varphi = \frac{y_s}{x_s}$) so that

$$(u', v') = (u, v) \cdot \exp(-i\varphi), \text{ leading to } u' = \frac{ux_s + vy_s}{a}, \; v' = \frac{vx_s - uy_s}{a}. \quad (7.4)$$

The disposal length l is diminished by the "consumed" length t. We are now at the label "inner" (fig. 7.4.2), and also in this case consecutive testings for jumps to "escol" are made:

(1) Sign of $w \cdot z$ (w = z-direction cosine). $w \cdot z > 0$ leads to "escol".

(2) Calculation of the distance t along the flight line to the intersection point $P_R(x_r, y_r, \pm k)$. $t > l$ leads to "escol".

(3) Situation of P_R. $x_r^2 + y_r^2 \geqslant a^2$ leads to "escol", otherwise the rod is hit.

Arriving at the label "escol", one ascertains whether a collision or a hitting of the cut-off cylinder has taken place. In the latter case, the neutron is reflected optically in the cut-off cylinder. The planes $z = \pm h$ reflect the flight simply by reversion of the sign of w. The curved surface reflection gives a slightly more complicated formula for the reflected direction vector (u_1, v_1, w_1):

$$u_1 = \frac{-ux_c - vy_c}{R}, \quad v_1 = \frac{vx_c - uy_c}{R}, \quad w_1 = w. \quad (R = \text{cut-off radius}), \quad (7.5)$$

corresponding to a normalizing of the mirror point from (x_c, y_c, z_c) to $(R, 0, z_c)$. If, on the other hand, collision occurs, one scores zone currents according to the previously mentioned "spraying" principle.

The output is processed in the usual way for the estimation of mean values and variances.

7.3.2. The grey rod in a homogeneous medium

The Monte-Carlo run of this problem is mapped in the flow diagram fig. 7.3. The neutrons start from the whole rod surface. Stratified sampling of position is feasible in this problem. The surface source strength should have the distribution calculated in the black rod problem. However, we decided instead to sample from a constant source and then compensate by ascribing the weight W(P) to the neutron. W(P) is a function of the points P on the total rod surface, normalized to an average value of unity over the rod. W(P) is given by the black rod calculation. The source directions are chosen from an inward cosine distribution, which is a good approximation in this problem. A track length l in the rod is sampled. One ascertains whether the neutron has collided in the rod or escaped from it. If a rod collision occurs, the score in the zone containing the collision point is increased by W. The weight after collision is

$$W \cdot \frac{\Sigma_o - \Sigma_{ao}}{\Sigma_o} ,$$

where Σ_{ao} and Σ_o are the absorption and the total cross section of the rod. If $W < W_{cut}$, one returns to "start", otherwise one proceeds to the isotropic scattering routine, after which a new flight in the rod is sampled, and so on. If the neutrons pass out from the rod, one applies a similar flight routine for the medium outside the rod (total cross section Σ, no absorption). After a certain number of collisions here, the neutron will hit either the rod or the cut-off cylinder. In the former case one continues to trace the neutron in the rod. In the latter case the neutron is transferred to a random point P of the rod surface, from which it starts with inward cosine distribution and the weight multiplied by W(P). The contents of the box in fig. 7.3 labelled "entrance in rod 2" are exactly the same as shown in fig. 7.4.2 for the black rod.

The flow diagram fig. 7.3 refers to the simple flux score routine discussed above. However, this routine has recently been modified. Instead of scoring the zone collisions, one makes a statistical estimate of the zone flux increment for every track length occurring in the zone. This procedure

is carried out in the following way: Track lengths in the rod are sampled from the scattering cross section Σ_{so} instead of the total Σ_{to}. This incorrect method of sampling is corrected as follows: each time a neutron track l_i in a zone i ceases - either by escape from the zone or by a collision - one multiplies the neutron weight W by $\exp(-\Sigma_{ao} \cdot l_i)$. The statistical estimate of the flux increment in zone i is then $W(1-\exp(-\Sigma_{ao} \cdot l_i))$. This modified flux scoring device, which is also introduced in the "heterogeneous" problem, has increased the calculation efficiency by a factor 4 for rods with rather thin zones.

7.3.3. The grey rod in a heterogeneous medium

Fig. 7.2 shows the geometry of this problem, and the Monte-Carlo run is mapped in fig. 7.5. The rather involved structure of this diagram derives from the routines which decide the momentary zone of the neutron. These routines are described in ref. 6.

The neutrons start stratified from the cylinder surface $x^2 + y^2 = a^2$, $z \leq h$. (2h = height of cut-off cylinder.) The directions have an inward cosine distribution. The planes $z = \pm h$ act as mirrors, while the neutrons, when passing through the curved surface of the cut-off cylinder, are killed.

7.4. The Computer Programme System

The computer programme system includes five codes:

(1) NETPROB, in GIER-ALGOL, preparing auxiliary input for MC5A.

(2) MC5A, in FORTRAN IV, solving problems of type (a) (subsec. 7.1).

(3) FITAB, in GIER-ALGOL, which processes the output of MC5A to be used as input in MC5B1.

(4) MC5B1, in GIER-ALGOL and FORTRAN IV, solving problems of type (b) (subsec. 7.1).

(5) MC5C1, in GIER-ALGOL and FORTRAN IV, solving problems of type (c) (subsec. 7.1).

The GIER-ALGOL programmes are run on the GIER computer at Risö, while the FORTRAN IV programmes are run on the IBM 7090, installed at the Technical University of Denmark in Lyngby.

NETPROB calculates the mesh probabilities to be used as input in MC5A.

MC5A gives as output the values for the neutron current (n/cm^2/time unit) in the radial as well as the axial zones.

FITAB is discussed in some detail below. It is a link code between MC5A and MC5B1. It carries out a smoothening of the stepwise varying currents which MC5A gives as output.

Fig. 7.6 shows a graph of such an output. The level is arbitrary. This representation is replaced by expressions of the form

$$F_1(z) = A'_0 \exp(-A'_2(k-|z|)) + A'_4 \quad \text{(axial current)} \tag{7.6}$$

and $$G_1(x) = B'_0 + B'_2 x^2 \quad \text{(radial current)} , \tag{7.7}$$

the fits being least square fits. After this one must normalize to an overall incoming current of the average unity, thus obtaining the final expressions

$$F(z) = A_0 \exp(-A_2(k-|z|)) + A_4, \qquad -k \leqslant z \leqslant k \tag{7.8}$$

$$G(x) = B_0 + B_2 x^2 , \qquad x \leqslant a \quad . \tag{7.9}$$

The forms of the fitting expressions above seem to be the simplest possible to extract the main features of the black rod current distribution obtained. If k is large enough to exclude coupling between the ends, then $F(z) \approx A_4$ will be valid for a range of z-values, i.e. the rod has a middle part with no axial perturbation of the flux. The only essential drawback of the form (7.8) is that F(z) has a bend at $z = 0$; however, this only matters if the rod is very short.

In order to obtain the form (7.6) in a straightforward manner, we simply set $A'_4 = f_1$ (fig. 7.6). Clearly, this requires that the level f_1 is sufficiently stable statistically, and that $k-z_1$ is large enough to ensure that the axial flux perturbation is small at z_1. These conditions should be borne in mind when one uses MC5A. The least square condition to be met by the axial fit is now applied to the logarithms of increments $f_i - f_1$:

$$\sum_{i=2}^{n} w_i(\ln(f_i-f_1) - \ln A'_0 + A'_2(k-t_i))^2 = \min. \tag{7.10}$$

with $t_i = \frac{1}{2}(z_i + z_{i-1})$

A natural choice for the weights w_i is

$$w_i = (f_i - f_1) \cdot (z_i - z_{i-1}) . \tag{7.11}$$

The solution of (7.10) is

$$A_2' = \frac{\Sigma w_i \zeta_i \; \Sigma w_i \eta_i - \Sigma w_i \; \Sigma w_i \eta_i \zeta_i}{\Sigma w_i \; \Sigma w_i \zeta_i^2 - (\Sigma w_i \zeta_i)^2} \tag{7.12}$$

and $$A_o' = \exp\left[\frac{\Sigma w_i \eta_i + A_2' \Sigma w_i \zeta_i}{\Sigma w_i}\right] \tag{7.13}$$

with the abbreviations $\zeta_i = k - t_i$ and $\eta_i = \ln(f_i - f_1)$.

The summations extend from i = 2 to i = n.

The form (7.7) is obtained by applying the least square condition to the integrated zone currents. This gives the equation

$$\sum_{i=1}^{m} \left[\frac{B_2'}{2}(x_i^4 - x_{i-1}^4) + B_o'(x_i^2 - x_{i-1}^2) - g_i(x_i^2 - x_{i-1}^2)\right]^2 = \min. \tag{7.14}$$

(notation, see fig. 7.6).

As the detailed shape of the radial fit is not very important, no weights have been carried along. The solution of (7.14) is

$$B_2' = \frac{h_3 h_4 - h_2 h_5}{h_1 h_4 - h_2^2} \qquad B_o' = \frac{h_1 h_5 - h_3 h_2}{h_1 h_4 - h_2^2} \tag{7.15}$$

with the abbreviations

$$h_1 = \Sigma \alpha_i^2, \quad h_2 = \Sigma \alpha_i \beta_i, \quad h_3 = \Sigma \alpha_i \beta_i g_i, \quad h_4 = \Sigma \beta_i^2, \quad h_5 = \Sigma \beta_i^2 g_i$$

$$\alpha_i = \frac{1}{2}(x_i^4 - x_{i-1}^4), \qquad \beta_i = x_i^2 - x_{i-1}^2,$$

the summation extending from 1 to m.

The normalized expressions (7.8) and (7.9) are finally obtained by requiring

$$(A_o, A_2, A_4, B_o, B_2) = (kA_o', A_2', kA_4', kB_o', kB_2') \tag{7.16}$$

and $$\int_o^a (B_o + B_2 x^2) 2\pi x dx + \int_o^k (A_o \exp(-A_2(k-z)) + A_4) 2\pi a dz = \int_o^a 2\pi x dx + \int_o^k 2\pi a dz$$

(7.17)

The final expressions (7.8) and (7.9) constitute the function W(P) in 7.3.2, and the constants (A_0, A_2, A_4, B_0, B_2) form the input of MC5B1.

However, MC5B1 has an option permitting automatic calculation of (A_0, A_2, A_4, B_0, B_2). This has been possible after a parameter study of black rod calculations, by varying α (eq. (7.1)). The said study has only been completed where there is no coupling between the ends of the rods and in cases with surface sources.

Both MC5B1 and MC5C1 give as output mean volume fluxes over the cylindrical zones into which the rod is divided. The division into zones is arbitrary apart from the requirement that the zones must lie symmetrically about the centre of the rod.

FITAB and the GIER version of MC5B1 and MC5C1 also present the output in graphic form by means of a plotter.

Running times:

NETPROB	about	2 hours
MC5A	"	2 hours
FITAB	"	1 min.
MC5B1	"	10 min. on IBM 7090, 3 hours on GIER
MC5C1	"	20 min. on IBM 7090, 5 hours on GIER.

All the figures for running times refer to typical cases with reasonably good statistics.

7.5. Presentation of Calculations and Comparisons with Experiments

7.5.1.

In this subsection a number of calculations are presented, and some are compared with measurements.

As the literature available on such experiments was very limited, it was decided that supplementary experiments should be carried out in the Risö facilities. The measurements were performed in a heavy-water exponential facility. A description of the experiments is given in 7.6.

Table 7.1 gives a summary of the comparisons.

Table 7.1

Model	Code	Experimental set-up	Carried out at	Results in fig.
Black rod	MC5A	Cadmium cylinder, 2.5 cm dia., in heavy water (exponential facility)	Risö	7.9.1
Grey rod in hom. medium	MC5B1	Natural uranium rod, 1.796 cm dia., in graphite (thermal column)	ANL	7.10.1
- " -	- " -	do., 2.54 cm dia.	- " -	7.10.2
Grey rod in het. medium	MC5C1	Copper rods (1.27 cm dia.) with lead spacers and heavy water outside (exponential facility)	Risö	7.11.1
- " -	- " -	do., 2.54 cm dia.	- " -	7.11.2

The experiments at ANL are described in ref. 18. This report also describes a number of experiments on rods with cadmium as the main absorbing component. However, it was recognized that thermal Cd-experiments were not feasible for testing one-group models because of the rapidly varying cross-section curve of Cd.

Most of the digital computer calculations have been performed at NEUCC (Northern Europe University Computing Center), Technical University of Denmark, on an IBM 7090 computer.

In the following, a short description of the results is given.

7.5.2. Black rod, a = 1, surface source. Comparison with Risö experiment

Fig. 7.9.1 shows the measured as well as the calculated axial current distribution on a black rod (Cd) in heavy water. The diameter of the rod was 2.5 cm. The scattering cross section (corrected for anisotropy) of the heavy water was taken to be 0.4012 cm^{-1}. So, in this case, $a = 2.5 \cdot 0.4012 = 1.00$.

In both experiment and calculation the current values were normalized to unity at the midpoint on the curved surface, where the current is essentially constant. As can be seen from fig. 7.9.1, a finer zone division was used in the experiment than in the calculation. Therefore a "converted" experimental curve has been drawn to meet the zone specification in the calculation. This curve agrees quite well with the calculated distribution. No statistical

error limits have been stated in the Monte-Carlo calculation because the error is here very small (~0.3 pct.).

The calculations were made with MC5A, a constant surface source on the cut-off cylinder being used to simulate the actual physical conditions.

7.5.3. a-parameter study on black rods (surface source)

To make possible an automatic black rod calculation preceding a routine grey rod calculation (see 7.2), a number of black rod calculations with different a-values (see 7.2) were carried out. The values a = 0.5, 1, 2, 3 were considered. The calculations refer to cases with no coupling between the ends and to cases where the surface source model is valid. The results of this parameter study are shown in figs.7.7 and 7.8. The radial distributions shown are not very reliable because of statistical errors. It is seen that the flux perturbation increases steadily with increasing a.

To extract the essential feature of these calculations, FITAB was used to smoothen the stepwise varying currents by fitting them to simple analytic expressions.

If one renormalizes the expressions (7.14) and (7.15) to the forms

$$f(z) = a_o \exp(-a_2 \frac{k-|z|}{a}) + 1 \qquad (7.18)$$

$$g(x) = b_o + b_2(\frac{x}{a})^2 \qquad (7.19)$$

(a = rod radius, k = half rod length),

corresponding to the current density unity at the midpoint of the axial surface (z = 0), then the constants (a_o, a_2, b_o, b_2) will depend only on a, provided the rods are long enough to exclude end coupling effects, and these constants themselves can be fitted to simple polynomial functions of a.

Our calculation gave the result shown in fig. 7.12, which shows both the 4 · 4 calculation points and the graphs of four fits, the equations of which were chosen as follows:

$$a_o = 0.0233\, a^2 + 0.1466\, a \qquad (7.20)$$

$$a_2 = 0.2\, a + 0.85 \qquad (7.21)$$

$$b_o = 1 + 0.12\, a \qquad (7.22)$$

$$b_2 = 0.02916\, a^2 + 0.02418\, a\ . \qquad (7.23)$$

a_2 for $\alpha = 0.5$ could be determined only very crudely from the MC5A result. The expression (7.21) is used for all $\alpha \leqslant 3$ because the perturbation is in any case small (a_0 small) for small α-values.

These functions have been built into MC5B1 to be used when an automatic black rod calculation is to precede a grey rod calculation.

The formulas (7.22), (7.23) for the constants in the radial distributions are not claimed to be very reliable, owing to statistical errors.

The Risö experiment mentioned in 7.5.2 has been used to make a test of the formulas (7.20) to (7.23). The mean radial current j_r and the mean axial current j_z,

$$j_r = \frac{\int_0^a j(x)\, 2\pi x\, dx}{\int_0^a 2\pi x\, dx}, \qquad j_z = \frac{\int_0^k j(z)\, 2\pi a\, dz}{\int_0^k 2\pi a\, dz} \qquad \begin{matrix}(a = \text{rod radius},\\ k = \text{half length}),\end{matrix} \quad (7.24)$$

are found both from the experiments and from the fits (7.20) to (7.23). j_r and j_z are in units of the current at the midpoint of the curved surface ($z = 0$). The results are seen in table 7.2.

Table 7.2

	j_z	j_r
experimental	1.047	1.138
fits (7.20) to (7.23)	1.049	1.147

The agreement is satisfactory.

A parameter study for the corresponding problems with volume sources instead of surface sources has not so far been made. However, in a single case ($\alpha = 3$), a calculation with constant volume sources between the rod and the cut-off cylinder was made and compared with the result for surface source, see fig. 7.9.2. It appears, as would be expected that the perturbation is not so great for volume sources as for surface sources.

7.5.4. Calculations on grey rods in a homogeneous medium. Comparisons with ANL measurements

Some calculations have been made with the code MC5B1 with the built-in formulas (7.20) - (7.23). The calculations refer to the two rods (table 7.1) for which ANL measurements have been reported. Results of Monte-Carlo calculations as well as of ANL measurements appear from fig. 7.10. There seems to be a slight gradient in the experimental flux at distances where the end effect cannot be significant. This complicates the comparisons somewhat. Otherwise the agreement seems to be satisfactory. In the calculations, the macroscopic cross section of natural uranium reported in ref.18 was applied, and for graphite the scattering cross section (corrected for anisotropy) was taken to be 0.3748 cm^{-1}.

7.5.5. Calculations on grey rods in a heterogeneous medium. Comparisons with Risö experiments

The heterogeneous model (MC5C1) has been compared with Risö experiments with copper rods of 8 cm length, separated by lead spacers of 10 cm length and surrounded by heavy water. Two diameters of the rods, 0.5" and 1", have been considered. The cross sections applied in the calculations are $\Sigma_s^{D_2O}(1-\mu) = 0.4012\ cm^{-1}$, $\Sigma_s^{Pb}(1-\mu) = 0.303\ cm^{-1}$, $\Sigma_a^{Pb} = 0.005\ cm^{-1}$, $\Sigma_s^{Cu}(1-\mu) = 0.604\ cm^{-1}$, $\Sigma_a^{Cu} = 0.285\ cm^{-1}$. For Pb, the scattering cross section has been obtained by averaging over a Maxwell spectrum.

7.6. The Risö Measurements

7.6.1. Measurements on a black rod

The experimental arrangement was as follows:

A cadmium cylinder (diameter 2.5 cm, length 10 cm) standing on four legs was placed centrally on the bottom of the exponential tank mentioned in 7.5 (diameter 76.4 cm, height 170 cm). This tank, filled with heavy water, is situated on the top of the DR1 reactor. Between the reactor core and the bottom of the tank there is 120 cm of graphite. In the activation position the cadmium ratio R_{Cd} was > 4500.

It is assumed that all neutrons entering the cadmium are absorbed. The scattering effect in the Cd-cylinder is neglected. This is a very good approximation. Manganese foil detectors (50 mg/cm^2) were glued to the Cd-cylinder both along a cylinder generator and on the end face. Their

activities are proportional to the neutron current perpendicular to the surface.

The result for the longitudinal distribution appears from fig.7.9.1 and was discussed in 7.5.2. The radial distribution was integrated over the surface as mentioned in 7.5.3 (table 7.2).

The neutron flux at the bottom of the tank was about 10^7 n/cm^2/sec. After activation for two hours the activity of the Mn-foils was measured with a gas flow counter.

7.6.2. Measurements on grey rods

The geometry was described in 7.5.5, and the set-up was identical with that in 7.6.1. The subdivision of the Cu-cylinder appears from fig. 7.11. The activity of the middle zone was used to normalize the results.

The irradiation time was 3 hours, and as before the neutron flux was 10^7 n/cm^2/sec.

As seen from fig. 7.11, the measurements were made in five zones. The corresponding five Cu-pellets were dissolved in nitric acid; thus the mean value of the absorption in the pellets was obtained. The Y-activity of this solution was measured in a NaI crystal with a well.

The figure shows good agreement between experiment and calculation.

REFERENCES

1) E. Aalto, L. Hjärne and M. Leimdörfer, A New Shield Design Method and some Attenuation Studies in Laminated Biological Shields. Proc. of the 3rd Conf. on the Peaceful Uses of Atomic Energy, Geneva, 1964.

2) G. D. Joanou, J. S. Dudek, A. J. Goodjohn, and N. F. Wikner, Nuclear Data for the GAM-I Data Tape. GA-2451 (1961).

3) J. Hughes and J. A. Harvey, Neutron Cross Sections. BNL 325 (1955).

4) M. D. Goldberg, V. M. May and J. R. Stehn, Angular Distributions in Neutron-Induced Reactions. BNL 400 (1962).

5) J. M. Hammersley and D. C. Handscomb, Monte Carlo Methods (Methuen and Co. Ltd., London, 1964).

6) E. D. Cashwell and C. J. Everett, A Practical Manual on the Monte Method for Random Walk Problems. LA-2120 (1957).

7) R. A. Mann, Gamma Ray Cross Section Data (Aircraft Nuclear Propulsion Department, DC-60-9-75, 1960).

8) H. Goldstein, Fundamental Aspects of Reactor Shielding (Addison-Wesley, Massachusetts, 1959).

9) M. Leimdörfer, On the Use of Monte Carlo Methods for Solving Gamma Radiation Transport Problems. Nukleonik 6 (1964) 14.

10) Reactor Handbook, vol. III, part B: Shielding (Wiley and Sons, New York, 1962).

11) F. E. Deloume, Gamma Ray Energy Spectra from Thermal Neutron Capture. APEX 407 (1958).

12) I. Bergqvist and N. Starfelt, Neutron Capture Cross Sections and Gamma-Ray Spectra (NAVALATOM, Oct. 1961).

13) M. Leimdörfer, A Monte Carlo Method for the Analysis of Gamma Radiation Transport from Distributed Sources in Laminated Shields. Nukleonik 6 (1964) 58.

14) M. Leimdörfer, On the Transformation of the Transport Equation for Solving Deep Penetration Problems by the Monte Carlo Method. Transactions of Chalmers University of Technology 286 (1964).

15) E. Aalto and R. Nilsson, Measurements of Neutron and Gamma Attenuation in Massive Laminated Shields of Concrete and a Study of the Accuracy of some Methods of Calculation. AE-157 (1964).

16) S. Glasstone and A. Sesonske, Nuclear Reactor Engineering (Van Nostrand, New York, 1963).

17) J. E. Wilkins, The Distribution of Thermal Neutrons in a Slug with Thick End Caps. CP-1989 (1944).

18) F. R. Taraba and S. H. Paine, The Longitudinal Distribution of Thermal Neutron Flux in Cylindrical Fuel Specimens during Irradiation. ANL-5945 (1959).

FIG. 2.1.

PRIGAM GEOMETRY

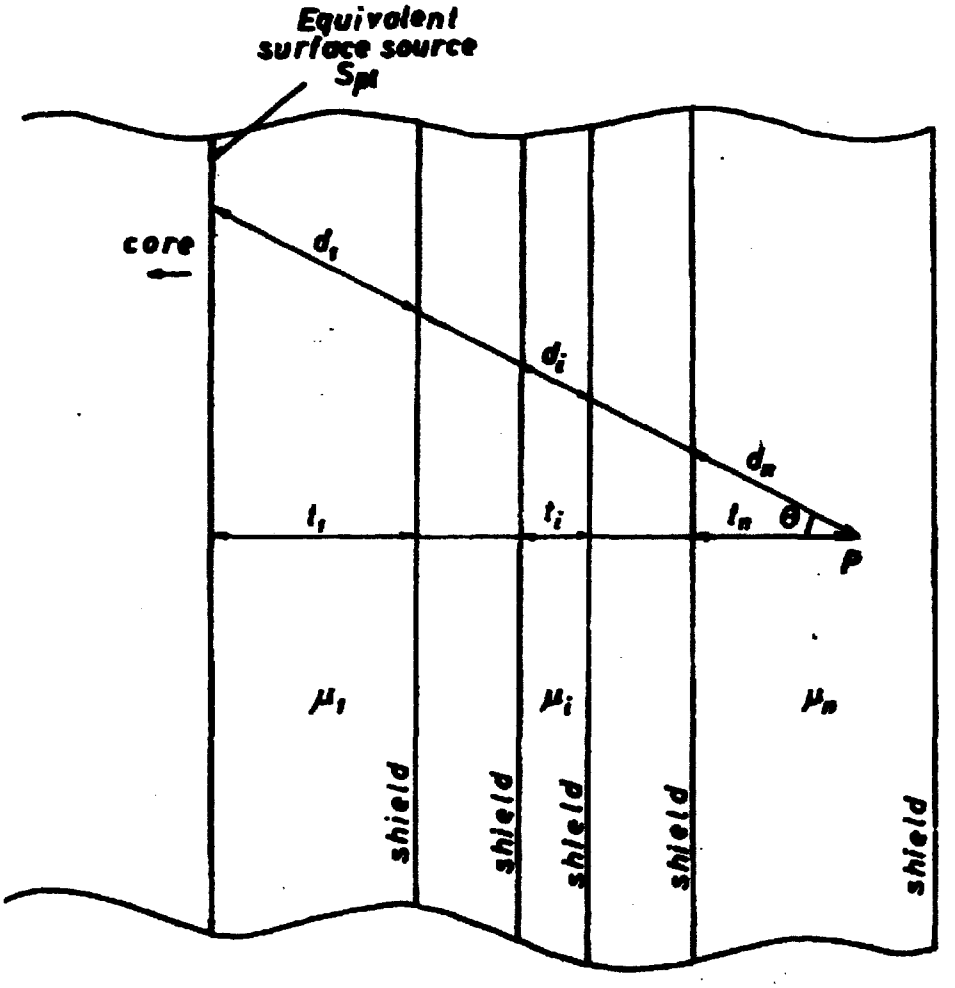

μ_i = linear total γ-absorption coefficient for the i'th shield

$$D_i = \mu_i \, d_i \qquad X_i = \mu_i \, t_i$$

$$D = \sum D_i \qquad X = \sum X_i = D \cos\theta$$

$$d = \sum_1^n d_i \qquad t = \sum_1^n t_i$$

FIG. 2.2.

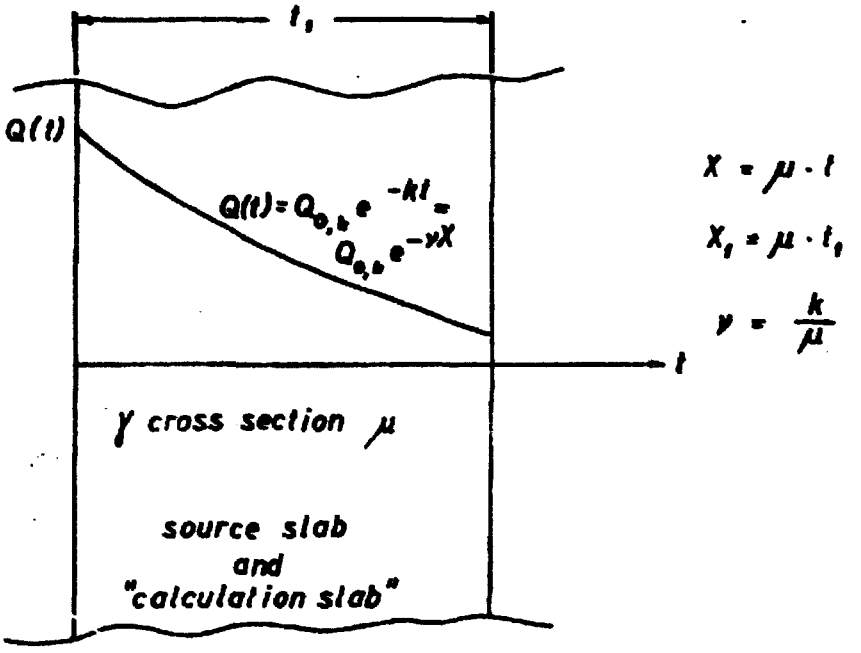

FIG. 2.2.1. SEGAM I GEOMETRY

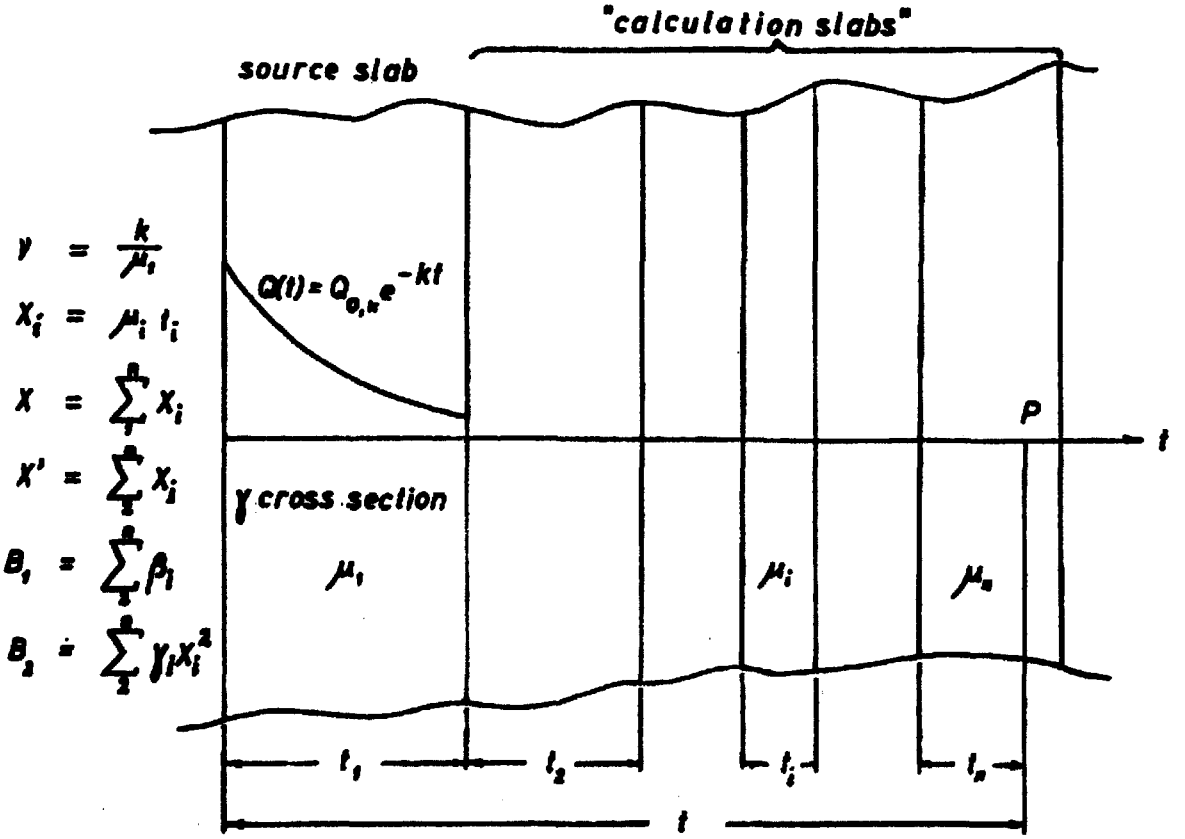

FIG. 2.2.2. SEGAM II GEOMETRY

FIG. 3.1.

REMDIFF GEOMETRY

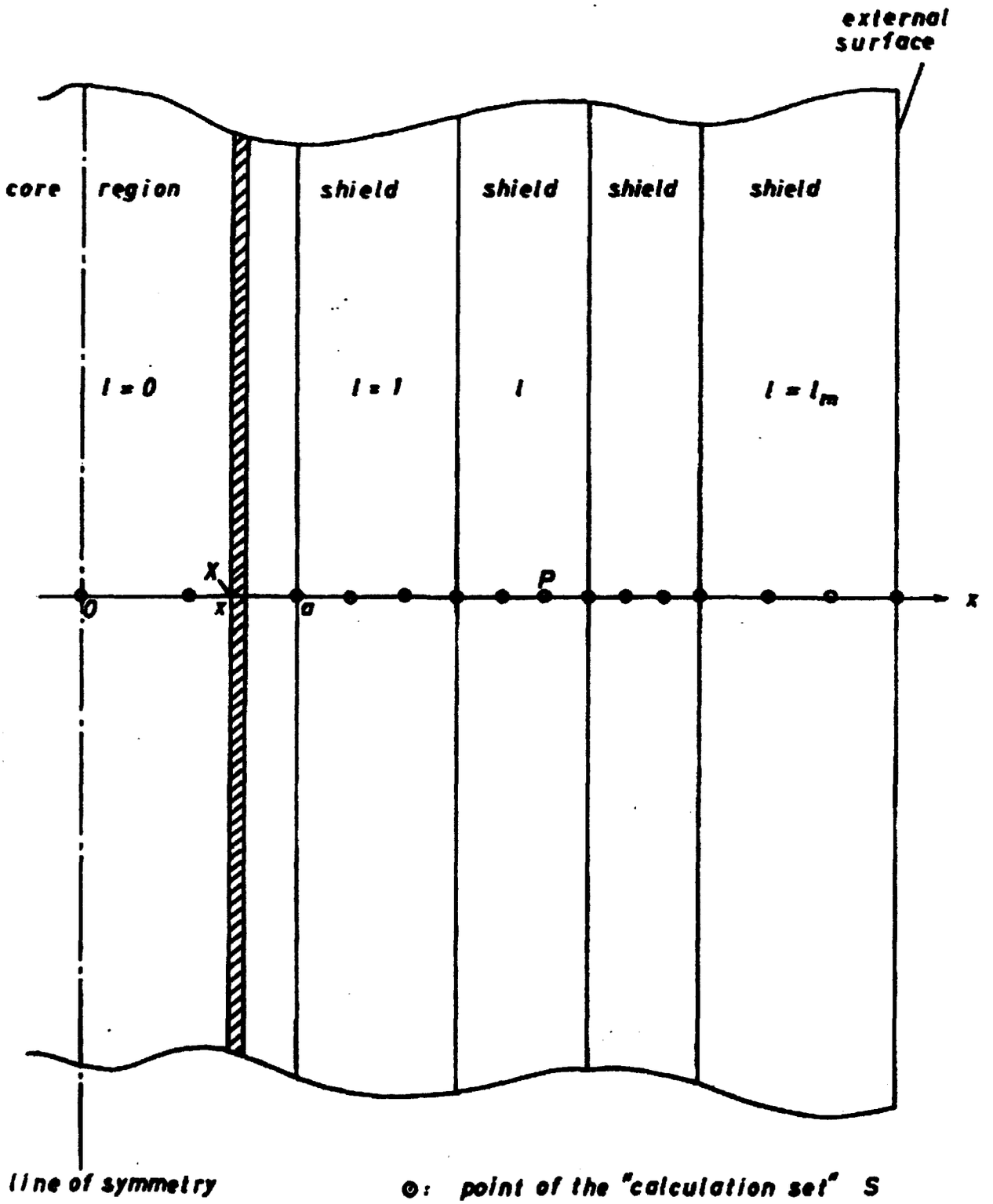

FIG. 3.2.

CONSTRUCTION OF DIFFUSION SOURCE FUNCTIONS

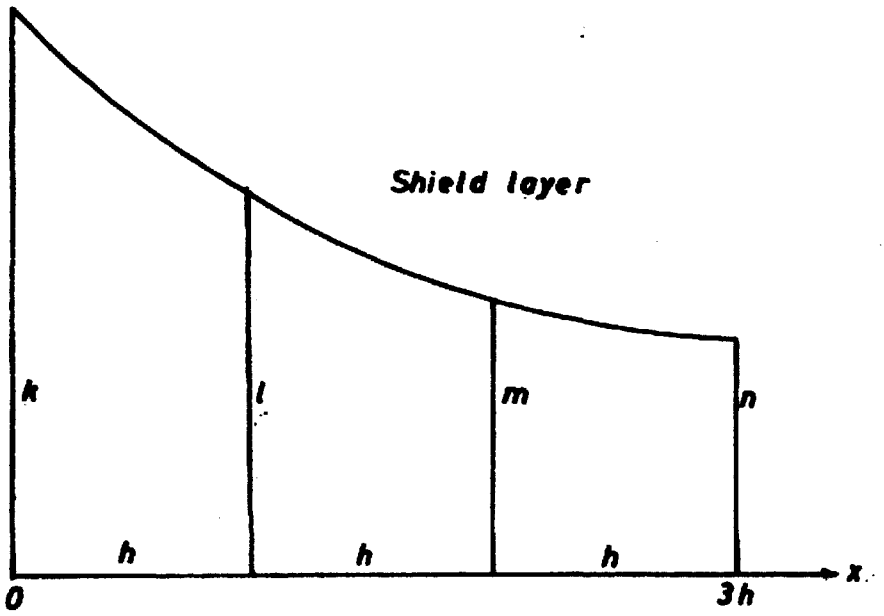

FIG. 3.2.1.

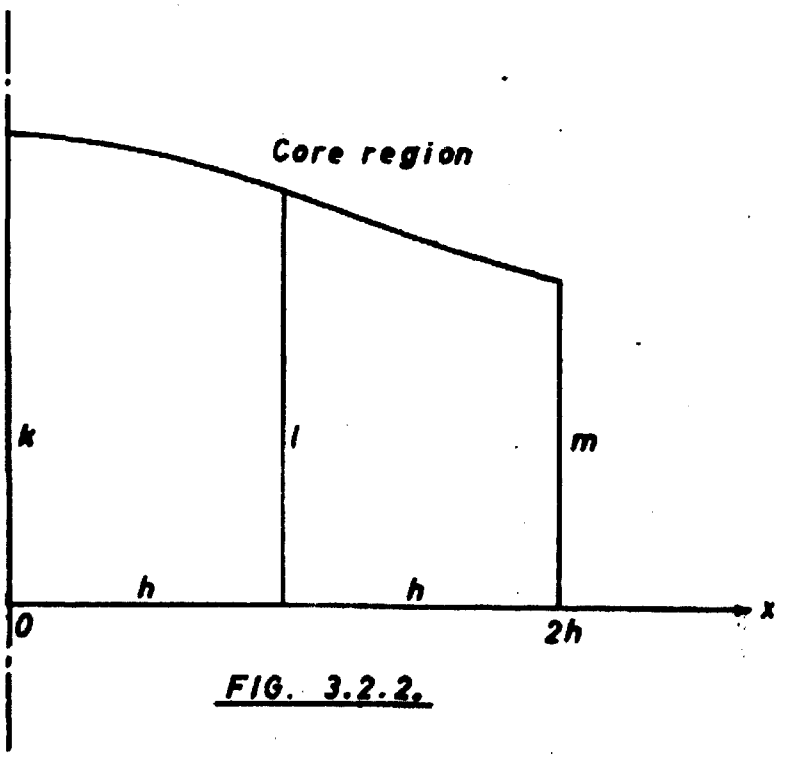

FIG. 3.2.2.

FIG. 3.3.

GROUP STRUCTURE FOR REMDIFF CROSS-SECTION LIBRARY

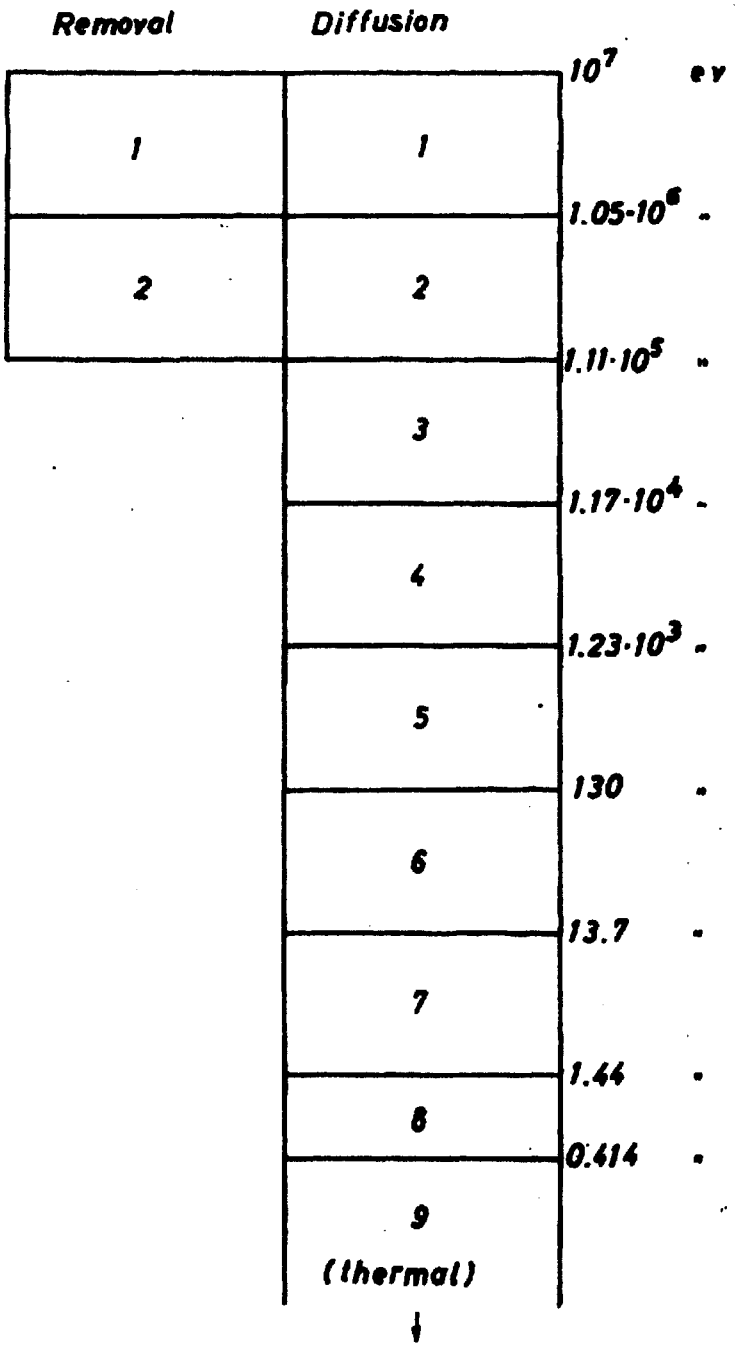

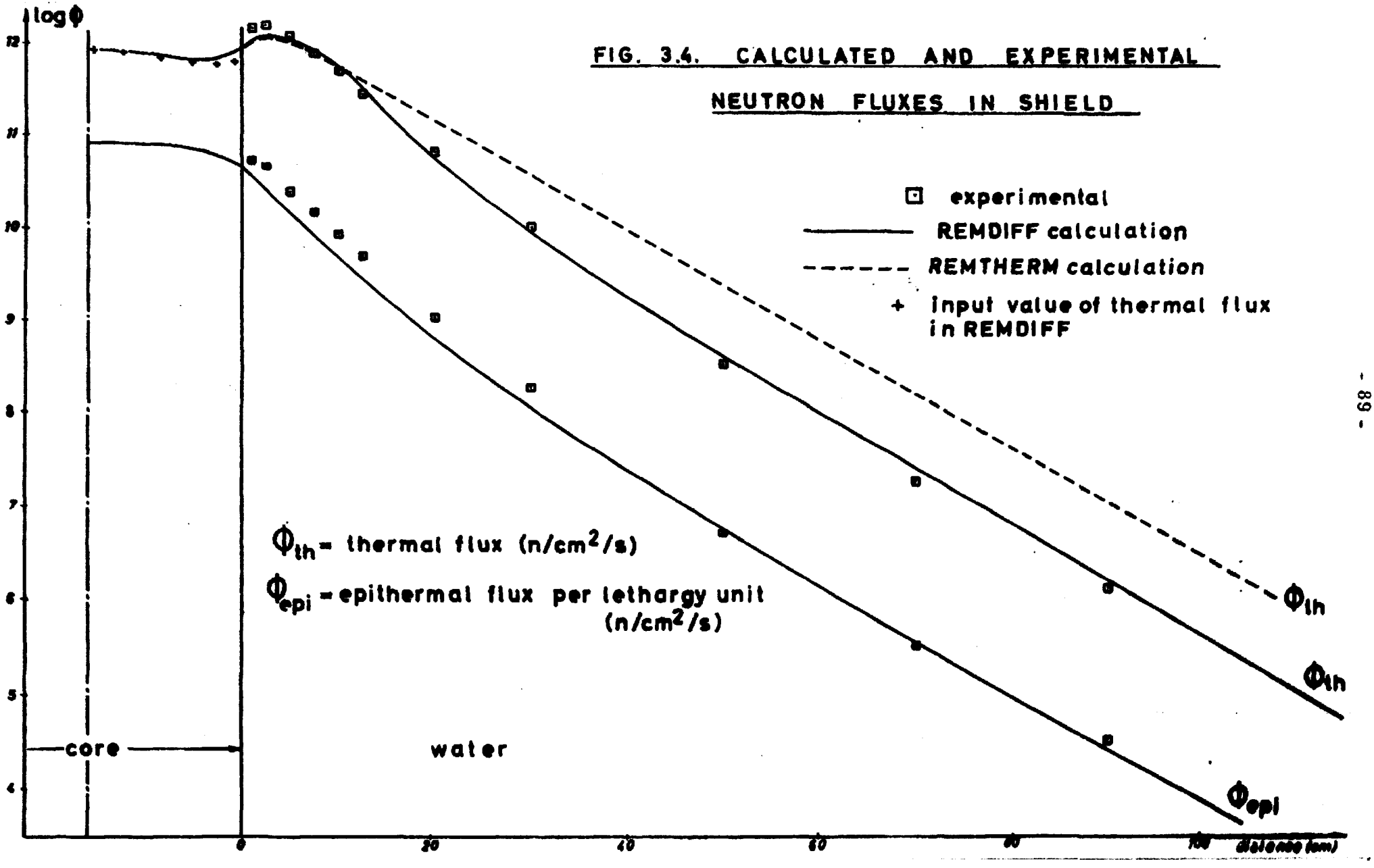

FIG. 3.4. CALCULATED AND EXPERIMENTAL NEUTRON FLUXES IN SHIELD

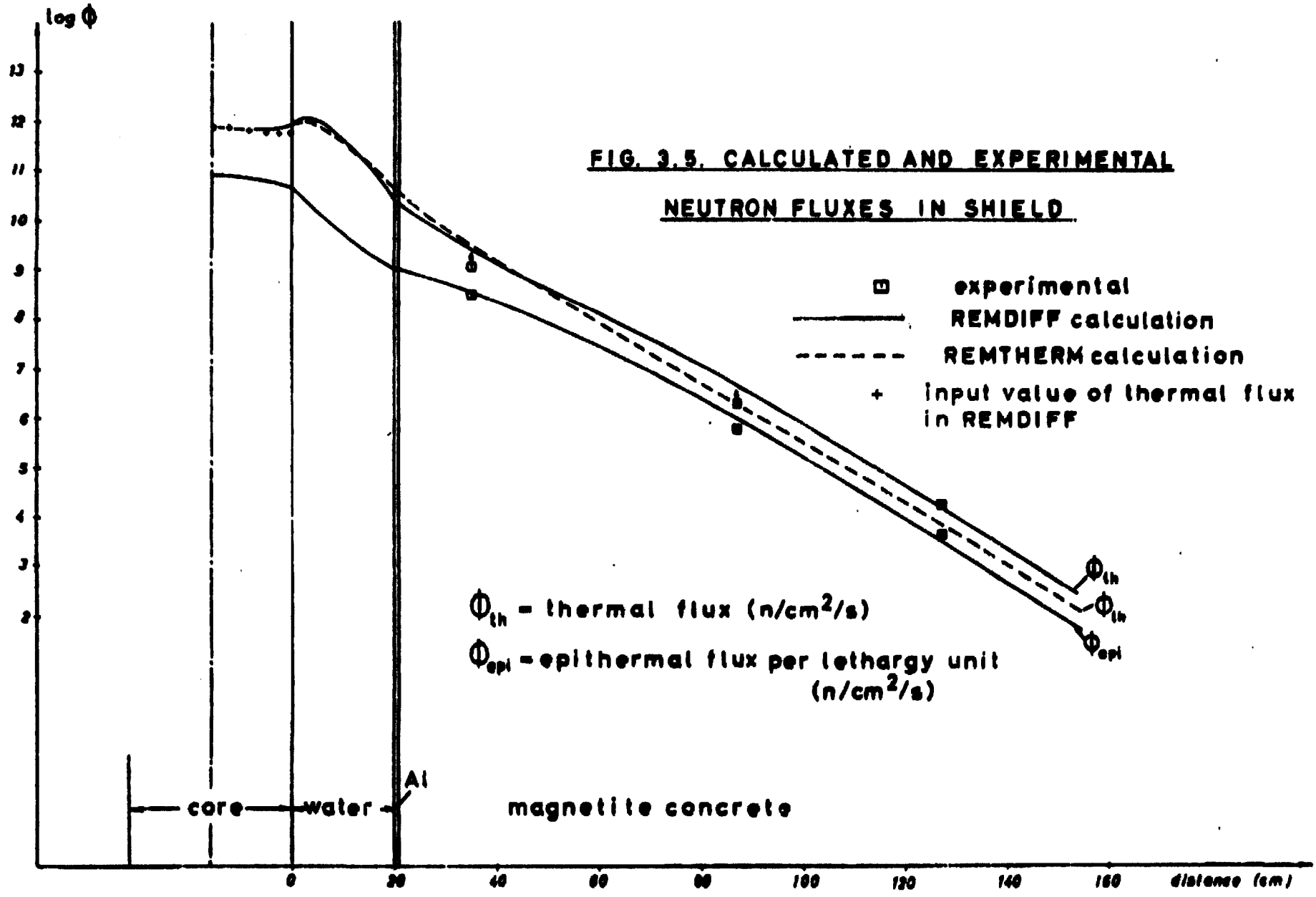

FIG. 3.5. CALCULATED AND EXPERIMENTAL NEUTRON FLUXES IN SHIELD

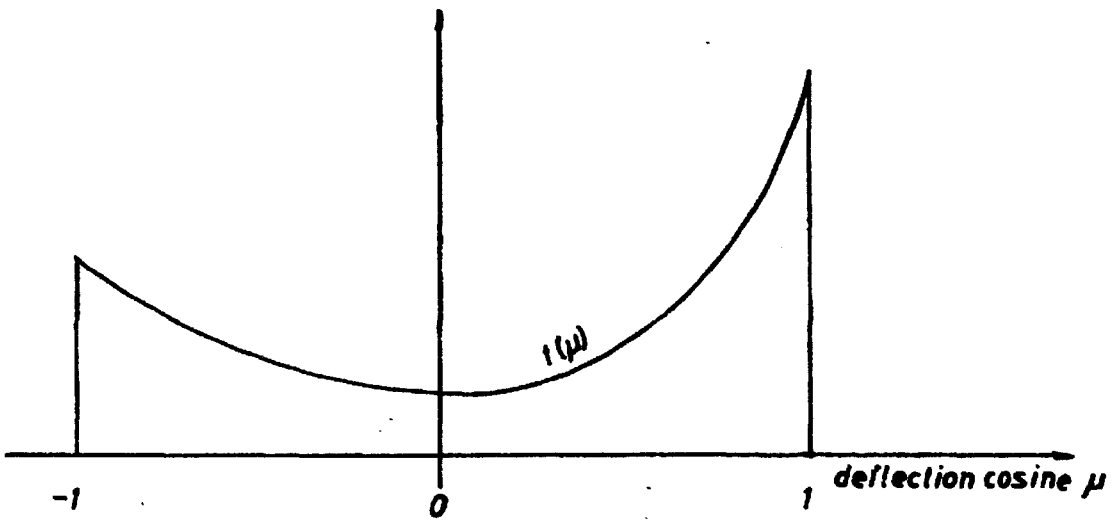

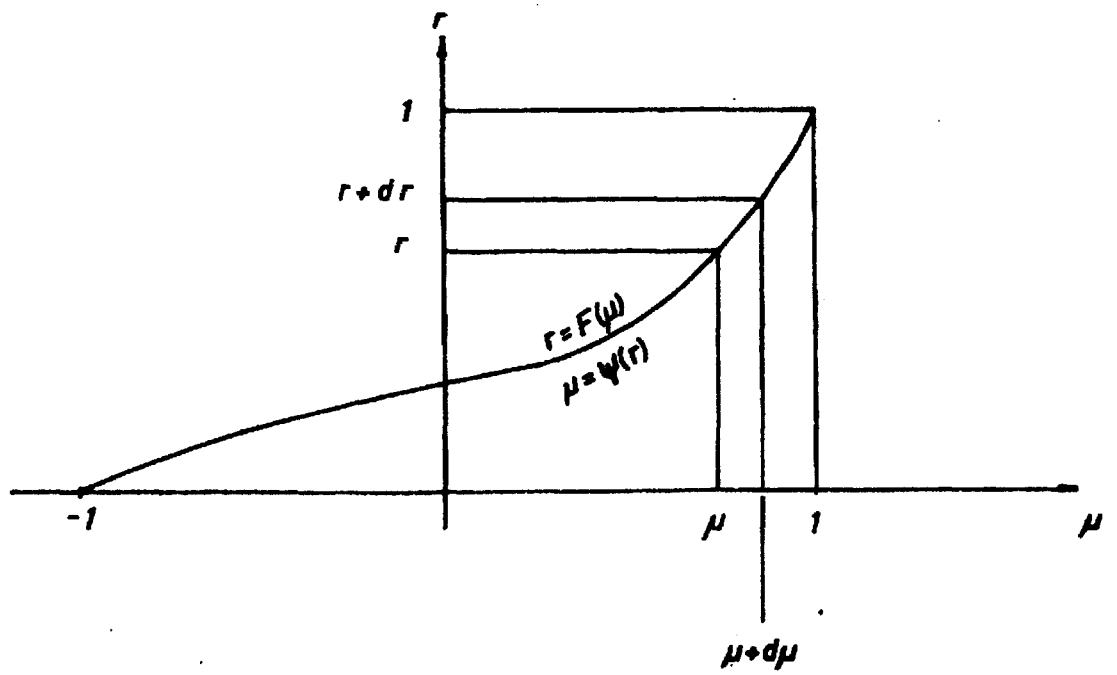

FIG. 4.1.

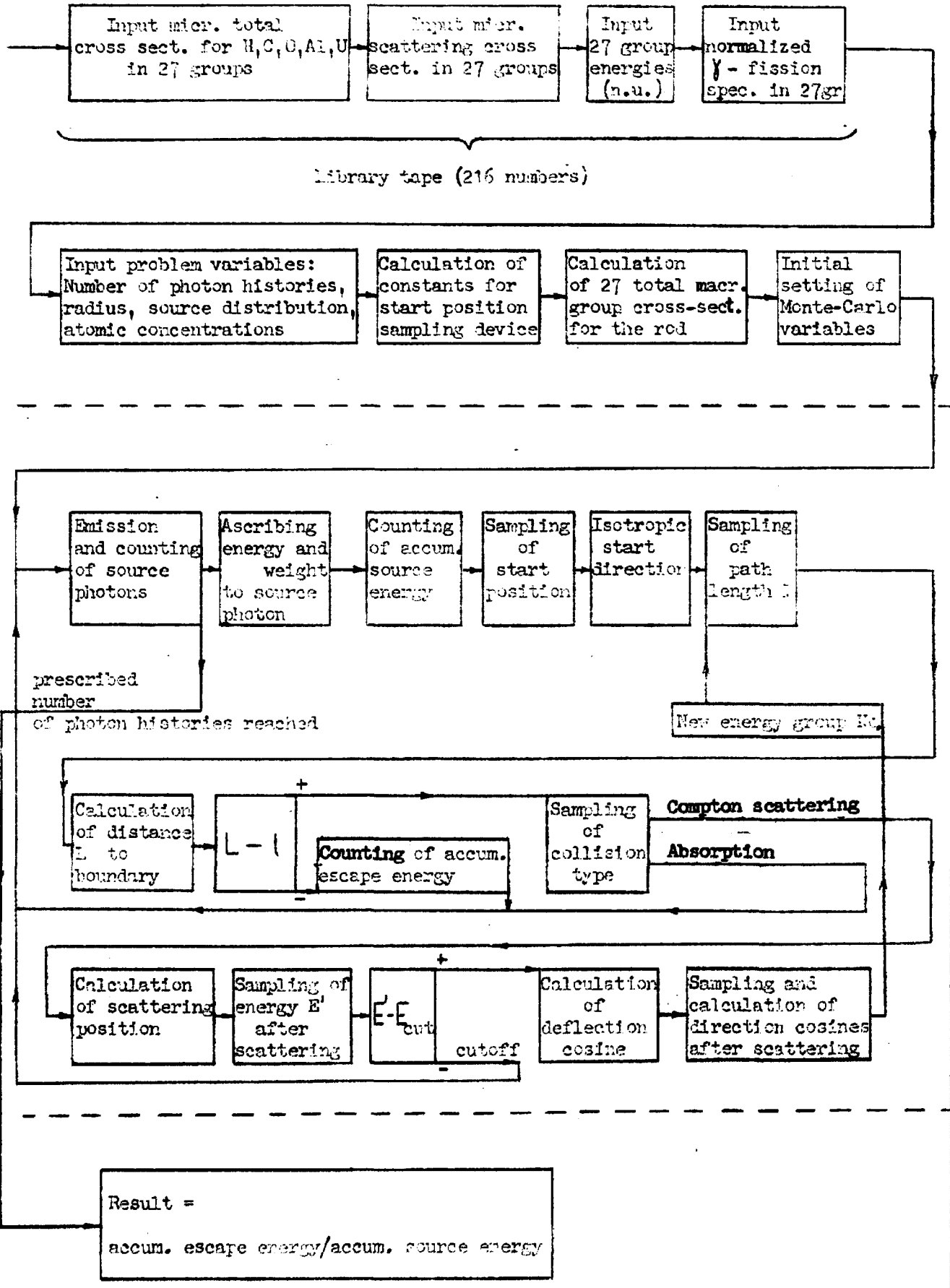
Input micr. total cross sect. for H,C,O,Al,U in 27 groups
Input micr. scattering cross sect. in 27 groups
Input 27 group energies (n.u.)
Input normalized γ - fission spec. in 27gr
Library tape (216 numbers)
Input problem variables: Number of photon histories, radius, source distribution, atomic concentrations
Calculation of constants for start position sampling device
Calculation of 27 total macr. group cross-sect. for the rod
Initial setting of Monte-Carlo variables
Emission and counting of source photons
Ascribing energy and weight to source photon
Counting of accum. source energy
Sampling of start position
Isotropic start direction
Sampling of path length
prescribed number of photon histories reached
New energy group No.
Calculation of distance L to boundary
L - l
+
-
Counting of accum. escape energy
Sampling of collision type
Compton scattering
Absorption
Calculation of scattering position
Sampling of energy E' after scattering
E'-E cut
+
-
cutoff
Calculation of deflection cosine
Sampling and calculation of direction cosines after scattering
Result =
accum. escape energy/accum. source energy

FIG. 5.1.

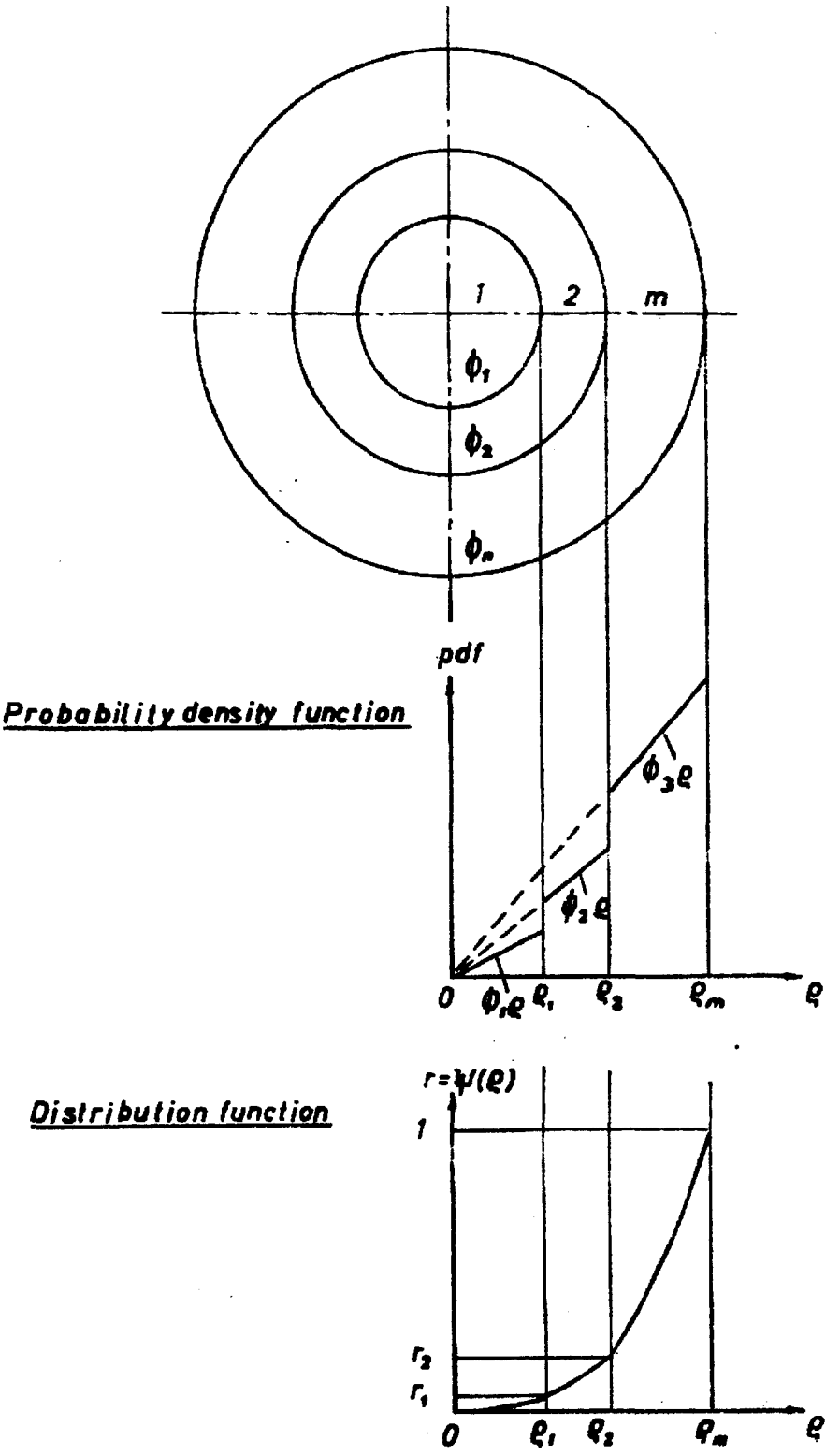

Probability density function

Distribution function

FIG.5.2.

FIG. 5.3.

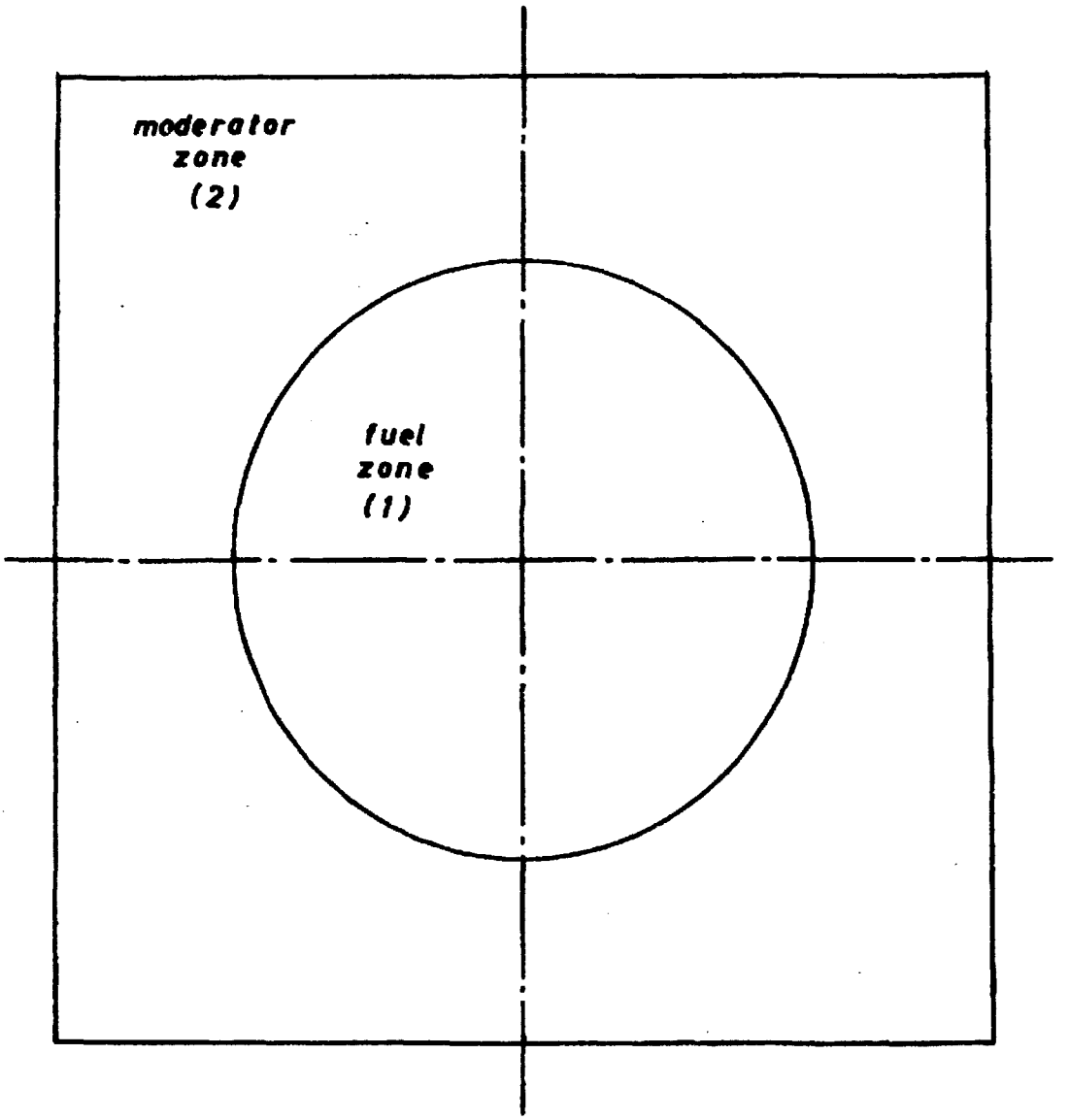

LATTICE CELL GEOMETRY

FOR MC1-MC2

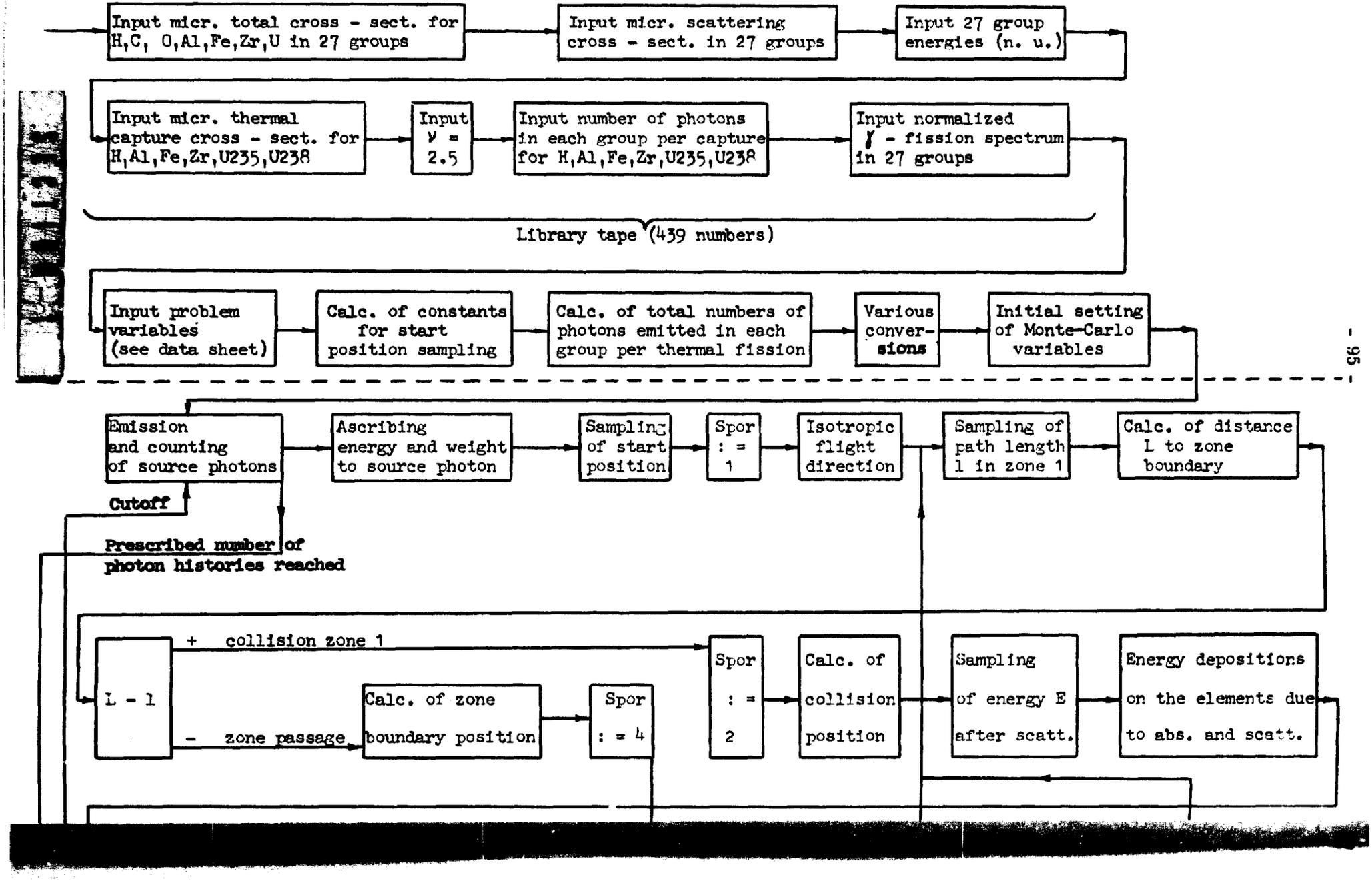
Input micr. total cross - sect. for H,C, O,Al,Fe,Zr,U in 27 groups
Input micr. scattering cross - sect. in 27 groups
Input 27 group energies (n. u.)
Input micr. thermal capture cross - sect. for H,Al,Fe,Zr,U235,U238
Input ν = 2.5
Input number of photons in each group per capture for H,Al,Fe,Zr,U235,U238
Input normalized γ - fission spectrum in 27 groups
Library tape (439 numbers)
Input problem variables (see data sheet)
Calc. of constants for start position sampling
Calc. of total numbers of photons emitted in each group per thermal fission
Various conversions
Initial setting of Monte-Carlo variables
Emission and counting of source photons
Ascribing energy and weight to source photon
Sampling of start position
Spor : = 1
Isotropic flight direction
Sampling of path length l in zone 1
Calc. of distance L to zone boundary
Cutoff
Prescribed number of photon histories reached
L - l
+ collision zone 1
- zone passage
Calc. of zone boundary position
Spor : = 4
Spor : = 2
Calc. of collision position
Sampling of energy E after scatt.
Energy depositions on the elements due to abs. and scatt.

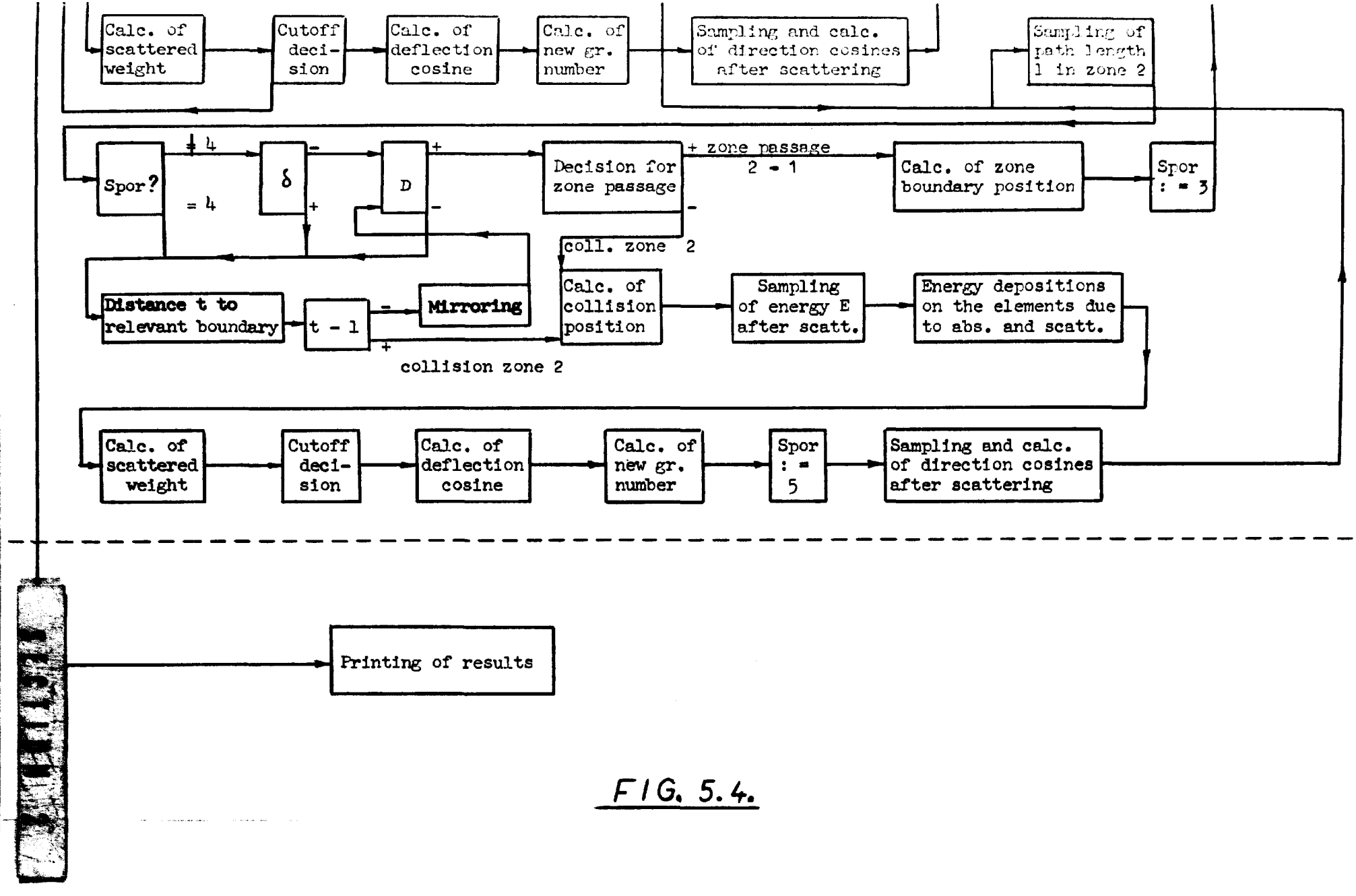
Calc. of scattered weight
Cutoff deci- sion
Calc. of deflection cosine
Calc. of new gr. number
Sampling and calc. of direction cosines after scattering
Sampling of path length l in zone 2
Spor?
≠ 4
= 4
δ
D
Decision for zone passage
+ zone passage
2 → 1
Calc. of zone boundary position
Spor : = 3
coll. zone 2
Distance t to relevant boundary
t - l
Mirroring
Calc. of collision position
Sampling of energy E after scatt.
Energy depositions on the elements due to abs. and scatt.
collision zone 2
Calc. of scattered weight
Cutoff deci- sion
Calc. of deflection cosine
Calc. of new gr. number
Spor : = 5
Sampling and calc. of direction cosines after scattering
Printing of results

FIG. 5.4.

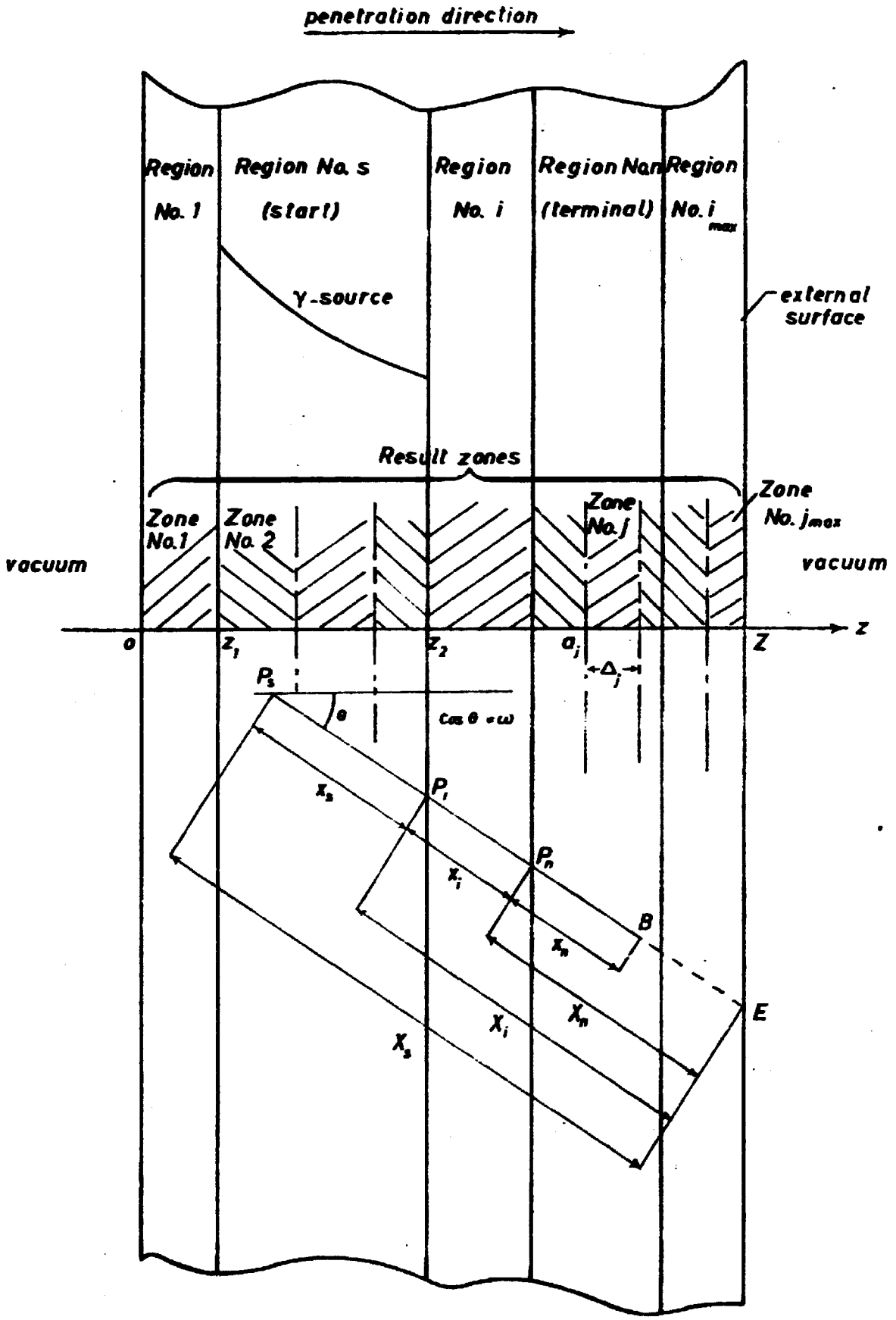
penetration direction
Region No. 1
Region No. s (start)
Region No. i
Region Nan (terminal)
Region No. i max
γ-source
external surface
Result zones
Zone No.1
Zone No. 2
Zone No. j
Zone No. j max
vacuum
vacuum
z
0
z1
z2
aj
Δj
Z
Ps
θ
cos θ = ω
Xs
Pi
Pn
Xi
B
Xn
E
Xi
Xn
Xs

FIG. 6.1.

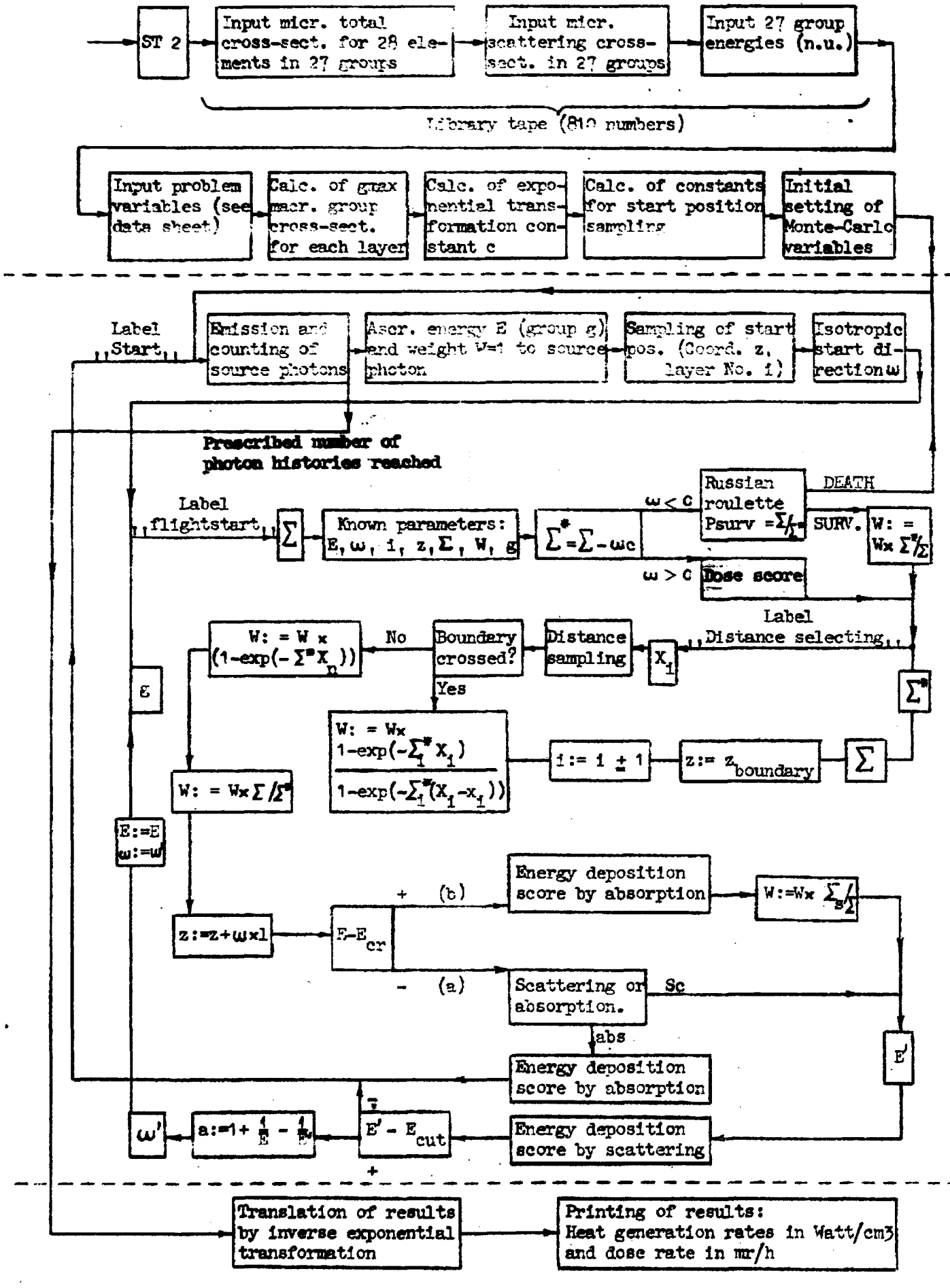
ST 2
Input micr. total cross-sect. for 28 elements in 27 groups
Input micr. scattering cross-sect. in 27 groups
Input 27 group energies (n.u.)
Library tape (810 numbers)
Input problem variables (see data sheet)
Calc. of gmax macr. group cross-sect. for each layer
Calc. of exponential transformation constant c
Calc. of constants for start position sampling
Initial setting of Monte-Carlo variables
Label Start
Emission and counting of source photons
Asgn. energy E (group g) and weight W=1 to source photon
Sampling of start pos. (Coord. z, layer No. i)
Isotropic start direction ω
Prescribed number of photon histories reached
Label flightstart
Known parameters: E, ω, i, z, Σ, W, g
ω < c
Russian roulette Psurv = Σ*/Σ
DEATH
SURV.
W: = W x Σ*/Σ
ω > c
Dose score
Label Distance selecting
Distance sampling
Boundary crossed?
No
Yes
W: = W x (1-exp(-Σ*X_n))
W: = W x 1-exp(-Σ_i* X_i) / 1-exp(-Σ_i*(X_i-x_i))
i := i ± 1
z := z_boundary
W: = W x Σ/Σ*
E:=E ω:=ω
z:=z+ω x l
E-E_cr
+ (b)
- (a)
Energy deposition score by absorption
W:=W x Σ_s/Σ
Scattering or absorption.
Sc
abs
Energy deposition score by absorption
Energy deposition score by scattering
E'
ω'
a:=1+ 1/E - 1/E'
E' - E_cut
+
Translation of results by inverse exponential transformation
Printing of results: Heat generation rates in Watt/cm3 and dose rate in mr/h

FIG. 6.2.

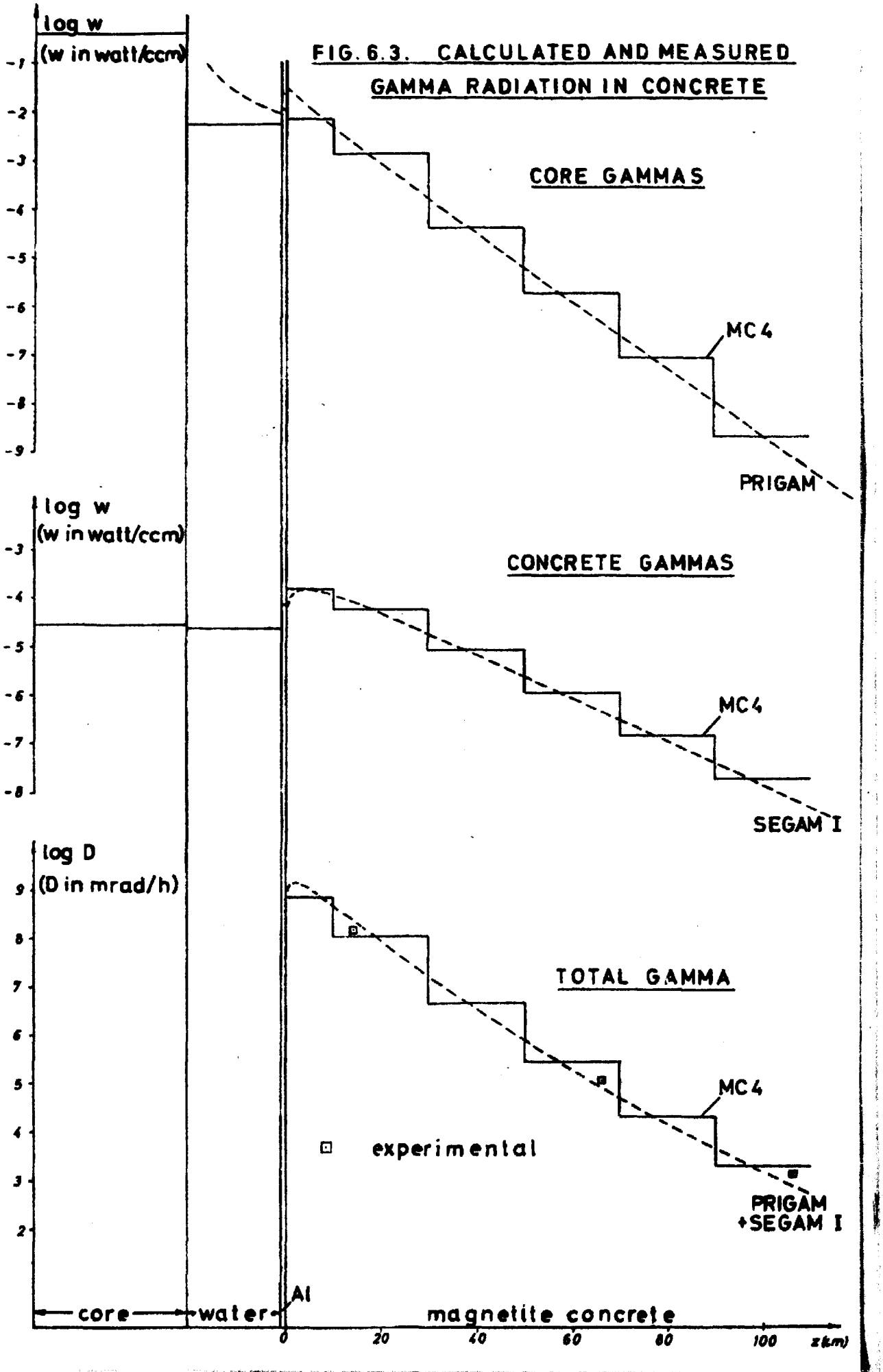

FIG. 6.3. CALCULATED AND MEASURED GAMMA RADIATION IN CONCRETE

FIG. 7.1.

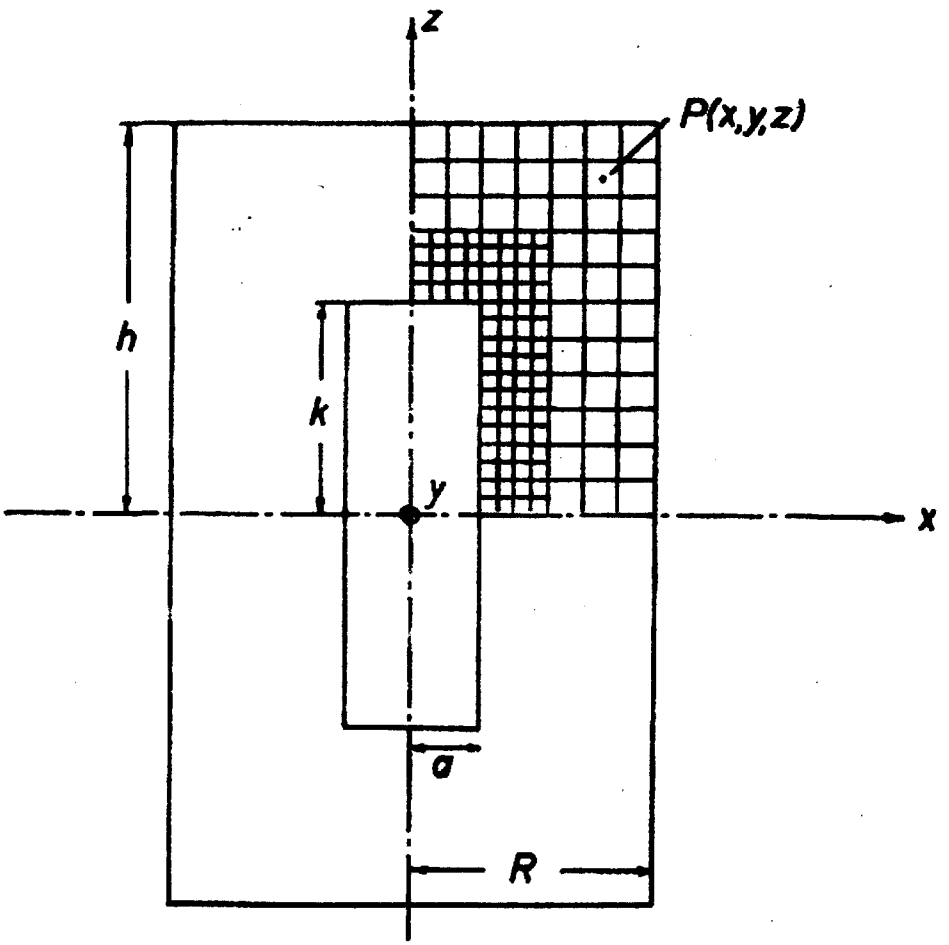

BLACK ROD GEOMETRY

FIG.7.2.

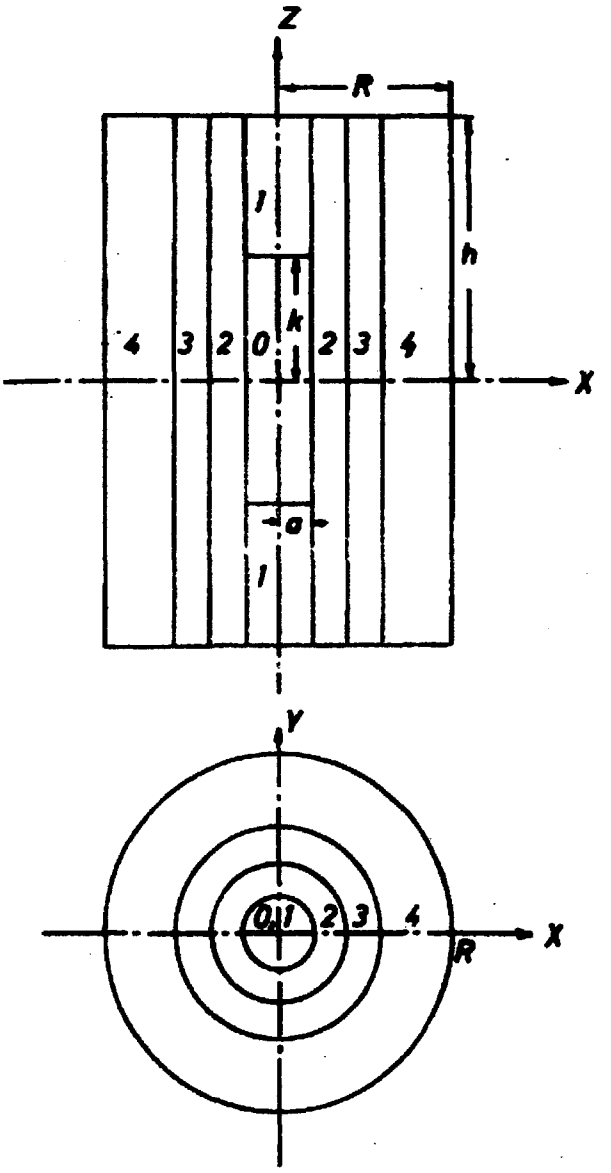

GEOMETRY FOR GREY ROD IN HETERO-GENEOUS MEDIUM.

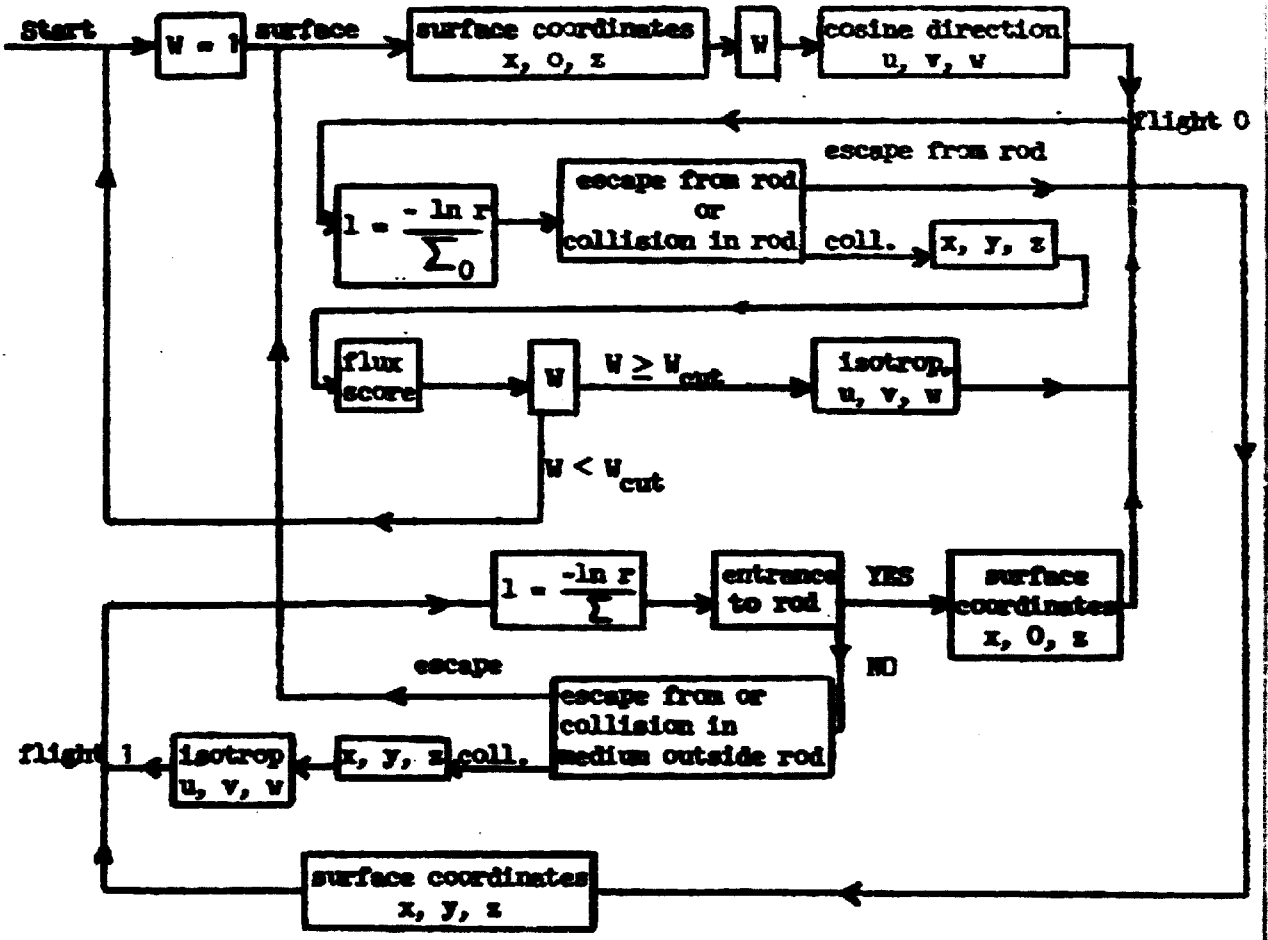

FIG. 7.3. FLOW DIAGRAM FOR GREY ROD IN HOMOGENEOUS MEDIUM.

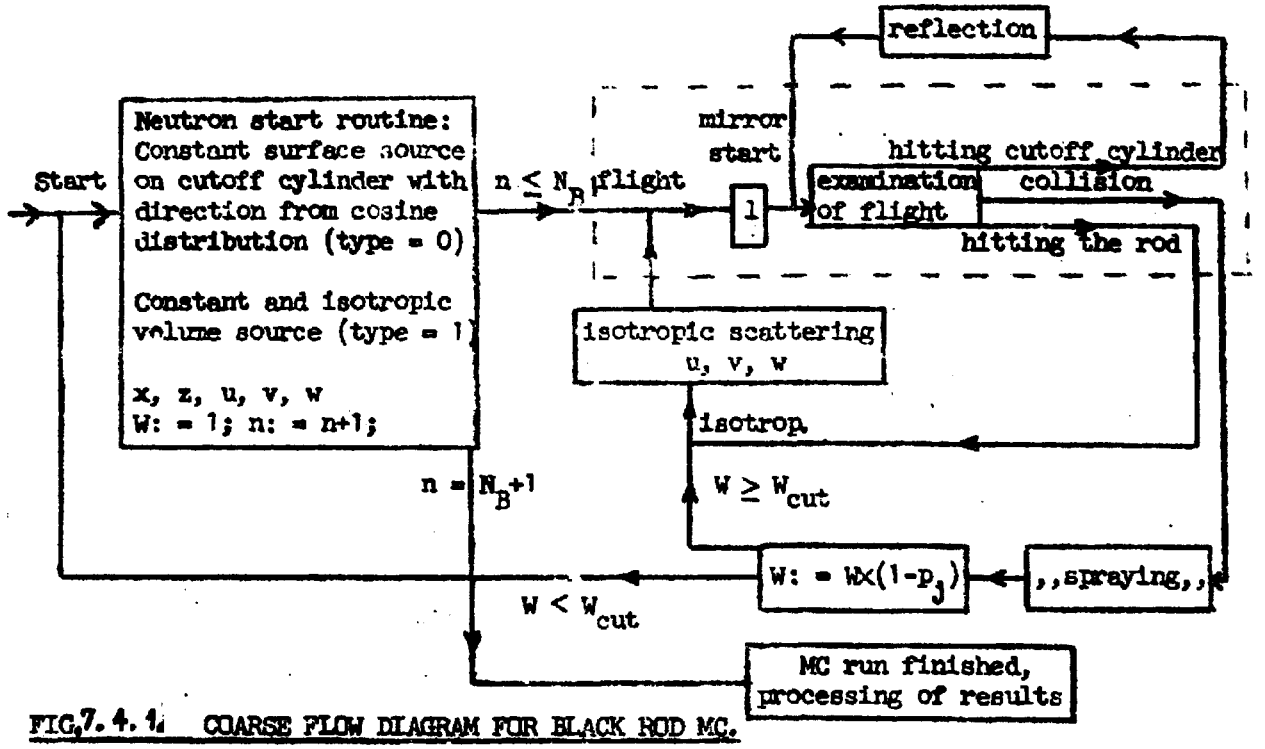

FIG.7.4.1 COARSE FLOW DIAGRAM FOR BLACK ROD MC.

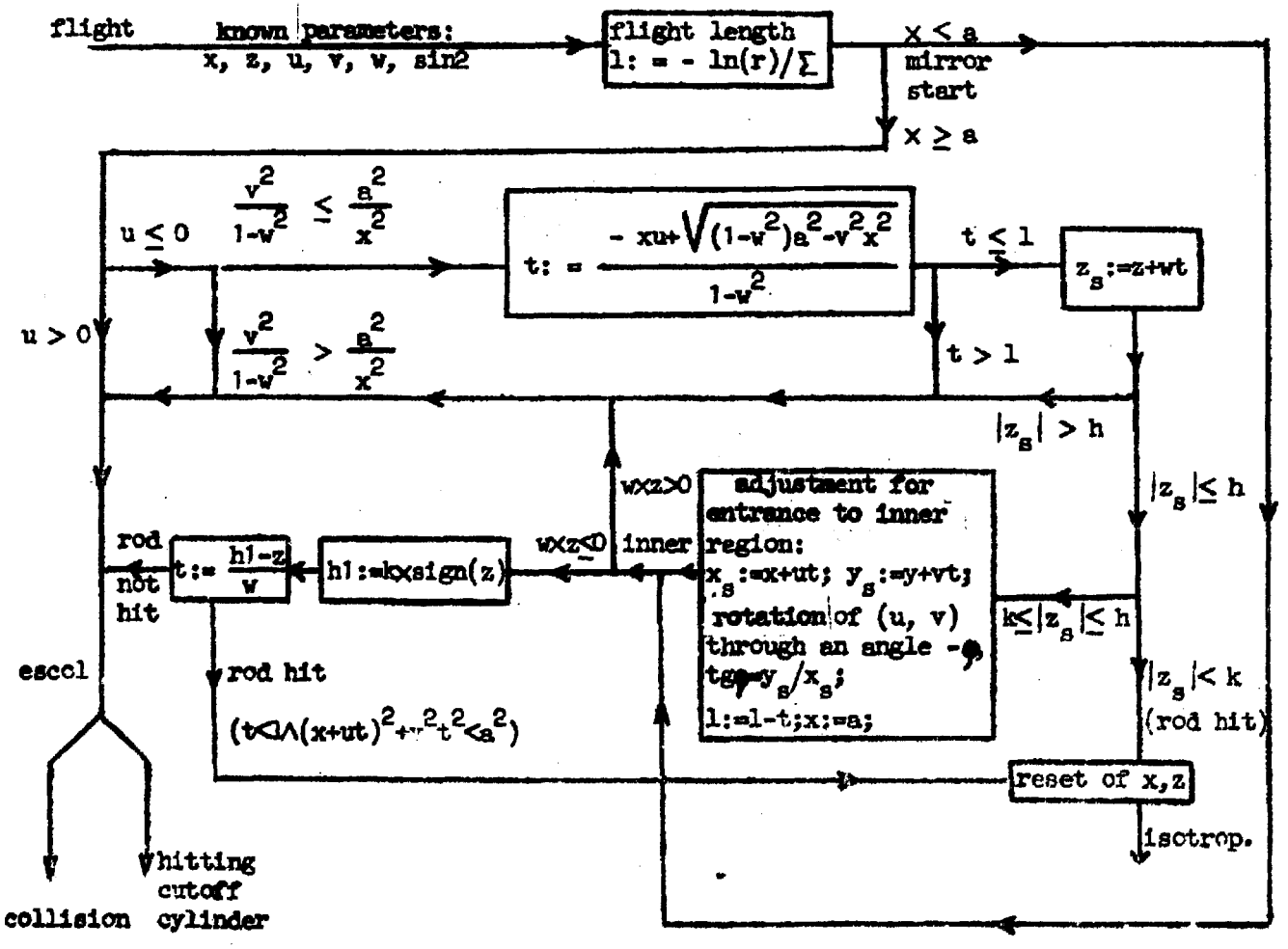

FIG.7.4.2 DETAILED FLOW DIAGRAM OF FLIGHT ROUTINE FOR BLACK ROD MC.

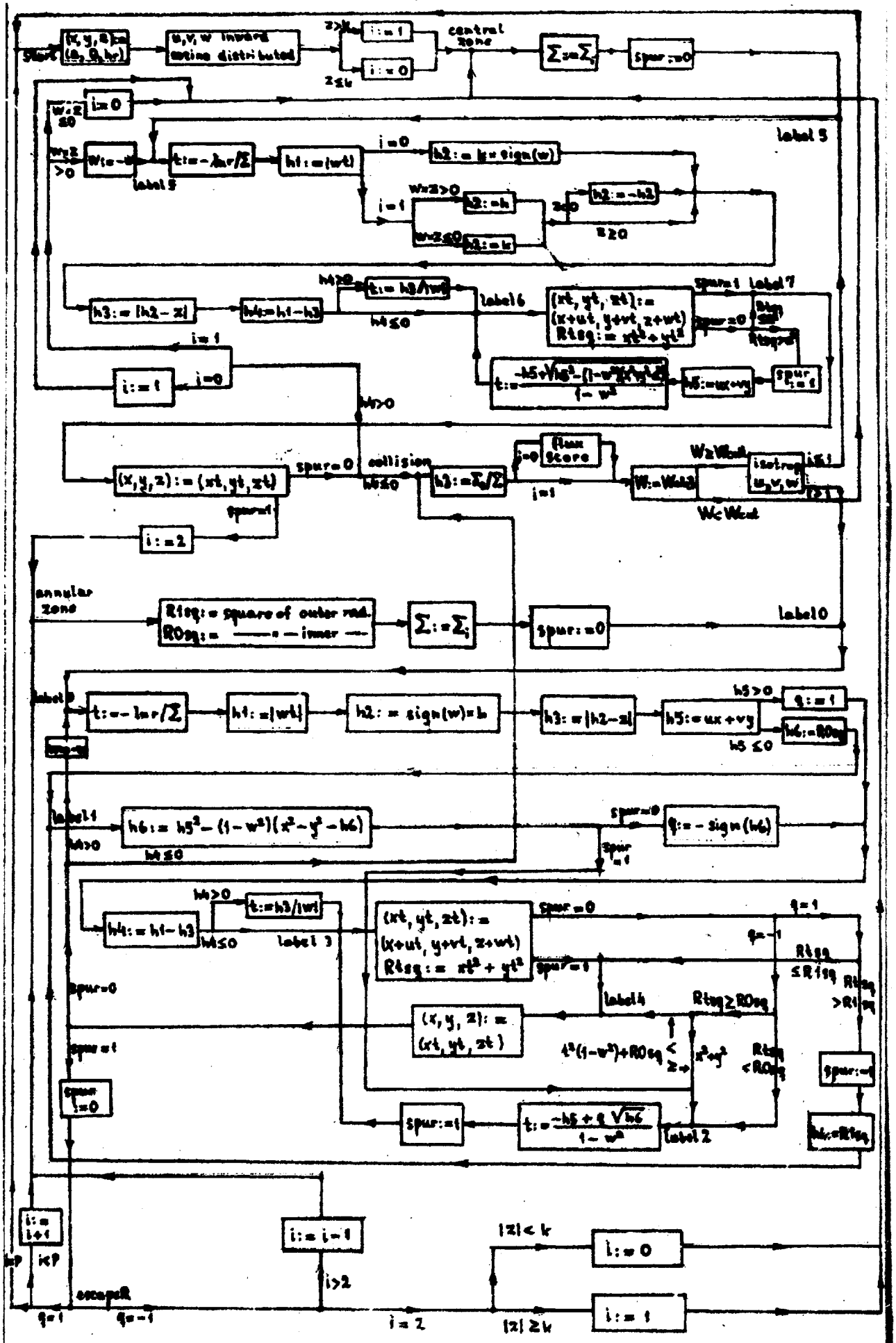

FIG. 7.5. FLOW DIAGRAM FOR GREY ROD IN HETEROGENEOUS MEDIUM.

FIG.7.6.

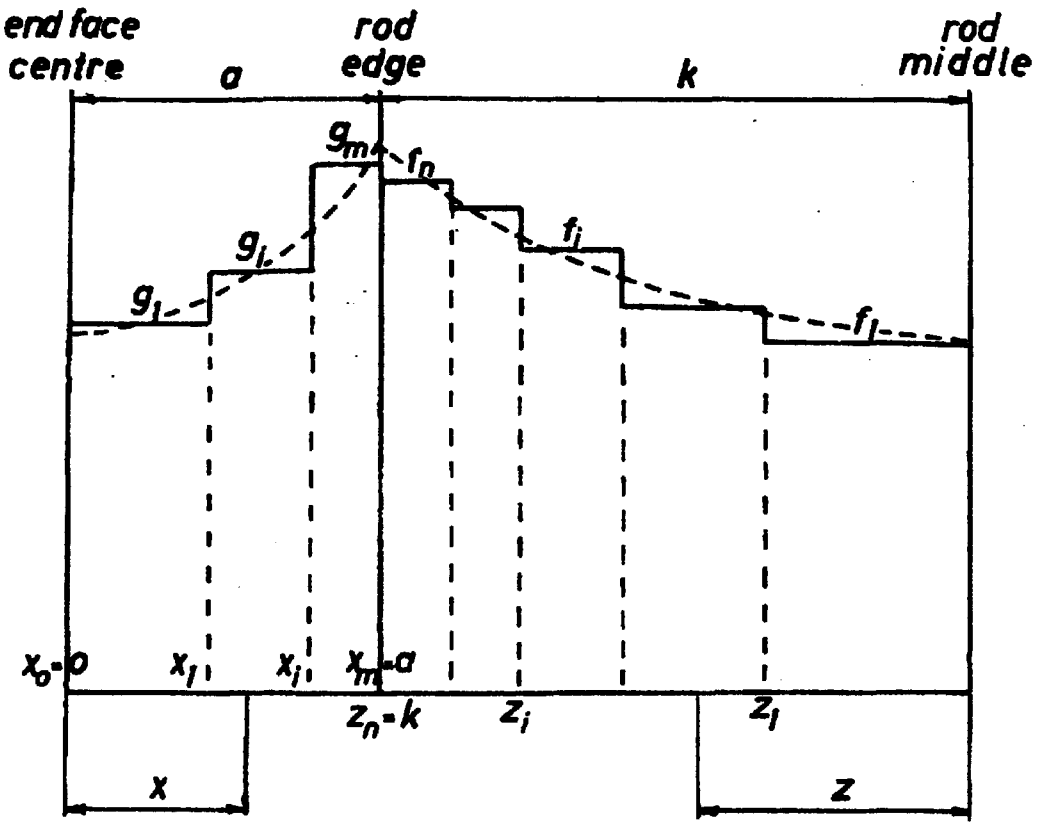

SMOOTHENING OF OUTPUT FROM MC5A.

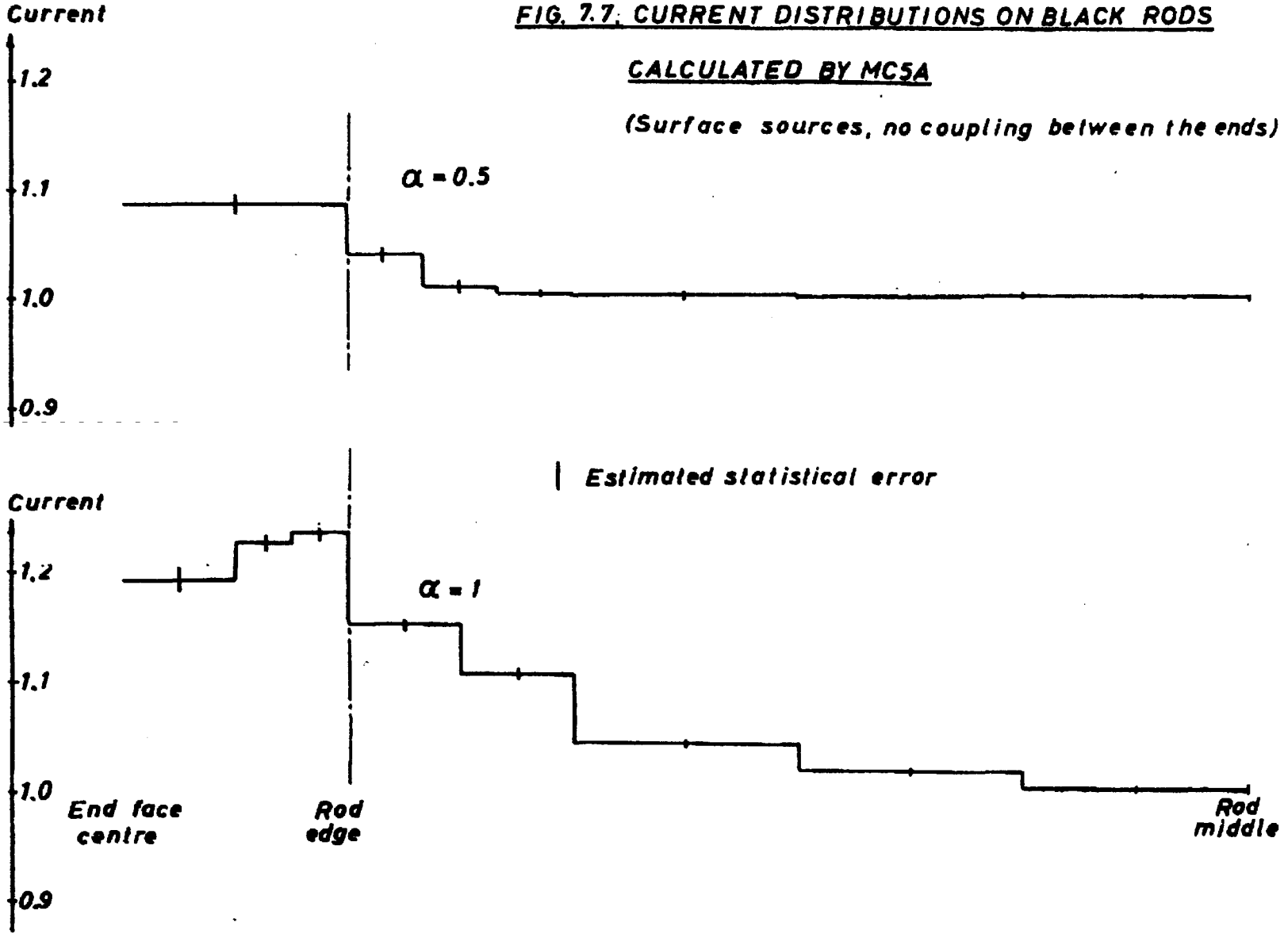

FIG. 7.7. CURRENT DISTRIBUTIONS ON BLACK RODS

CALCULATED BY MC5A

(Surface sources, no coupling between the ends)

FIG. 7.8. CURRENT DISTRIBUTIONS ON BLACK RODS CALCULATED BY MC5A

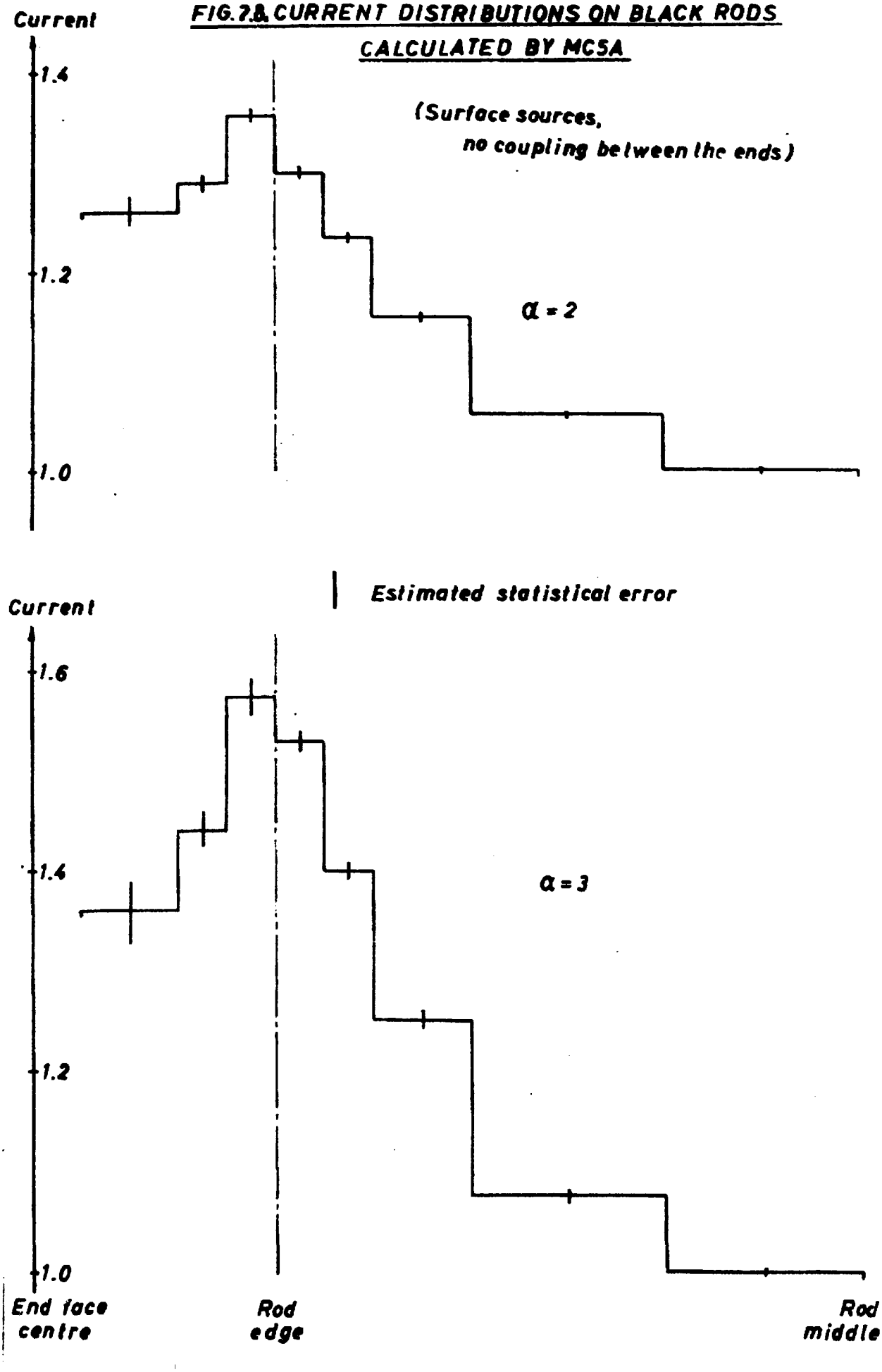

FIG. 7.9.1. MEASURED AND CALCULATED LONGITUDINAL CURRENT DISTRIBUTION ON BLACK ROD

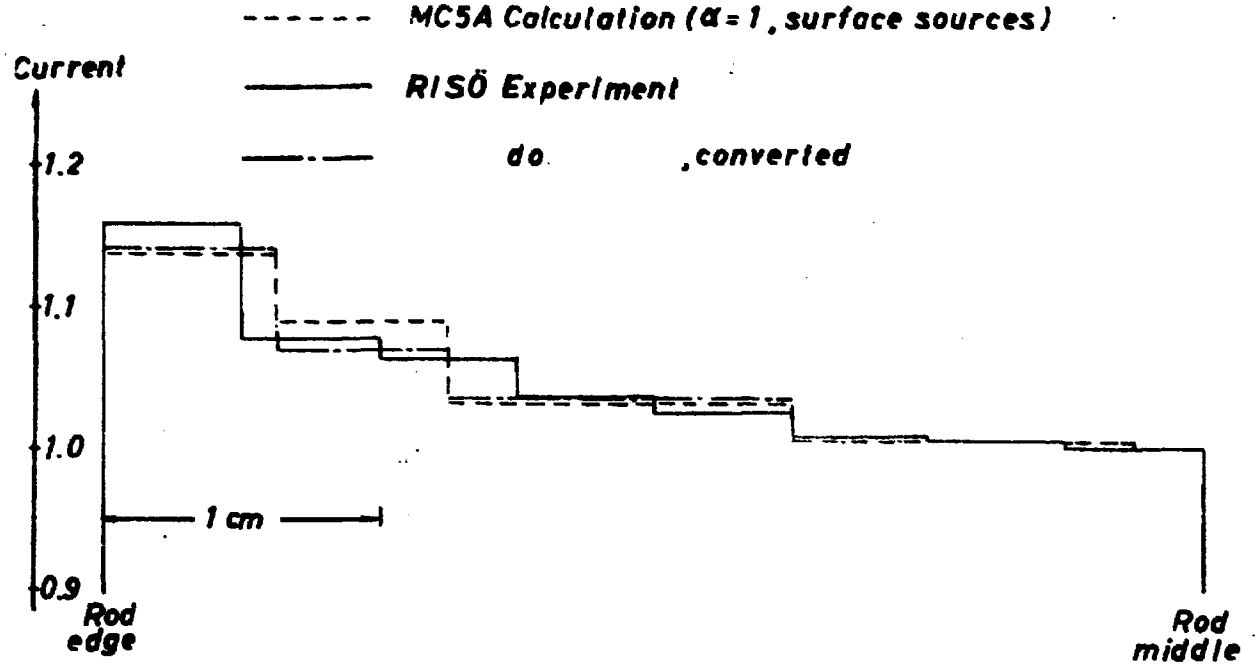

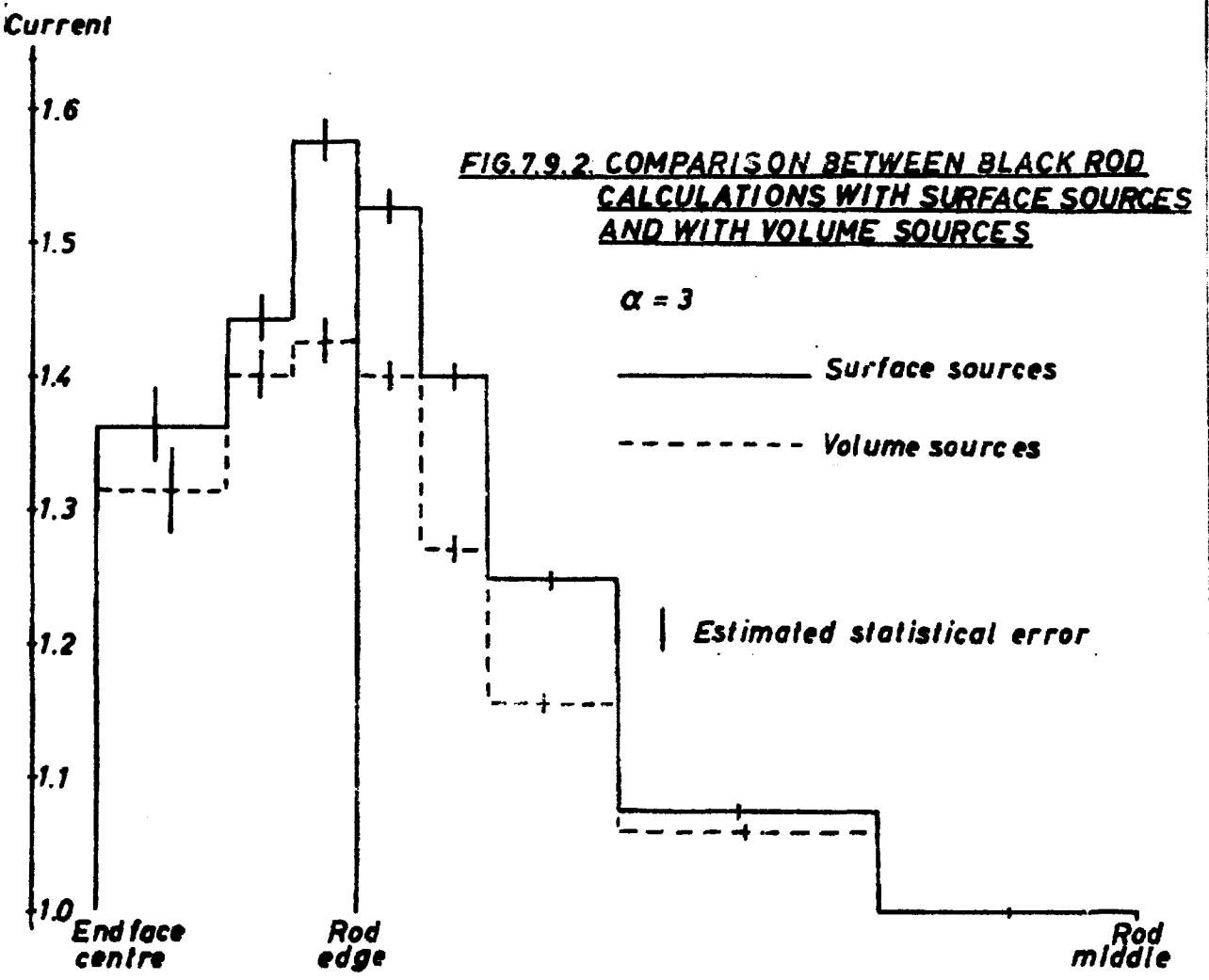

FIG. 7.9.2. COMPARISON BETWEEN BLACK ROD CALCULATIONS WITH SURFACE SOURCES AND WITH VOLUME SOURCES

FIG. 7.10.

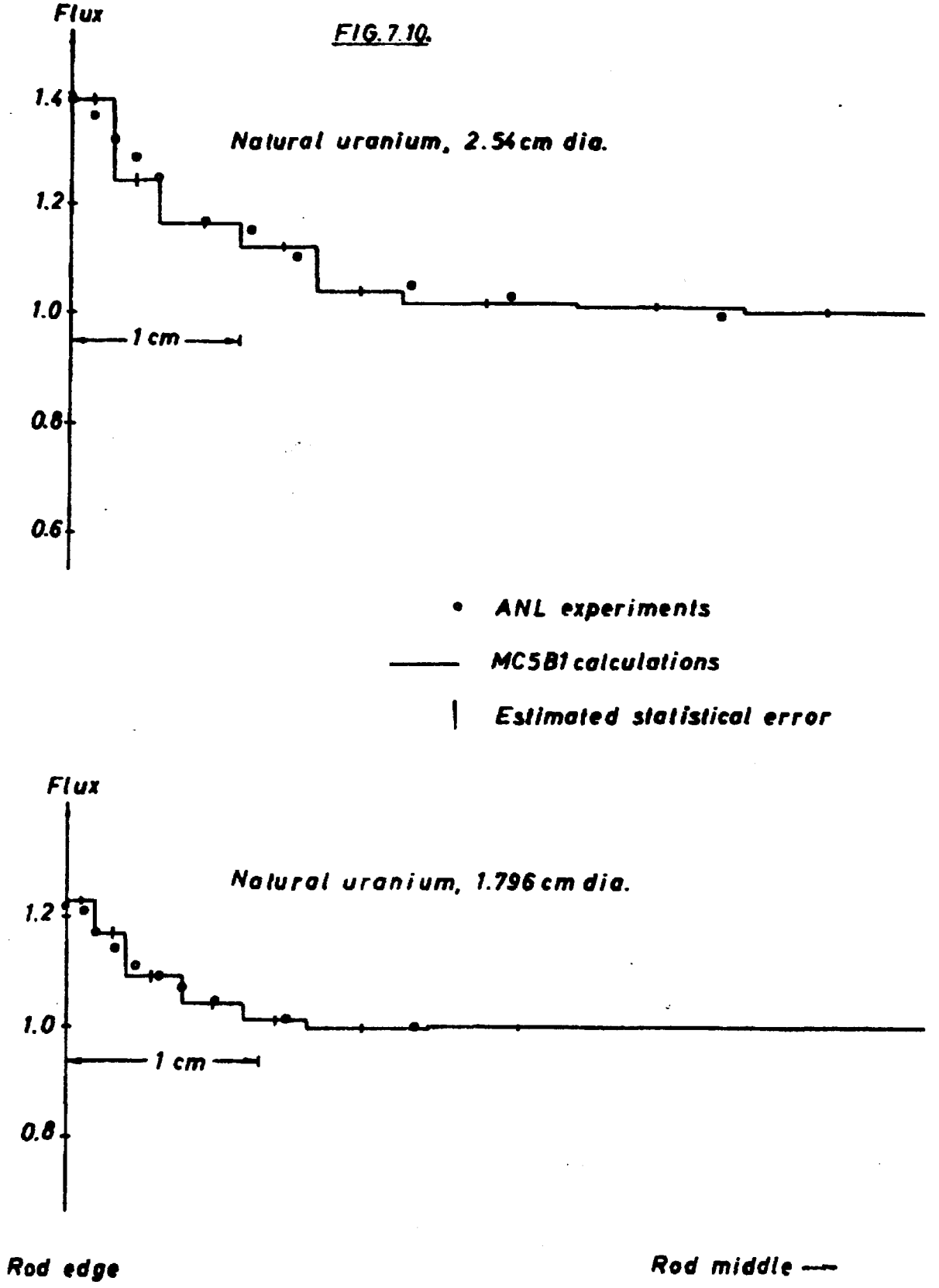

COMPARISON BETWEEN ANL MEASUREMENTS AND MC5B1 CALCULATIONS

FIG. 7.11.

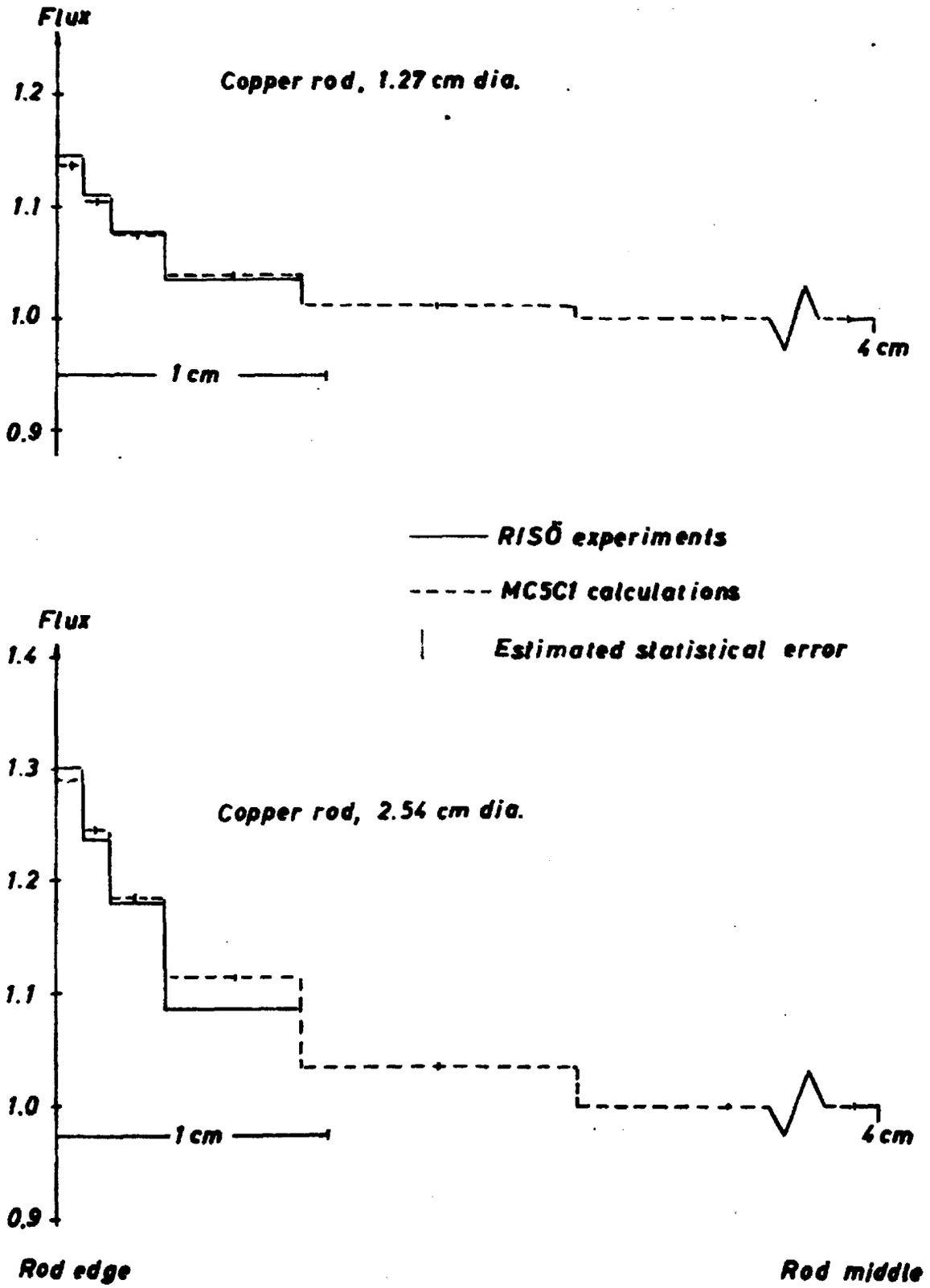

COMPARISON BETWEEN RISÖ MEASUREMENTS AND MC5C1 CALCULATIONS

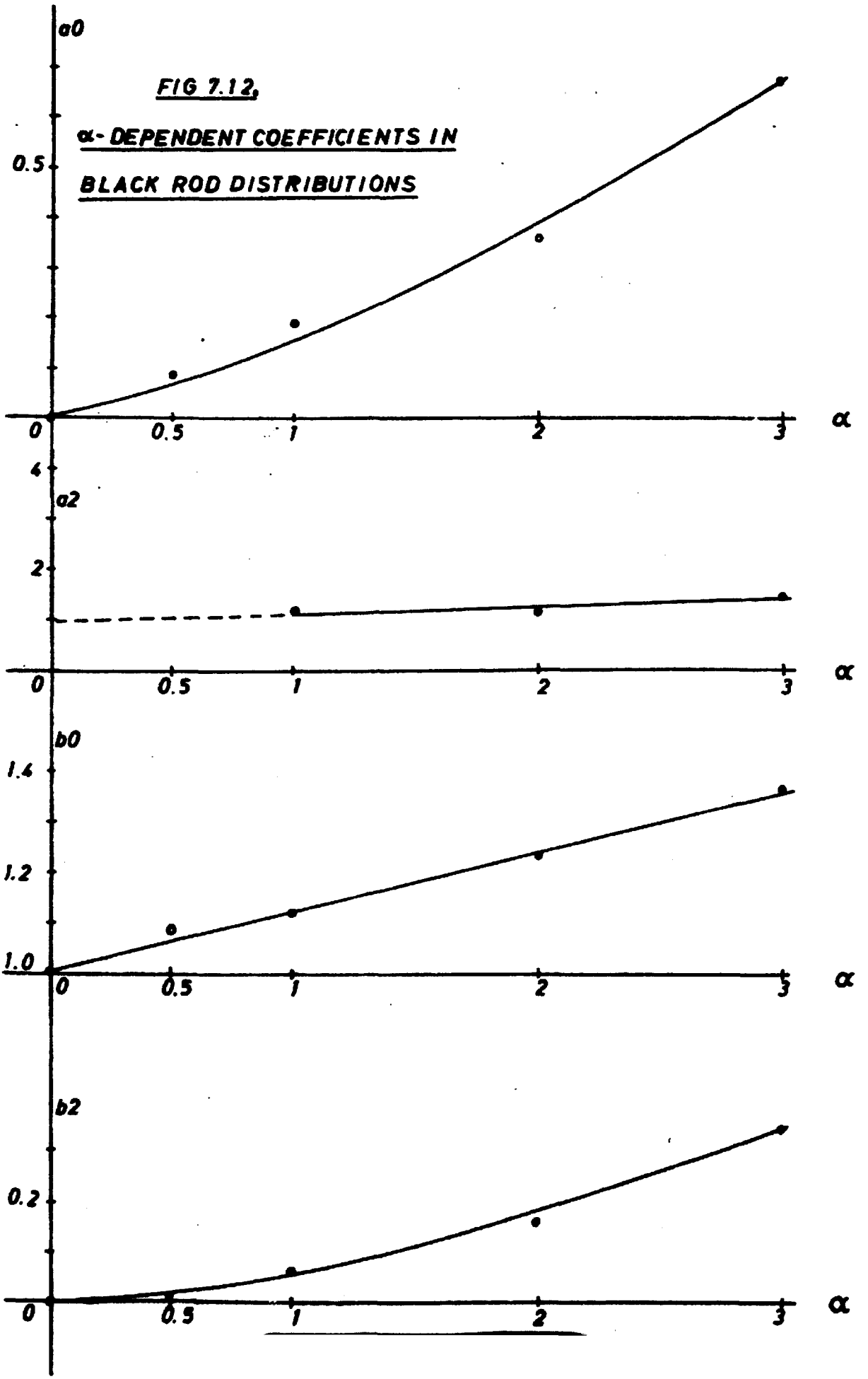

FIG 7.12,

α- DEPENDENT COEFFICIENTS IN BLACK ROD DISTRIBUTIONS